# Development of an open-source ecohydrology model using Landlab with applications in semi-arid landscapes

Sai Siddhartha Nudurupati

A dissertation

submitted in partial fulfillment of the

requirements for the degree of

Doctor of Philosophy

University of Washington

2020

Reading Committee:

Erkan Istanbulluoglu, Chair

Faisal Hossain

Gregory Tucker

Program Authorized to Offer Degree:

Department of Civil and Environmental Engineering

University of Washington

**Abstract**

# Development of an open-source ecohydrology model using Landlab with applications in semi-arid landscapes

Sai Siddhartha Nudurupati

Chair of the Supervisory Committee:
Professor Erkan Istanbulluoglu
Department of Civil and Environmental Engineering

Ecosystems are in transition globally with critical societal consequences. Global warming, growing climatic extremes, land degradation, human-introduced herbivores, and climate-related disturbances (wildfires, diseases, insect outbreaks) drive rapid changes in ecosystem productivity and structure, with complex feedbacks in watershed hydrology, geomorphology and biogeochemistry. There is need to develop models that can represent ecosystem changes by incorporating the role of individual plant patches. In my research I developed ecohydrologic components in Landlab, an open source toolkit written in Python (http://landlab.github.io/#/), to study global change drivers in watersheds with emphasis on woody plant encroachment (WPE).

I will first discuss the development of Landlab, its design, architecture, and illustrate examples of building models with Landlab. I will then present the development of ecohydrologic components and illustrate examples of coupling these components for simulating local soil moisture and plant dynamics with spatially explicit cellular automaton (CA)-based plant establishment, mortality, fire, and grazing processes. Several key features of arid and semiarid ecosystems will be discussed. Coexistence of tree-grass cover on north facing slopes (NFS) and shrub cover on south facing slopes (SFS) in central New Mexico is attributed to the competitive advantage of trees due to their longer seed dispersal range against shrubs in cooler and moist NFS. Incorporating a rule to represent inhibitory effects of shrubs on grasses enhance modeled shrub cover, while both trees and grasses are favored when runon is included in the local soil moisture model. Feedbacks among livestock grazing, grassland fire frequency and size, resource redistribution on woody plant encroachment are investigated using different ecohydrologic model configurations. These feedbacks have led to a three-phase woody plant expansion processes in the model, with rates of encroachment controlled by the state transition probabilities of vegetation types in relation to plant susceptibility to fires, grazing, and age-related mortality. A critical area of woody plant emerges in the model with which a negative feedback between fire size and woody plant expansion begins, providing a spatially-explict modelling evidence to the alternative stable states hypothesis.

Finally, I investigate the transient ecosystem response to climate variability since the Late Pleistocene using paleoclimatic reconstructions of precipitation and temperature in central New Mexico, USA. The interplay between ecosystem state, change in climate, resultant grass connectivity, and hence fire frequency, and topography are explored with an ecohydrologic model discussed earlier. A transition from cool-wet climate to a warm-dry climate leads to shrub

expansion due to drought-induced loss of grass connectivity. Shrubs dominate the ecosystem if dry conditions persist longer. Transition back to a tree or grass dominated ecosystem from shrub dominated ecosystem can only happen when climate shifts from dry to wet. The importance of length of dry or wet spells on ecosystem structure is highlighted. Aspect plays a critical role in providing topographical refugia for trees during dry periods and influences the rate of ecosystem transitions during climate change.

# TABLE OF CONTENTS

# LIST OF FIGURES

# LIST OF TABLES

# ACKNOWLEDGEMENTS

I would like to thank my advisor, Dr. Erkan Istanbulluoglu for his immense support, guidance, and mentorship. I thank him for this opportunity to pursue my research ambition. I would like to thank my committee members Dr. Faisal Hossain, Dr. Gregory Tucker, and Dr. Brittany Johnson for their invaluable guidance, support, and feedback.

I would like to thank my wife Divya for her love, patience, and support throughout this journey. I want to thank my parents Sarada and Shyam Sundar Sai, my sister Sravanthi and brother-in-law Deepak for their never-ending love and support. I want to thank Dr. Arun Natarajan for his love, mentorship, support, and advice.

I want to thank Dr. Steve Burges for all the enlightening conversations in Wilcox. I would also like to thank my Hydrology colleagues and officemates for all their support, guidance, and friendship, especially Ronda Strauch, Christina Bandaragoda, Omer Yetemen, Nicoleta Christea, Claire Beveridge, Amanda Manaster, Chris Frans, Jeff Keck, Susan Dickerson-Lange, Xiaodong Chen, Ryan Currier, Yifan Cheng, Shashank Bhusan, Kaiwen Wang, Gu Wenquen, Domenico Caracciolo, Jimmy Phuong, and Nishan Biswas.

I am very grateful to the Landlab team, especially Greg, Nicole, Dan, Eric, Jordan, Katy, Jenny, and Nathan for teaching me so much. I consider myself very fortunate to be a part of this team. I also want to thank CSDMS for connecting numerical modelers in the field earth surface dynamics. Their annual meetings are the best. I loved volunteering for Puget Sound Programming Python meetup. I am very thankful to Don Sheu, Alan Vezina, Quentin Caudron, Kurt Maurer, and Jacob Deppen for their friendship and support.

I want to thank my friends Ananth, Mahanth, Chaitanya, Apoorva, Dhairya, Uday, Shailesh, and Hardik for their support and encouragement.

I would like to prostrate to Shri Sai Baba for this life and beyond.

# DEDICATION

Dedicated to my father, Shyam Sundar Sai, my mother, Sarada, my wife, Divya, my brother-in-law, Deepak, and my sister, Sravanthi.

# Chapter 1. INTRODUCTION

## 1.1 MOTIVATION

Woody Plant Encroachment (WPE) is defined as an increase in density, cover, and biomass of native trees or shrubs in grasslands (e.g., Fig. 1-1, Fig. 1-2). WPE has been observed to be a major cause for dramatic changes in arid and semiarid grasslands and savannas of the world over the last 100 years (Naito and Cairns, 2011; Myers-Smith et al., 2011; D'Odorico et al., 2013; Ravi and D'Odorico, 2009; Stevens et al., 2017). WPE into grasslands has important eco-hydro-geomorphic implications (e.g. Huxman et al., 2005). It leads to loss of grass cover and increase in overall bare soil. This in turn results in intensification of fluvial and aeolian erosion of nutrient-rich top soil (Parsons et al., 1996; Schlesinger et al., 1999; Wainwright et al., 2000; Li et al., 2007; Li et al., 2008).

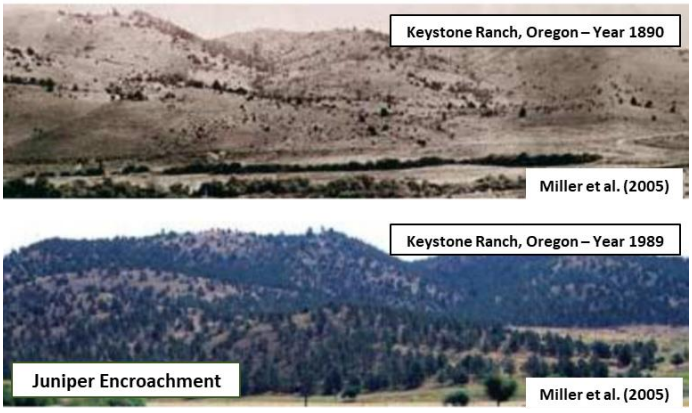


Figure 1-1: Illustration of WPE using repeat photography of Keystone Ranch, Oregon. Photographs provided by Stu Garret and Rick Miller (Miller et al., 2005).

Exogenic factors like increased CO2 concentrations (Polley, 1997), regional changes in disturbance patterns (e.g. change in fire frequency and grazing intensity due to new human settlement) (Van Auken, 2000; van de Koppel et al., 2002), and global changes in temperature or rainfall (Idso, 1992; Brown et al., 1997) can cause a shift in competitive advantage of one Plant Functional Type (PFT) over the other. Endogenic factors such as microclimate, interactions of fire dynamics with vegetation cover, erosion dynamics, and grazing due to small animals,

contribute to the shift in one ecosystem state to another, likely initiated by exogenic factors, through a series of self-sustained processes (Archer et al., 1995; D'Odorico et al., 2012).

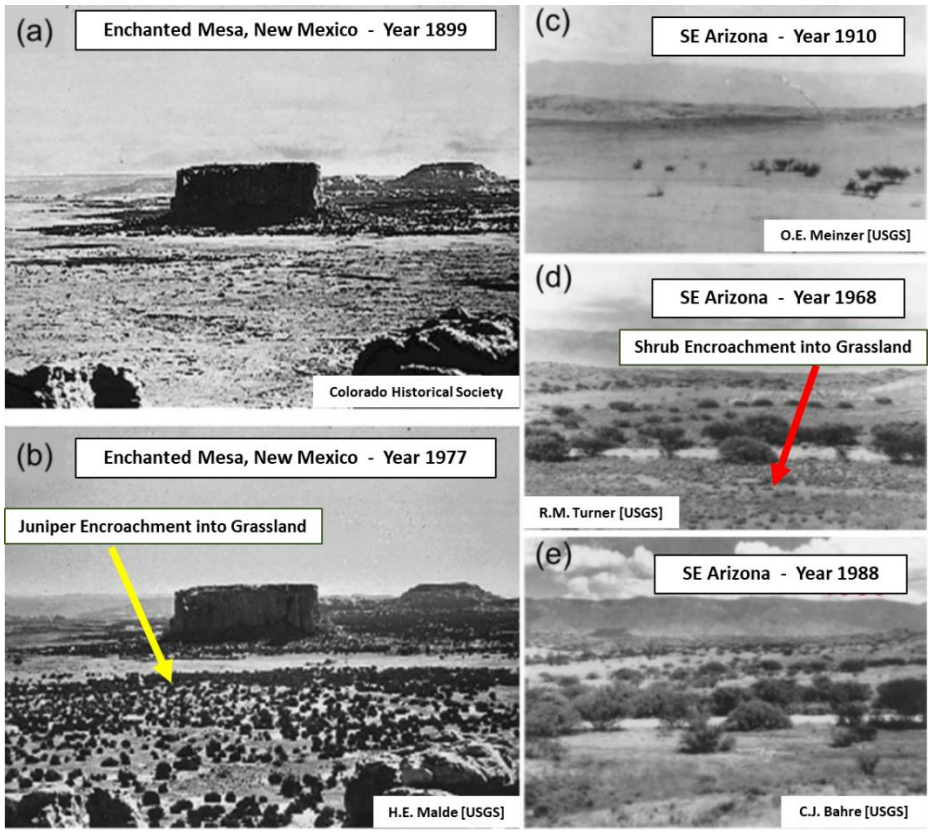


Figure 1-2: Illustration of WPE using repeat photography. (a, b) Jupiter Encroachment into grasslands. Photos of Enchanted Mesa, west of Albuquerque, New Mexico, USA taken from Acoma Pueblo in 1899 taken by W. H. Jackson, and 1977 taken by H. E. Malde. (c, d, & e) Shrub encroachment. Photos taken in 1910 by O. E. Meinzer (USGS), 1968 by R. M. Turner (USGS), and 1988 by C. J. Bahre (USGS).

Physically based numerical models have been used to predict the influence of climatic drivers on the water, energy, and carbon dynamics. The topographic controls on solar energy and water distribution influence the spatial patterns of vegetation (Ivanov et al., 2008; Fatichi et al., 2016). Growing applications of spatially explicit discrete cellular automaton (CA) and flow models provide computational flexibility for the integration of a range of concepts from reaction-advection-diffusion (RAD), kernel-based, and process-based terrestrial biosphere models. In CA models each cell is occupied by one plant functional type (PFT). Changes in PFTs are governed

by transition probabilities, obtained in relation to one or more of the following: field observations, hypothesized establishment, resource uptake and utilization processes (Lanzer and Pillar, 2002; Scanlon et al., 2007; Colasanti et al., 2007), modeled ecohydrologic variables such as plant water stress, grazing intensity, seed dispersal, and climate variability (van Wijk and Rodriguez-Iturbe, 2002; Fernandez-Illescas and Rodriguez-Iturbe, 2004; Zhou et al., 2013; Foti and Ramirez, 2013; King and Franz, 2016). CA models are suitable for studying ecotone shifts. Among the CA models, the Cellular Automaton Tree-Grass-Shrub Simulator (CATGraSS) provides a conceptual framework to couple basic functionality of a simplified TBM, which includes the dynamics of local daily water balance, plant life cycle processes, and a rule-based probabilistic CA component that simulates seed dispersal and plant establishment processes (Caracciolo et al., 2014, 2016, 2017; Zhou et al., 2013).

My dissertation focuses on developing ecohydrologic components and models using Landlab, a component-based software toolkit, that can be deployed to study the influence of WPE in transient semiarid ecosystems. In this research, I address the following questions:

- Can the key plant-to-plant and plant-environment interactions that drive the spatio-temporal ecosystem response be identified?
- Are there any thresholds and tipping points that lead to regional ecosystems shifts?
- Do anthropogenic factors cause rapid ecosystem shifts? If they do, can we reverse them through land management?

## 1.2 DISSERTATION STRUCTURE

My dissertation is organized into three main chapters, following this introduction chapter. Chapter 2 details the development of the Landlab modeling framework. In this chapter I discuss the goals of Landlab, the underlying design principles, its architecture, and building numerical models with Landlab. Chapter 3 discusses the development of various ecohydrologic components in Landlab, building models using these components, and applying them to investigate the ecosystem dynamics in semiarid landscapes of southwest United States. In chapter 4, I investigate the role of historical climate variability on ecosystem change since late Pleistocene in central New Mexico.

Paleoclimate reconstructions of precipitation and temperature time series presented by Hall and Penner (2013) are used to drive an ecohydrology model discussed in Chapter 3.

## REFERENCES


Archer, S., Schimel, D. S., & Holland, E. A. (1995). Mechanisms of shrubland expansion: land use, climate or CO2?. Climatic change, 29(1), 91-99.

Brown, J. H., Valone, T. J., & Curtin, C. G. (1997). Reorganization of an arid ecosystem in response to recent climate change. Proceedings of the National Academy of Sciences, 94(18), 9729-9733.

Caracciolo, D., Noto, L. V., Istanbulluoglu, E., Fatichi, S., & Zhou, X. (2014). Climate change and Ecotone boundaries: Insights from a cellular automata ecohydrology model in a Mediterranean catchment with topography controlled vegetation patterns. Advances in water resources, 73, 159-175.

Caracciolo, D., Istanbulluoglu, E., Noto, L. V., & Collins, S. L. (2016). Mechanisms of shrub encroachment into Northern Chihuahuan Desert grasslands and impacts of climate change investigated using a cellular automata model. Advances in water resources, 91, 46-62.

Caracciolo, D., Istanbulluoglu, E., & Noto, L. V. (2017). An ecohydrological cellular automata model investigation of juniper tree encroachment in a western North American landscape. Ecosystems, 20(6), 1104-1123.

D'odorico, P., Okin, G. S., & Bestelmeyer, B. T. (2012). A synthetic review of feedbacks and drivers of shrub encroachment in arid grasslands. Ecohydrology, 5(5), 520-530.

D'Odorico, P., Bhattachan, A., Davis, K. F., Ravi, S., & Runyan, C. W. (2013). Global desertification: drivers and feedbacks. Advances in water resources, 51, 326-344.

Fatichi, S., Pappas, C., & Ivanov, V. Y. (2016). Modeling plant–water interactions: an ecohydrological overview from the cell to the global scale. Wiley Interdisciplinary Reviews: Water, 3(3), 327-368.

Hall, S. A., & Penner, W. L. (2013). Stable carbon isotopes, C3–C4 vegetation, and 12,800 years of climate change in central New Mexico, USA. Palaeogeography, Palaeoclimatology, Palaeoecology, 369, 272-281.

Huxman, T. E., Wilcox, B. P., Breshears, D. D., Scott, R. L., Snyder, K. A., Small, E. E., ... & Jackson, R. B. (2005). Ecohydrological implications of woody plant encroachment. Ecology, 86(2), 308-319.

Idso, S. B. (1992). Shrubland expansion in the American Southwest. Climatic Change, 22(1), 85-86.

Ivanov, V. Y., Bras, R. L., & Vivoni, E. R. (2008). Vegetation-hydrology dynamics in complex terrain of semiarid areas: 1. A mechanistic approach to modeling dynamic feedbacks. Water Resources Research, 44(3).

Li, J., Okin, G. S., Alvarez, L., & Epstein, H. (2007). Quantitative effects of vegetation cover on wind erosion and soil nutrient loss in a desert grassland of southern New Mexico, USA. Biogeochemistry, 85(3), 317-332.

Li, J., Okin, G. S., Alvarez, L., & Epstein, H. (2008). Effects of wind erosion on the spatial heterogeneity of soil nutrients in two desert grassland communities. Biogeochemistry, 88(1), 73-88.

Miller, R. F., Bates, J. D., Svejcar, T. J., Pierson, F. B., & Eddleman, L. E. (2005). Biology, ecology, and management of western juniper. Tech. Bull, 152.

Myers-Smith, I. H., Forbes, B. C., Wilmking, M., Hallinger, M., Lantz, T., Blok, D., ... & Boudreau, S. (2011). Shrub expansion in tundra ecosystems: dynamics, impacts and research priorities. Environmental Research Letters, 6(4), 045509.

Naito, A. T., & Cairns, D. M. (2011). Patterns and processes of global shrub expansion. Progress in Physical Geography, 35(4), 423-442.

Nudurupati, S. S., Istanbulluoglu, E., Tucker, G. E, Gasparini, N. M., Hobley, D. E., Hutton, E. W., Barnhart, K, & Adams, J. M. On Transient semi-arid ecosystem dynamics using Landlab. (Submitted for Publication)

Parsons, A. J., Abrahams, A. D., & Wainwright, J. (1996). Responses of interrill runoff and erosion rates to vegetation change in southern Arizona. Geomorphology, 14(4), 311-317.

Polley, H. W. (1997). Implications of rising atmospheric carbon dioxide concentration for rangelands. Rangeland Ecology & Management/Journal of Range Management Archives, 50(6), 562-577.

Ravi, S., D'Odorico, P., & Okin, G. S. (2007). Hydrologic and aeolian controls on vegetation patterns in arid landscapes. Geophysical Research Letters, 34(24).

Ravi, S., & D'Odorico, P. (2009). Post-fire resource redistribution and fertility island dynamics in shrub encroached desert grasslands: a modeling approach. Landscape Ecology, 24(3), 325-335.

Schlesinger, W. H., Abrahams, A. D., Parsons, A. J., & Wainwright, J. (1999). Nutrient losses in runoff from grassland and shrubland habitats in Southern New Mexico: I. Rainfall simulation experiments. Biogeochemistry, 45(1), 21-34.

van de Koppel, J., Rietkerk, M., van Langevelde, F., Kumar, L., Klausmeier, C. A., Fryxell, J. M., ... & Stroosnijder, L. (2002). Spatial heterogeneity and irreversible vegetation change in semiarid grazing systems. The American Naturalist, 159(2), 209-218.

Van Auken, O. W. (2009). Causes and consequences of woody plant encroachment into western North American grasslands. Journal of environmental management, 90(10), 2931-2942.

Wainwright, J., Parsons, A. J., & Abrahams, A. D. (2000). Plot-scale studies of vegetation, overland flow and erosion interactions: case studies from Arizona and New Mexico. Hydrological Processes, 14(16-17), 2921-2943.

Zhou, X., Istanbulluoglu, E., & Vivoni, E. R. (2013). Modeling the ecohydrological role of aspect-controlled radiation on tree-grass-shrub coexistence in a semiarid climate. Water Resources Research, 49(5), 2872-2895.

# Chapter 2. DEVELOPMENT OF THE LANDLAB MODELING FRAMEWORK

This chapter summarizes the design and development of Landlab, an open source software. I am a member of the core development team and have participated in the design process, developed, and contributed code, documentation, and training material, and have coauthored multiple publications describing this framework such as Hobley et al., 2017. In this chapter, I have reproduced, with permission, Figures 2, 5, 12a, and 14 from Hobley et al., 2017, Figure 2 from Barnhart et al., 2020, and Figure 9 from Strauch et al., 2018 that are published in the following Open-Access journals (Creative Commons Attribution 4.0 License).

Hobley, D., Adams, J. M., Nudurupati, S. S., Hutton, E. W., Gasparini, N. M., Istanbulluoglu, E., & Tucker, G. E. (2017). Creative computing with Landlab: an open-source toolkit for building, coupling, and exploring two-dimensional numerical models of Earth-surface dynamics. Earth Surface Dynamics, 5, 21-46.

Barnhart, K. R., Hutton, E. W., Tucker, G. E., Gasparini, N. M., Istanbulluoglu, E., Hobley, D. E., Lyons, N. J., Mouchene, M., Nudurupati, S. S., Adams, J. M., & Bandaragoda, C. (2020). Landlab v2. 0: A software package for Earth surface dynamics. Earth Surface Dynamics, 8(2).

Strauch, R., Istanbulluoglu, E., Siddhartha Nudurupati, S., Bandaragoda, C., Gasparini, N. M., & Tucker, G. E. (2018). A hydroclimatological approach to predicting regional landslide probability using Landlab. Earth Surface Dynamics, 6 (1), 49–75.

## 2.1 INTRODUCTION

Numerical models are widely used to study processes that operate on and across the Earth's land surface, sub-surface, and oceans. Researchers use these models to develop insights into these systems by testing quantitative hypotheses. These models also serve as decision-support tools by forming a link between measurable small-scale processes and long-term implicit outcomes (Tucker et al., 2001). Examples of applications in Science and Engineering vary from short-term flood forecasting (e.g. Dutta et al., 2000; Horritt and Bates, 2002; Kulkarni et al., 2014), predicting regional landslide probability (Strauch et al., 2018), to simulating the evolution of Earth's landscape over geologic time scales (e.g. Tucker et al., 2001; Tucker and Hancock, 2010; Yetemen et al., 2015). These models may vary widely in temporal and spatial scales but often encapsulate similar elements of software, such as code used to represent the modeling domain and the data structure framework. The developers of these models typically create them from scratch, duplicating efforts recreating the building blocks. Some of the reasons for this loss of human hours may be that the potentially reusable software is (a) inaccessible; (b) not maintained; (c) hard to understand; or (d) lack of confidence in the codebase. In this chapter, I will discuss the development of the Landlab modeling framework that seeks to mitigate some of these redundancies (Hobley et al., 2017).

## 2.2 DESIGN PRINCIPLES

Advances in computational systems, data and information management, visualization environments, and software literacy is boosting scholarly productivity enabling breakthroughs and discoveries. These advances, however, are also increasing the technical qualifications required for numerical modeling (Bandaragoda et al., 2019). The implicit design structure of curriculum in schools and colleges across the world can at best train the students (would-be researchers) in generic programming. The development and adaptation of newer software tools often outpace the refinement of these curriculum. The sheer diversity of research software that is currently used further reduces the possibility to adequately train the students and researchers prior to their entry into numerical modeling. As a result, many of the numerical modelers are therefore "self-taught" software developers. To lower this bar of entry, the Landlab modeling framework was developed by (Hobley et al., 2017):

- Facilitating easy and rapid creation of grids that represent the model domain.
- Creating an accessible, flexible, and robust set of data structures to store and manipulate data across the grid.
- Enabling control of boundary conditions on the grid.
- Developing a suite of handy functions that help map data from one type of data structures to another or perform a quick calculation across a data structure.
- Creating and enabling creation of process representing numerical models encapsulated into modular and reusable components.
- Facilitating building enhanced models by coupling two or more components.
- Providing an interface for importing and exporting data. For example, reading Digital Elevation Models (DEMs) in ESRI ASCII formats, reading data in NetCDF format.
- Developing and enable developing utility functions, that may complement and supplement components, but do not represent any processes. For example, tracking all contributing upstream nodes, converting ESRI ArcGIS derived flow directions into *RasterModelGrid* node ids, etc…

Landlab is *open source*, and hence a community resource. It is licensed under MIT free software license. Its source code is maintained in a version-controlled Git repository. The master repository is hosted on the Github website "https://github.com/landlab/landlab". Landlab can be installed with either a precompiled version, i.e. release versions that are available through *pip* and *conda* Python package managers, or a developer version, i.e. by forking the Git repository.

The execution of a numerical model involves performing a series of mathematical calculations and is often computer-time intensive. To select the programming language for the development of Landlab, the early developer team weighed the tradeoffs between C++, a time-proven robust but relatively lower-level language, and Python, a higher-level language with a rising adaptability among the scientific community. Lower level languages are relatively efficient, in terms of computation time, but require more development time. Python was voted the preferred language for Landlab because of its relative ease of adaptability serving the Landlab's goal of community adaptation. Other advantages of Python include its open-source availability, cross operating system portability, rising number of scientific packages, ease of execution, and availability of modules

that provide an interface with code written in other programming languages, such as C, C++, and Fortran. Landlab v1.0 supports both Python 2 and Python 3. Support for Python 2 has been dropped from Landlab v2.0 onwards.

Landlab users can be broadly classified into three categories: (a) *user-developers*, e.g. core Landlab developers that use, modify, and contribute to the source code; (b) *users*, e.g. people that use but do not contribute code; and (c) *teachers-students*, e.g. students using Landlab in a classroom (Barnhart et al., 2020). To make Landlab sustainable for these users into the future, we adopted many of the key guidelines outlined by authors of white papers on academic design best practices (e.g., Adams et al., 2014; Katz et al., 2015; Stewart et al., 2010; Wilson et al., 2017). These include extensive integrated testing, documentation, continuous integration, lint checking, and releasing binaries. Landlab testing is achieved by automated unit testing of key code functionality, issue-tracking through Github, code-reviews, and doctesting. Documentation for Landlab is hosted at http://landlab.github.io. This includes manually edited summary documents and tutorials, and automatically generated documentation from docstrings in the code. To increase the adaptation of Landlab, we have been conducting classes and workshops at international conferences, giving webinars online, aiding adaptation of Landlab exercises in a classroom setting, and hosting researchers through exchange programs.

The community plays a vital role in sustaining Landlab. It contributes to Landlab by (a) testing the software first-hand and giving feedback via *Github issues*, and (b) by contributing new code to the repository. The development team adheres to a strict pipeline for modification of the contents of the *master* branch. The user, member of the core development team or otherwise, creates a *pull request* via Github that encompasses all the proposed code changes. A subset of the core development team reviews these changes and determines whether they adhere to the Landlab principles and standards, such as whether the new code includes unit tests and relevant documentation, and iterate with the user for refinement if required, or accept the *pull request* (Barnhart et al., 2020; Hobley et al., 2017).

## 2.3 LANDLAB ARCHITECTURE

The Landlab package is designed to be modular. This modularity is achieved by individualizing the elements of a numerical model. Each element connects with the rest of the model through standard interfaces. These three elements are (a) a gridding engine; (b) process representing components; and (c) utilities (Figure 2-1).

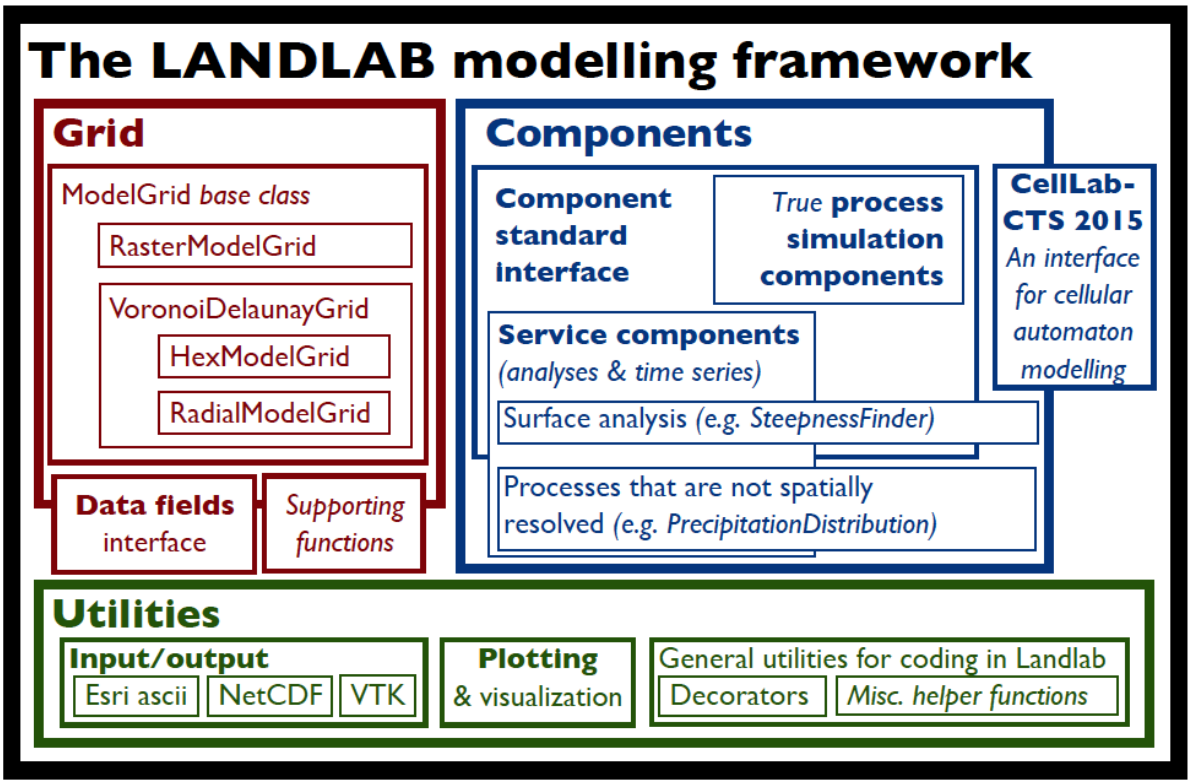


Figure 2-1: Schematic representation of the Landlab modeling framework (Hobley et al., 2017, reproduction of their Fig. 2).

### 2.3.1 *Gridding Engine*

The *grid* represents a modeling domain and comprises of two sets of interlocking and offset *grid elements* which are: points (*nodes* and *corners*), lines connecting these points (*links* and *faces*), and the polygons encompassing these points (*patches* and *cells*) (Figure 2-2). In Landlab, a *grid* can be generated with a single line of code that generates a Python *object*. This *object* encapsulates the data describing the geometry of the domain, data structures associated with the grid elements, and provides access to a set of *methods*, which can be accessed as *grid.method()*.

The user can generate a *grid* by just specifying the shape, or choose to provide the location of *nodes*, e.g. creating a *grid* by importing a Digital Elevation Model (DEM). Landlab supports both regular and irregular grids.

Data can be assigned to the element of choice, e.g. *cells*, as *data fields*, e.g. *grid.at_cell["soil_moisture__saturation_fraction"]*. These data fields are 1D *numpy* arrays with lengths equal to the total number of the corresponding *grid* elements. The geometric interrelationships between the various grid element types are implicitly provided through grid mappings and properties, e.g. *grid.cell_at_node*, *grid.cellarea*, *grid.cells_at_corners_of_grid*, etc.. Landlab follows a standard numbering scheme for all its elements where the IDs start with 0 at bottom left, and are ordered by y-coordinate first, and then by x-coordinate of the geometric centers (Figure 2-2c). Right-hand-rule, *anticlockwise* from positive *x-axis*, is followed for rotational ordering. Landlab v1.0 partially implemented *diagonals*, where *nodes* cross *corners*. Handling of these *diagonals* is improved and standardized from v2.0 onwards (Barnhart et al., 2020). Landlab *grid* also provides a set of handy computational methods, e.g. *grid.calc_flux_div_at_node* that can perform calculations on data stored across the grid elements. The *grid* object allows control of boundary conditions at each *grid* location. Each boundary condition type is associated with an integer value, e.g. integer value for *fixed value* at *node* is 1.

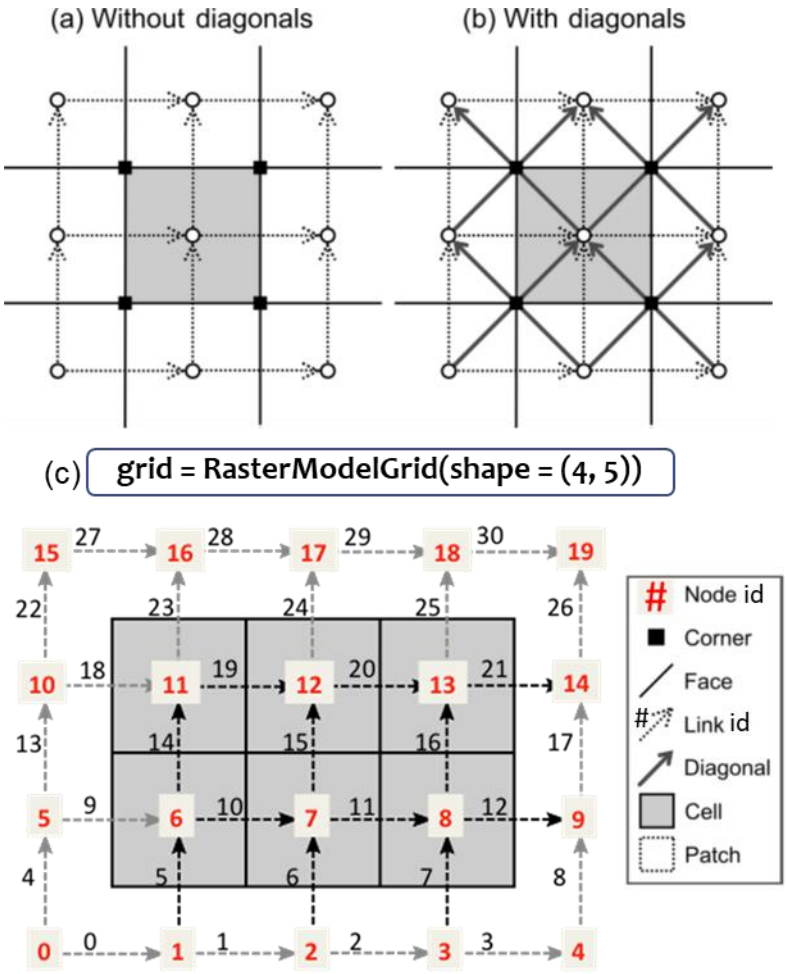


Figure 2-2: (a, b) Conceptual representation of *diagonals* of a *RasterModelGrid* (Barnhart et al., 2020, reproduction of their Fig. 2), (c) Illustration of *RasterModelGrid* elements and the numbering system (Hobley et al., 2017, reproduction modified from their Fig. 5)

### 2.3.2 *Components*

*Components* are numerical process representing, typically a single earth surface process, Python classes. These are designed to be coupled with other components in a "plug-and-play" style.
For example, *PotentialEvapotranspiration* component can calculate potential evapotranspiration on a *cellular grid* using the meteorological inputs. The outputs of this *component* can be ingested into *SoilMoisture* component that simulates the local soil moisture balance. These *components* follow a standard interface to provide interoperability between other Landlab modules or external interfaces such as Basic Model Interface (BMI) (Peckham et al., 2013). The standard interface comprises of the following:

(a) *initialization* method - *__init__(self, *args, **kwds)*. This method is a constructor, which means that this method will be executed automatically when the component is instantiated. A typical component requires an input of *grid* for instantiation. Other arguments and keywords include those parameters that are not expected to change during the timeline of the entire model run. The *args* are component specific and required to be defaulted to a certain value, i.e. If the user does not provide a value for these then these parameters assume the default value. *kwds* on the other hand allows these parameters to be optional and can be initialized from a file. From v2.0 onwards, passing parameters to the components as *kwds* is not allowed.

(b) *run* or *update* method – *run_one_step*(*self, *args, **kwds*). This method runs the process represented by this component for a time step. A time step is generally ingested as an input by this method. From v2.0 onwards, run_one_step() or equivalent methods are restricted to read only a time step or nothing. The input arguments need to be altered using *getter* and *setter* properties.

(c) *header properties.* Each component has a set of properties, *name, input_var_names, output_var_names, var_units, var_mapping, and var_definition*, that constitute the metadata for the data fields with which the component interacts with. From v2.0 onwards, this metadata is organized into a single Python dictionary.

### 2.3.3 *Utilities*

Landlab offers a suite of handy *utilities* that control input and output of data, data format translation, plotting, BMI model interfaces, etc... The main purpose of *utilities* is to include tools that are essential but do not represent any numerical model to be qualified as a component, e.g. create a *grid* by reading a DEM in ESRI ASCII format.

## 2.4 DOCUMENTATION, TESTING, AND VALIDATION

Landlab's code is quality controlled by using Python's native documentation and code testing systems that includes *unit tests* and *doctests*. *Unit tests* are separate testing scripts written by the developer supplementing their code. These scripts are designed to test specific portions of the code and to verify if they match the expected outcomes. *Doctests* are pieces of code that are included inline with the code as an integral part of docstrings and serve dual purpose, (a) as examples of

code usage; and (b) check the functioning of the code. Both *unit tests* and *doctests* are triggered automatically by continuous integration systems, Travis (for Linux and Mac OS) and Appveyor (for Windows), every time a pull request is created to alter the contents of the *master* branch. These integration systems perform these tests on multiple versions of Python and across OS platforms remotely making sure that Landlab is operable on various platforms. Docstrings are also scraped and are included in the online documentation (Hobley et al., 2017).

## 2.5 CREATING NUMERICAL MODELS WITH LANDLAB

A numerical model can be built using Landlab modules or a mix of both Landlab and external modules. Since Landlab can be installed as a Python package, it can be imported and can be treated like any other package in Python. Therefore, any compatible Python environment can host the Landlab modeling framework. In general, a Landlab model is nothing but a Python script, also referred as *driver*, that has a sequential set of commands. An example set of steps are (Figure 2-3):

- Import grid class, e.g. *RasterModelGrid*
- Import input data, e.g. read DEM
- Instantiate a *grid* that represents the modeling domain
- Set boundary conditions, e.g. Set boundary nodes to closed boundary
- Load data onto the *grid*, i.e. create data fields
- Import the desired *components* and *utilities*
- *Initialize* the components
- Call the *update* or *run_one_step* method
- Alternatively, include the calls to *update* in a temporal or spatial loop
- Collect output data, e.g. record temporal data in the loops into a *numpy ndarray*
- Use *utilities* to visualize or export the data, e.g. use *landlab.plot.imshow_grid*

In this section, a few examples of numerical models built with Landlab will be discussed.

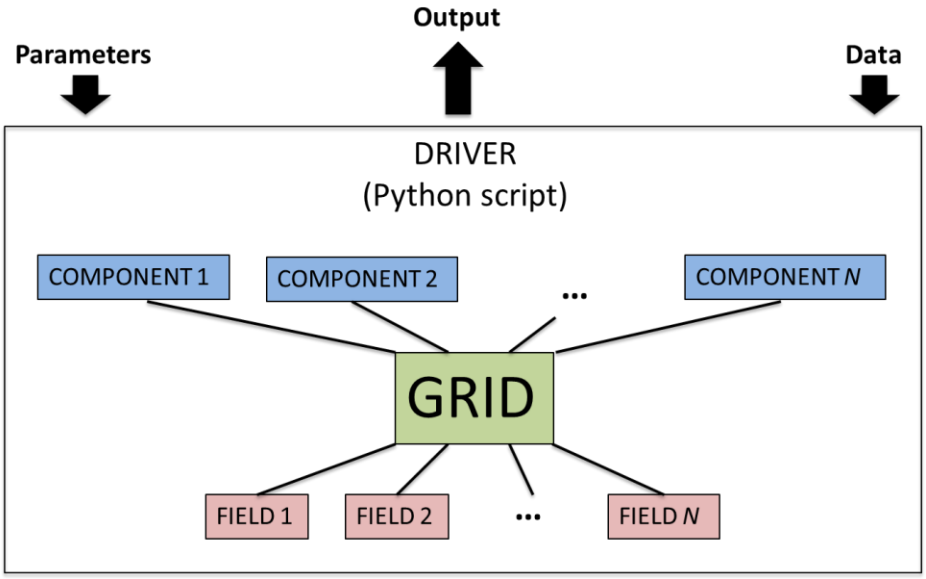


Figure 2-3: Illustration of the elements and their interfaces in a generic *driver* that represents a numerical model developed with Landlab

### 2.5.1 *Coupled Hillslope and Channel Evolution Model*

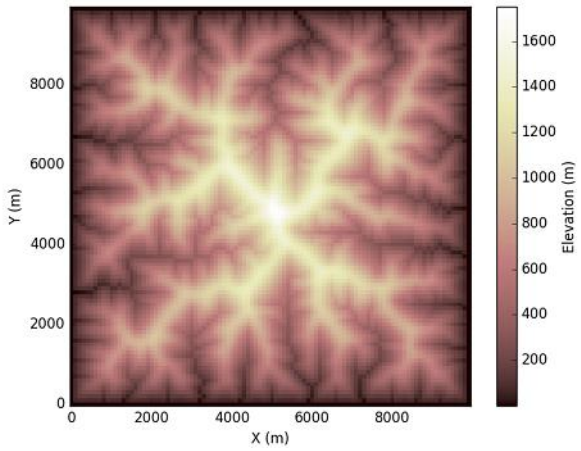


Figure 2-4: Modeled topography produced by implementing the coupled hillslope and channel evolution model on a *RasterModelGrid* (Hobley et al., 2017, reproduction of their Fig. 12a).

In this example, a coupled Landlab model that simulates landscape evolution, explicitly representing hillslope and channel incision processes, is illustrated. This coupled model is applied

to a flat surface represented by a *RasterModelGrid* with arbitrary roughness of an order $10^{-3}$ m. The area of the domain is 10 $km^2$. Stochastic storms generated using the *PrecipitationDistribution* component drive this model. *LinearDiffuser* simulates the hillslope diffusion. *FlowRouter* routes the water on the landscape and computes total channel discharge at each node. *StreamPowerEroder* simulates fluvial diffusion, by estimating channel incision using the channel bed slope and channel discharge, at each node. In this example, the model is run for 3 million years. The time step is determined by the duration between consecutive storms. During each interstorm period (dt), the landscape is uplifted with a fixed uplift rate (0.001 m $yr^{-1}$), *LinearDiffuser* is run (with linear diffusivity of 0.05 $m^2$ $yr^{-1}$), *FlowRouter* routes the water, *StreamPowerEroder* simulates fluvial erosion (m = 0.5, K = $10^{-5}$ $m^{-0.5}yr^{-0.5}$, C = $10^{-5}$ m $yr^{-1}$). The resultant topography at the end of the simulation period is shown in Figure 2-4 (see Sect. 5.2, Fig. 12, and code S4 of Hobley et al., 2017).

### 2.5.2 *Predicting Regional Landslide Probability*

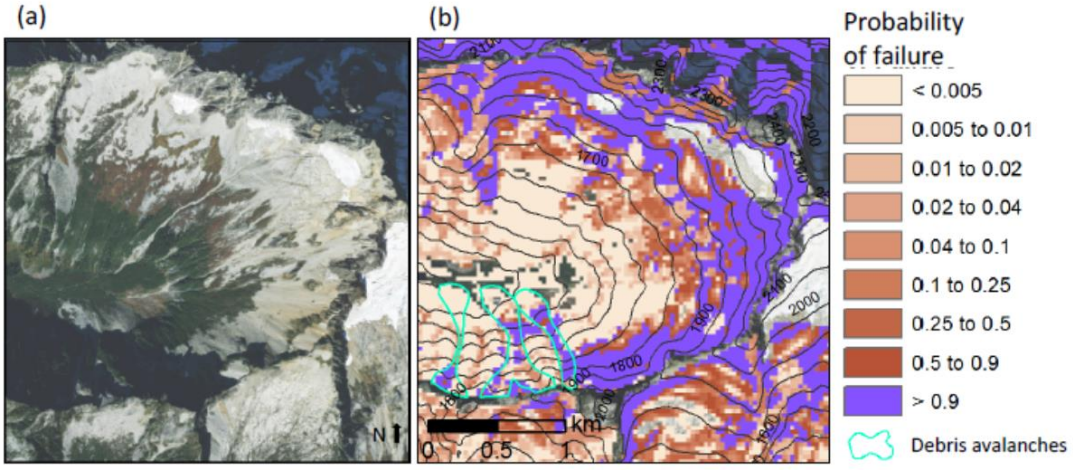


Figure 2-5: Performance of regional landslide model developed in Landlab in NOCA. (a) Image of a steep mountain in NOCA [World Imager, Esri Inc. Copyright Esri©]; (b) Simulated probability of failure on this steep landscape (Strauch et al., 2018, reproduction of their Fig. 9).

In this section, a regional landslide model presented by Strauch et al., 2018 is discussed. This work serves as an example of novel Landlab *component* development by one of the early *user-developers* outside the core development team. This work involved development of *LandslideProbability component* and inception of the same into the Landlab's library of

*components*. This *component* is initialized with a *RasterModelGrid*, desired number of Monte Carlo iterations, a choice of recharge distribution, and other recharge parameters. *calculate_landslide_probability()* is the process representing method (equivalent to *run_one_step()).* A Landlab *utility*, *source_tracking_algorithm*, was also developed. This utility was used to resample data from one grid resolution to another, and route local recharge in the downstream direction. This model predicts landslide hazard based on the hydroclimatological inputs. Figure 2-5 illustrates the model predictions of annual probability of failure of shallow landslides in North Cascades National Park in Washington (NOCA), USA.

### 2.5.3 *Modeling Ecosystem Dynamics with Landlab*

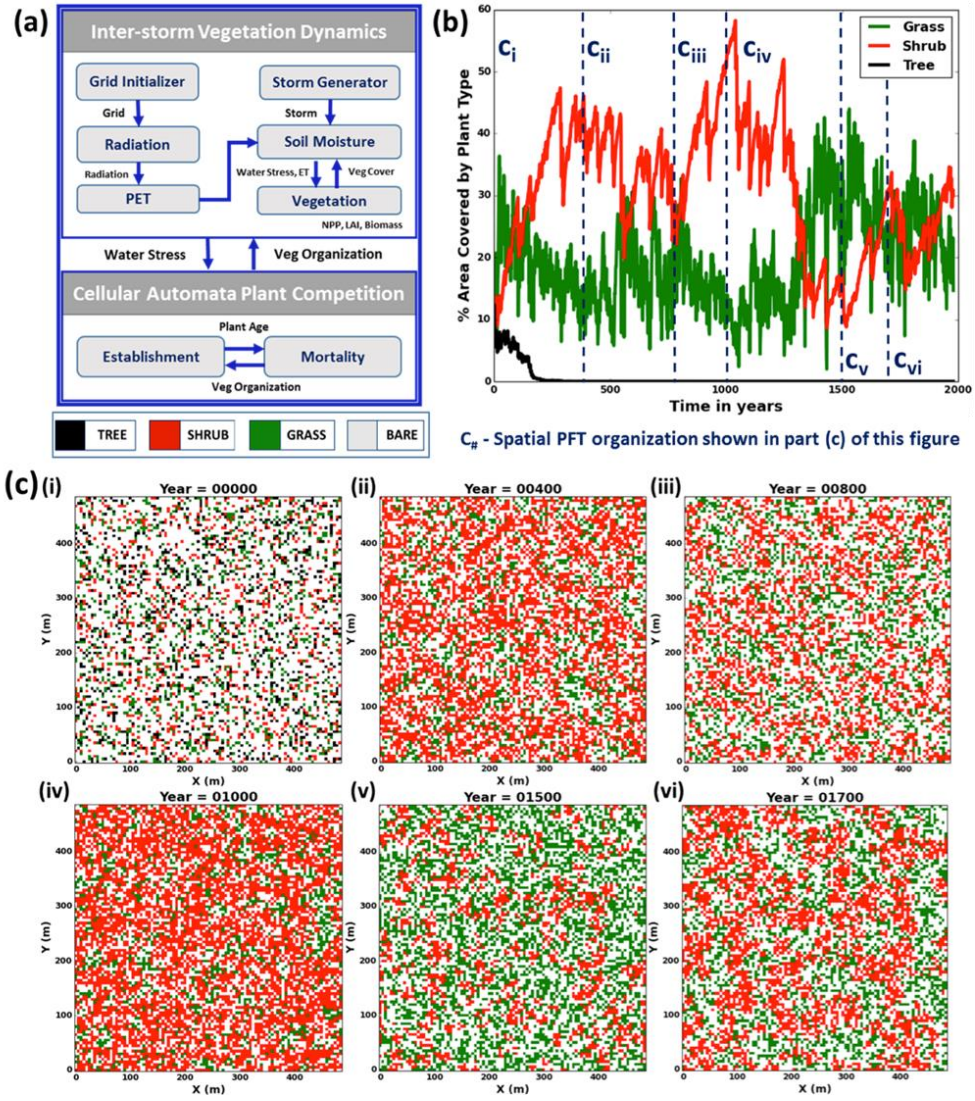


Figure 2-6: Demonstration of Ecosystem Dynamics model implementation on *RasterModelGrid* driven by present day's semi-arid climate at a headwater basin in Sevilleta LTER, central New Mexico, USA. (a) Schematic illustration of the model constituents. (b) Model results depicting the abundance of each PFT with respect to time. (c) Spatial maps of PFT occupancy at time steps marked in (b). The ecosystem shifts between grass-dominant to shrub-dominant ecosystems. (Hobley et al., 2017, reproduction of their Fig. 14).

Landlab houses a suite of ecohydrologic *components*. Development of these *components* and ecohydrologic modeling forms the basis for this dissertation and will be discussed in detail in

subsequent chapters. In this section, an implementation of Cellular Automata Tree-Grass-Shrub Simulator (CATGraSS), a coupled ecohydrologic model described by Zhou et al., 2013, is discussed to demonstrate the development of complex models using discrete *components*. This model was developed by coupling the following *components* (Figure 2-6a): *PrecipitationDistribution*, *Radiation*, *PotentialEvapotranspiration*, *SoilMoisture*, *Vegetation*, and *VegCA* (similar to Model A discussed in detail in Chapter 3). Each of these processes can be run independently outside the context of this model. In this example, the model is driven by stochastic rainfall pulses and solar insolation generated by PrecipitationDistribution and *Radiation components* consecutively to simulate ecosystem dynamics on a flat domain represented by a *RasterModelGrid*. Each cell in the domain can be occupied by one of the following Plant Functional Types (PFT); Grass, Shrub, Tree, Shrub Seedling, or Tree Seedling, or left bare. *PotentialEvapotranspiration* calculates the unstressed evapotranspiration rate using outputs of the Radiation. The *SoilMoisture* model determines the local PFT occupancy and models local root-zone soil moisture dynamics accordingly. The local soil moisture dynamics drives the simulation of above-ground Net Primary Productivity (NPP) of biomass by the *Vegetation*. The spatial interactions among the plants in the neighborhood is simulated by *VegCA*, through a set of rules for plant establishment and mortality, representing the competition between the plant species. These rules are based on a combination of probabilistic and deterministic rules (Caracciolo et al., 2014, 2016, 2017; Nudurupati et al., 2020; Zhou et al., 2013).

## 2.6 LANDLAB ON HYDROSHARE

To serve Landlab's mission to increase adaptability, the development team has consistently conducted a series of workshops. During the earlier workshops, we encountered issues with giving a hands-on experience to the attendees of these workshops. One of the main bottle necks at that time was the adopted installation method. We solved most, but not all, of these issues by releasing binaries and making them available through conda and pip. The pre-requirement for a Python environment installation remained. The advancements in cyberinfrastructure has led to the emergence of avenues, such as Hydroshare (http://www.hydroshare.org), to address these bottlenecks. Hydroshare is an online collaborative infrastructure that support data and model sharing in the form of resources. It provides a mechanism to move this data to the CUAHSI JupyterHub service seamlessly. The CUAHSI JupyterHub provides a pre-configured computing

environment that is launched on a web browser, and now hosts Landlab (Bandaragoda et al., 2019). Landlab on Hydroshare is therefore accessible to anyone through a web browser.

## 2.7 SUMMARY

Landlab is an open-source software toolkit written in Python programming language hosted on Github. The modular structure of Landlab makes it flexible and allows development of numerical models for diverse applications. The design principles and the model architecture of Landlab are discussed. The Landlab is designed to be sustainable and adheres to many best practices outlined for academic software development. Three examples of model building and application using Landlab are discussed. Landlab is hosted on Hydroshare and can be accessed through a web browser. In Chapters 3 and 4, I will discuss development of various ecohydrologic components and models with Landlab and their application towards semi-arid ecosystem dynamics research.

## REFERENCES


Adams, J. M., Nudurupati, S. S., Gasparini, N. M., Hobley, D., Hutton, E., Tucker, G. E., & Istanbulluoglu, E. (2014, November). Landlab: Sustainable software development in practice. In The Second Workshop on Sustainable Software for Science: Practice and Experiences (WSSSPE2), New Orleans, LA, USA (Vol. 16).

Adams, J. M., Gasparini, N. M., Hobley, D. E., Tucker, G. E., Hutton, E. W., Nudurupati, S. S., & Istanbulluoglu, E. (2017). The Landlab v1. 0 OverlandFlow component: a Python tool for computing shallow-water flow across watersheds. Geoscientific Model Development, 10(4), 1645-1663.

Bandaragoda, C., Castronova, A., Istanbulluoglu, E., Strauch, R., Nudurupati, S. S., Phuong, J., ... & Hobley, D. E. J. (2019). Enabling collaborative numerical Modeling in Earth sciences using Knowledge Infrastructure. Environmental Modelling & Software, 120, 104424.

Barnhart, K. R., Hutton, E. W., Tucker, G. E., Gasparini, N. M., Istanbulluoglu, E., Hobley, D. E., ... & Bandaragoda, C. (2020). Landlab v2. 0: A software package for Earth surface dynamics. Earth Surface Dynamics, 8(2).

Caracciolo, D., Noto, L. V., Istanbulluoglu, E., Fatichi, S., & Zhou, X. (2014). Climate change and Ecotone boundaries: Insights from a cellular automata ecohydrology model in a Mediterranean catchment with topography controlled vegetation patterns. Advances in water resources, 73, 159-175.

Caracciolo, D., Istanbulluoglu, E., Noto, L. V., & Collins, S. L. (2016). Mechanisms of shrub encroachment into Northern Chihuahuan Desert grasslands and impacts of climate change investigated using a cellular automata model. Advances in water resources, 91, 46-62.

Caracciolo, D., Istanbulluoglu, E., & Noto, L. V. (2017). An ecohydrological cellular automata model investigation of juniper tree encroachment in a western North American landscape. Ecosystems, 20(6), 1104-1123.

Dutta, D., Herath, S., & Musiake, K. (2000). Flood inundation simulation in a river basin using a physically based distributed hydrologic model. Hydrological Processes, 14(3), 497-519.

Hobley, D., Adams, J. M., Nudurupati, S. S., Hutton, E. W., Gasparini, N. M., Istanbulluoglu, E., & Tucker, G. E. (2017). Creative computing with Landlab: an open-source toolkit for building,

coupling, and exploring two-dimensional numerical models of Earth-surface dynamics. Earth Surface Dynamics, 5, 21-46.

Horritt, M. S., & Bates, P. D. (2002). Evaluation of 1D and 2D numerical models for predicting river flood inundation. Journal of hydrology, 268(1-4), 87-99.

Katz, D. S., Choi, S. C. T., Wilkins-Diehr, N., Hong, N. C., Venters, C. C., Howison, J., ... & de Val-Borro, M. (2015). Report on the second workshop on sustainable software for science: Practice and experiences (WSSSPE2). arXiv preprint arXiv:1507.01715.

Kulkarni, A. T., Mohanty, J., Eldho, T. I., Rao, E. P., & Mohan, B. K. (2014). A web GIS based integrated flood assessment modeling tool for coastal urban watersheds. Computers & Geosciences, 64, 7-14.

Nudurupati, S. S., Istanbulluoglu, E., Tucker, G. E, Gasparini, N. M., Hobley, D. E., Hutton, E. W., Barnhart, K, & Adams, J. M. On Transient semi-arid ecosystem dynamics using Landlab. (Submitted for Publication)

Peckham, S. D., Hutton, E. W., & Norris, B. (2013). A component-based approach to integrated modeling in the geosciences: The design of CSDMS. Computers & Geosciences, 53, 3-12.

Strauch, R., Istanbulluoglu, E., Nudurupati, S. S., Bandaragoda, C., Gasparini, N. M., & Tucker, G. E. (2018). A hydroclimatological approach to predicting regional landslide probability using Landlab.

Stewart, C. A., Almes, G. T., & Wheeler, B. C. (2010). Cyberinfrastructure Software Sustainability and Reusability: Report from an NSF-funded workshop.

Tucker, G. E., & Hancock, G. R. (2010). Modelling landscape evolution. Earth Surface Processes and Landforms, 35(1), 28-50.

Tucker, G. E., Hobley, D. E., Hutton, E., Gasparini, N. M., Istanbulluoglu, E., Adams, J. M., & Nudurupati, S. S. (2016). CellLab-CTS 2015: continuous-time stochastic cellular automaton modeling using Landlab. Geoscientific Model Development, 9(2), 823.

Tucker, G. E., Lancaster, S. T., Gasparini, N. M., and Bras, R. L.: The Channel-Hillslope Integrated Landscape Development Model (CHILD), in: Landscape Erosion and Evolution Modeling, Springer US, Boston, MA, USA, 349–388, 2001.

Wilson, G., Bryan, J., Cranston, K., Kitzes, J., Nederbragt, L., & Teal, T. K. (2017). Good enough practices in scientific computing. PLoS computational biology, 13(6).

Yetemen, O., Istanbulluoglu, E., Flores-Cervantes, J. H., Vivoni, E. R., & Bras, R. L. (2015). Ecohydrologic role of solar radiation on landscape evolution. Water Resources Research, 51(2), 1127-1157.

Zhou, X., Istanbulluoglu, E., & Vivoni, E. R. (2013). Modeling the ecohydrological role of aspect-controlled radiation on tree-grass-shrub coexistence in a semiarid climate. Water Resources Research, 49(5), 2872-2895.

# Chapter 3. ON TRANSIENT SEMI-ARID ECOSYSTEM DYNAMICS USING LANDLAB

Note: At the time of this writing, this chapter has been submitted for publication and is under review.

Nudurupati, S. S., Istanbulluoglu, E., Tucker, G. E, Gasparini, N. M., Hobley, D. E., Hutton, E. W., Barnhart, K, & Adams, J. M. On Transient semi-arid ecosystem dynamics using Landlab. (Submitted for Publication)

## ABSTRACT

Transition of grasslands and savannas to woodlands have been observed globally for more than a century. We present ecohydrology components of the Landlab modelling toolkit (Hobley et al., 2017) that can be used to design simulation experiments to test hypotheses on ecosystem transition. We illustrate examples that couple components for local soil moisture and plant dynamics with spatially explicit cellular automaton (CA)-based plant establishment, mortality, fire and grazing processes. Several key features of arid and semiarid ecosystems are discussed. Coexistence of tree-grass cover on north facing slopes (NFS) and shrub cover on south facing slopes (SFS) in central New Mexico is attributed to the competitive advantage of trees due to their longer seed dispersal range against shrubs in cooler and moist NFS. Incorporating a rule to represent inhibitory effects of shrubs on grasses enhance modeled shrub cover, while both trees and grasses are favoured when runon is included in the local soil moisture model. Feedbacks among livestock grazing, grassland fire frequency and size, resource redistribution on woody plant encroachment are investigated using different ecohydrologic model configurations. These feedbacks have led to a three-phase woody plant expansion processes in the model, with rates of encroachment controlled by the state transition probabilities of vegetation types in relation to plant susceptibility to fires, grazing, and age-related mortality. A critical area of woody plant emerges in the model with which a negative feedback between fire size and woody plant expansion begins, providing a spatially-explict modelling evidence to the alternative stable states hypothesis.

## 3.1 INTRODUCTION

Climate and its spatial manifestation on topography act as a critical driver for the distribution of natural ecosystems on the landscape (e.g., Grimm et al., 2013). Widespread ecosystem reorganizations evident in paleoecological records have been attributed to climate fluctuations over a range of temporal and spatial scales (Fritz, 2013; Hall and Penner, 2013; Machadoa and Froehnerb, 2016). Superimposed on the natural variability of climate, anthropogenic climate change, land degradation, herbivore grazing, changing regimes of wildfires, disease and insect outbreaks push ecosystems of the Anthropocene beyond their natural limits, triggering changes in ecosystem productivity, type and structure (Miller and Rose, 1999; Van Aueken, 2009; Grimm et al., 2013), with complex feedbacks in watershed hydrologic and geomorphic processes (Waters and Haynes, 2001; Istanbulluoglu and Bras, 2005; Pelletier et al., 2016) and biogeochemical cycles (Finzi et al., 2011; Puttock et al., 2014). In this paper we focus on modeling transient ecosystem processes in arid to semiarid ecosystems.

On a broad scale climate controls the distribution of biomes (Woodward et al., 2011) and sets an upper limit for woody plant canopy cover (Sankaran et al., 2005; Stevens et al., 2017). Since the Last Glacial Maximum, wetter and cooler climate in most arid semiarid regions has generally transitioned to drier and warmer conditions, establishing their characteristic (i.e., today's native) ecosystems and fire regimes 3,000 - 5,000 years B.P. (Whitlock et al., 2003; Grosjean et al., 2007). For example, transition from a green Sahara with tropical tree-grass savanna (~ 250 mm/y rainfall) to a hyper-arid desert (< 50 mm/y rainfall) took place over a few thousand years that began roughly 4,300 years BP (Kröpelin et al. 2008). Similarly, in the southwest United States (US), conifer forests at high elevations were replaced by woodlands, and desert shrub and grass vegetation established in the low elevations nearly 4,000 years BP (Holmgren et al., 2007; Hall and Penner, 2013). However, climate alone is not sufficient in explaining ecotone shifts, local vegetation patterns, global increase in woody plant cover and the large degree of variability in woody plant density under similar climates, which often require local environmental factors, disturbances and feedbacks (Archer et al., 2017).

Increase in the density of native woody plants (shrubs and trees) has been reported within the last 100 years or more in semiarid grasslands and savannas and high-latitude alpine tundra ecosystems of the Arctic (Naito and Cairns, 2011; Myers-Smith et al., 2011; D'Odorico et al., 2013; Stevens et al., 2017). Notable examples in the US include encroachment of western Juniper (*Juniperus Occidentalis, var. occidentalis*) and Sierra Juniper (*J. occidentalis* var. *australis*) trees into shrub-steppe communities in the western US (e.g., Miller et al., 2005); spreading of *Juniperus* trees from high- into low-elevation grasslands of the Chihuahuan and Sonoran Deserts; encroachment of *Prospocis* (mesquite) tree species and *Larrea tridentata* (creosotebush) shrubs in the Southwest US; and Eastern redcedar (*Juniperus virginiana*) and Rocky Mountain juniper (*Juniperus scopulorum*) in the great plains (Van Auken, 2009; Symstad and Leis, 2017). In the central great plains less than half a century was sufficient to convert some grasslands to full (up to 95%) woodland coverage (e.g., Briggs et al., 2002, 2005; Knapp et al., 2008), but in most other cases WPE that started in mid to late 1800s continued throughout most of the 1900s (Van Auken, 2009).

WPE follows several phases. In the initiation phase pioneering new woody plants gradually establish in grasslands, in response to changes in one or more exogenous drivers such as trends in precipitation, temperature and atmospheric $CO_2$, grazing of domestic herbivores and suppression of grassland fires (Brown et al., 1997; Van Auken, 2009; D'Odorico et al., 2018). This phase is followed by rapid expansion and canopy closure phases. Observational studies increasingly associate the rapid expansion of WPE to multiple endogenous feedback mechanisms that require vegetation cover interacting with another variable such as fire frequency and size, water and wind erosion, soil moisture and surface energy balance (see reviews by Bond, 2008; D'Odorico et al., 2012; Grimm et al., 2013; Archer et al., 2017). For example, historical heavy livestock grazing in the Chihuahuan Desert had reduced ground cover, which accelerated wind erosion in the upwind bare soil areas and deposition in downwind areas, causing grass mortality. By trapping nutrient-rich eolian sediments, established shrubs formed "islands of fertility" around them, enabling the development of highly resistant shrub communities to external disturbances (Charley and West , 1975; Schlesinger et al., 1990; Okin and Gillette, 2001; and Ravi and D'Odorico, 2009). Another endogenous feedback mechanism in grasslands is the fine fuel-fire feedback. Frequent grassland fires, often initiated by lightning, is considered the main factor limiting woody plant cover. Fires interact with grazing as both modify the grass cover. Intense grazing reduces fine fuel density of

grasslands, impairing fine fuel-fire feedback, causing less-frequent and smaller fires. Loss of fires enables established woody plant seedlings to mature, eventually causing ecosystem transition to woodland (Anderies et al., 2002; Ravi and D'Odorico, 2009; Wilcox et al., 2018).

Physically-based ecohydrology models are developed to predict the influence of climatic drivers and atmospheric $CO_2$ on terrestrial water, energy and carbon (biomass) dynamics; spatial patterns of vegetation only emerge out of topographic controls on solar energy and water distribution (Ivanov et al., 2008; Fatichi et al., 2017). Spatial processes for plant establishment, competition, mortality, and disturbances (fires and grazing), critical to simulate transient ecosystems, are only beginning to be incorporated in stochastic rule-based cellular automaton (CA) models (e.g., Van Wijk and Rodriguez-Iturbe, 2003; Zhou et al., 2013).

Three major questions should be addressed to advance the modeling of transient semiarid ecosystems:

1) What are the key plant-to-plant and plant-environment interactions and feedbacks that control ecosystem response in space and time?
2) Are there any thresholds and tipping points that lead to regional ecosystem shifts?
3) What are the key anthropogenic drivers that cause rapid changes in ecosystems, and can we reverse undesired ecosystem shifts by land management?

In this paper we introduce ecohydrologic modeling tools in Landlab, a component-based earth surface modeling toolkit coded in Python (Hobley et al., 2017), and develop illustrative examples of WPE in arid to semiarid climates that address the questions posed above. Simple algorithms are discussed as initial steps for developing plant-to-plant and plant-environment feedback mechanisms.

## 3.2 Background and Motivation: Vegetation models

Vegetation models can be broadly viewed in three classes: macro-scale Terrestrial Biosphere Models (TBMs), watershed ecohydrology models, and vegetation pattern (self-organization) models. Since the 1970s, empirical and process-based formulations have been developed that

attempt to explain local plant life processes (physiology, phenology, carbon allocation, and senescence) coupled with vertical water and energy balance, from the level of a cell within the interior of a leaf, to individual plants and plant communities in a region. Many TBMs (includes >20 different model types) have been developed using a collection of these process representations at the macro-scale (from 10 km to 10s of km grid sizes) (Fisher et al., 2014). TBMs are now effectively used within Earth System Models (ESM) at the global scale (Quillet et al., 2010; Wenzel et al., 2014). TBMs rely on two key assumptions: 1) process formulations are scale-independent; 2) topography is flat with no laterally connectivity; 3) fluxes and state variables predicted in a macro-scale model represent cell-average conditions defined at the center of a flat surface. To add heterogeneity in species representation at the plot-scale, a special case of TBMs, called forest gap models have been developed. Forest gap models statistically simulate the birth, growth and death of individual trees (see review by Shugart et al., 2018). Because of their macro-scale applications TBMs do not explicitly account for topography. Implicit representation of aspect and slope variability is only beginning to be introduced in forest gap models (e.g., Foster et al., 2017).

Ecohydrology models have adopted formulations used in TBMs but focused on the two-way interactions between hydrologic fluxes, moisture storages, and plant function over time scales relevant for both hydrologic and ecosystem predictions (see review by Fatichi et al., 2017). Ecohydrology models have advanced from point models which focus on analytical solutions for water balance, plant water stress and plant productivity driven by statistically represented rainfall variability (Eagleson, 2002; Rodriguez-Iturbe and Porporato, 2004) to transient point models that can simulate time series of above and below ground biomass (Montaldo et al., 2005; Kirschbaum et al., 2007). Transient point models have later morphed into distributed watershed ecohydrolgy models that explicitly account for topography on solar radiation and lateral exchange of soil water (Tague and Band, 2004; Ivanov et al., 2008; Fatichi et al., 2012).

Recent advances in ecohydrology and TBMs include paramaterizations for plant hydraulics and stomatal controls on transpiration and carbon assimilation (Loranty et al., 2010; Bonan et al., 2014; Mackay et al., 2015), representation of spatial and temporal dynamics of roots (Wu et al., 2007; Fatichi et al., 2012; Dunbabin et al., 2013; Javaux et al., 2013), canopy structure (Bohrer et al.,

2005; Nikinmaa et al, 2014), and microbial processes for decomposition and soil carbon dynamics (Wider et al., 2013; Li et al., 2014). These advances continuously improve skills for predicting the direct impacts of climate on carbon balance, however topographic controls on lateral redistribution of soil moisture and solar radiation have been the only mechanisms that lead to spatial patterns in biomass predictions (e.g. Ivanov et al., 2008; Fatichi et al., 2016).

Development of regular vegetation patterns, such as fairy rings, labyrinth, tiger bush, and stripes have been investigated with two general types of models and their hybrid. (1) dynamical system models that use reaction-advection-diffusion (RAD) equations to represent cell-by-cell plant interactions. These models demonstrate pattern formation through local interactions driven by gradients (Turing, 1952; Crampin and Maini, 2001; Berenstein, 2012); (2) Kernel-based models that employ kernel functions for characterizing non-local interactions in which growth of plant biomass is a function of multiplicative short-range cooperative interactions (community benefits to individuals), and long-range inhibitory interactions for plant competition, such as growing lateral roots for resource competition (Rietkerk and van de Koppel, 2008; Lefever and Lejeune, 1997; D'Odorico et al., 2006), as well as allelopathic autotoxic compounds released by decaying plant litter (Zhou et al., 2013; Vincenot et al., 2017); (3) Hybrid models in which the plant biomass term in the coupled RAD formulations is amplified by a non-local seed dispersion kernel (Thompson et al., 2008; Vincenot et al., 2016).

By coupling differential equations for water flow, diffusion of seeds, and plant growth, studies using RAD models commonly found that faster infiltration in vegetated patches and runoff contribution into vegetated patches from bare ground were sufficient to form patterns; while positive feedbacks due to plant facilitation among neighbors, plant-mediated changes in soil properties and nutrients have secondary effects (Klausmeier, 1999; HilleRisLambers et al., 2001; Rieterk et al., 2002; Foti and Ramirez, 2013). The roles of geomorphic processes and microtopographic feedbacks have been recognized by incorporating advective and diffusive processes of sediment transport in vegetation pattern models. The switch from banded to striped vegetation patterns, and their associated micro-topographic patterns, has been related to the relative strength of diffusive and fluvial sediment transport rates (Saco et al., 2007; Saco et al., 2015). RAD and kernel-based vegetation models provide conceptual frameworks for investigating

conditions for pattern formation and properties, shifts between patterns, and pattern migration (Sherratt, 2005; Siteaur et al., 2014; Escaff et al., 2015). However, these models use relatively simplistic and conjectural process representations, do not differentiate individual storms and seasonal behavior of ecosystems for plant growth, water balance, and surface runoff. Thus, they are difficult to confirm in field studies, and could only provide limited opportunities for studying environmental change (Siteaur et al., 2014).

Growing applications of spatially-explicit discrete cellular automaton (CA) and flow models provide computational flexibility for the integration of a range of concepts from RAD, kernel-based, and process-based terrestrial biosphere models. In CA models each cell is occupied by one plant functional type (PFT). Changes in PFTs are governed by transition probabilities, obtained in relation to one or more of the following: field observations, hypothesized establishment, resource uptake and utilization processes (Lanzer and Pillar, 2002; Scanlon et al., 2007; Colasanti et al., 2007), modeled ecohydrologic variables such as plant water stress, grazing intensity, seed dispersal, and climate variability (van Wijk and Rodriguez-Iturbe, 2002; Fernandez-Illescas and Rodriguez-Iturbe, 2004; Zhou et al., 2013; Foti and Ramirez, 2013; King and Franz, 2016). CA models are suitable for studying ecotone shifts. A key aspect to improve the skill of CA models to study global change is to relate transition probabilities to the well-being of a PFT occupying a particular cell. Among the CA models, the Cellular Automaton Tree-Grass-Shrub Simulator (CATGraSS) provides a conceptual framework to couple basic functionality of a simplified TBM, which includes the dynamics of local daily water balance, plant life cycle processes, and a rule-based probabilistic CA component that simulates seed dispersal and plant establishment processes (Zhuo et al., 2013; Caracciolo et al., 2014, 2016, 2017).

## 3.3 LANDLAB ECOHYDROLOGY:

Landlab is an open-source programming library and a modeling framework written in Python, developed for modeling coupled earth surface processes (e.g., Hobley et al., 2017). Landlab provides a 2D gridding engine to create structured and unstructured grids; data structures for storing and managing data on the grid during a simulation; a library of pre-developed components that implement a variety of Earth surface processes; mappers allowing data transfer from one data structure to another; tools for importing and exporting commonly used ESRI ASCII and netCDF formats; and basic tools for visualization of Landlab grids and data structures. Landlab's modular architecture allows the user to build multi-process models by coupling two or more *components* in a "plug-and-play" style.

Table 1: Description of existing ecohydrology components in Landlab

| **Component brief** | **What data it returns** (*fields* of) | **What data it needs (**fields of) |
|---|---|---|
| *Radiation*(): daily calculation of solar radiation for a given latitude, day of year, slope, aspect. | radiation__incoming_shortwave_flux [W/m$^2$],<br>radiation__net_shortwave_flux [W/m$^2$]<br>radiation__ratio_to_flat_surface [W/m$^2$] | topographic__elevation [m] |
| *PotentialEvapotranspiration*(): calculate potential evapotranspiration based on Priestly and Taylor, Penman Monteith, and Cosine method. | surface__potential_evapotranspiration_rate [mm/d] | radiation__ratio_to_flat_<br>surface [-] |
| *SoilMoisture*(): local soil moisture balance during interstorm, following instantaneous pulse of rain/runon input. | surface__evapotranspiration [mm/d],<br>soil_moisture__root_zone_leakage [mm],<br>soil_moisture__saturation_fraction [-],<br>surface__runon [mm],<br>surface__runoff [mm],<br>vegetation__water_stress [-] | rainfall__daily_depth [mm],<br>surface__potential_evapotranspiration_rate [mm/d],<br>surface__potential_evapotranspiration_rate__grass [mm/d],<br>soil_moisture__initial_saturation_fraction [-],<br>vegetation__cover_fraction [-],<br>vegetation__live_leaf_area_index [-],<br>vegetation__plant_functional_type |

| | | |
|---|---|---|
| *Vegetation*(): plant biomass balance during interstorm driven by transpiration. | vegetation__live_biomass [gr DM/$m^2$], vegetation__dead_biomass [gr DM /$m^2$], vegetation__live_leaf_area_index [$m^2/m^2$], vegetation__dead_leaf_area_index [$m^2/m^2$], vegetation__cover_fraction [$m^2/m^2$] | vegetation__plant_functional_type [-], vegetation__water_stress [-], surface__evapotranspiration [mm/d], surface__potential_evapotranspiration_rate [mm/d], surface__potential_evapotranspiration_30day_mean [mm/d] |
| *VegCA*(): cellular automaton (CA) vegetation component simulates tree, grass, shrub competition. | vegetation__plant_functional_type [-], plant__live_index [-], plant__age [years] | vegetation__cumulative_water_stress [-], vegetation__plant_functional_type [-] |
| *ResourceRedistriution*(): CA model with two state variables, vegetation cover and soil resource storage. | vegetation__plant_functional_type [-], soil__resources [$m^2/m^2$] | vegetation__plant_functional_type [-], soil__resources [$m^2/m^2$] |
| *SpatialDisturbance*(): simulates disturbances by grazing and wildfires. | vegetation__plant_functional_type [-] | vegetation__plant_functional_type [-] |

A typical modeling exercise using Landlab involves the following steps: 1) creating a grid, which in all ecohydrology applications uses Landlab's RasterModelGrid objects; 2) loading data on the grid using Landlab's data *fields,* a data structure attached to the grid and is associated with one of the grid elements (e.g. *grid.at_cell[''vegetation__plant_functional_type'])*; 3) initializing *components* that constitute the model; 4) running a time loop that execute calls to *run_one_step* or equivalent methods of the *components* in a sequence that create or update data on *fields*; 5) analysing and visualizing simulation outputs; and 6) saving plots and outputs. A driver script, e.g. a *.py* file, which includes code to perform the above steps, constitutes a typical model. All Ecohydrology components described in this paper are limited to structured rectilinear grids (represented by the *RasterModelGrid* class) in Landlab. Table 1 presents existing ecohydrology components of Landlab and their functionality. All Landlab components, including the ones presented in this paper, extensively use Python's native documentation and code-testing techniques, and adhere to the testing standards outlined by Hobley et al. (2017).

Landlab ecohydrology components include local processes for daily solar radiation, potential evapotranspiration, water balance dynamics (soil moisture, actual evapotranspiration, runoff);

plant dynamics (biomass production, allocation, senescence); and spatial processes of plant establishment, mortality, wildfires, grazing, and resource redistribution each represented in a CA structure. The current design strives for parsimony such that the model can be used for long-term paleo-ecologic studies, ensemble simulations for future global change, as well as eco-geomorphic landscape evolution modeling (Pelletier et al., 2017).

In this paper we illustrate three coupled model examples that use the components listed in Table 1, Models A, B, and C (Figure 3-1). Model A constitutes the coupling of local vegetation dynamics, which links six Landlab components to model local temporal dynamics of soil moisture and biomass for a given PFT, with the CA plant competition model that tracks the spatial behavior of individual PFTs through probabilistic establishment and mortality phenomena. These two models are coupled through the exchange of two variables- water stress of the vegetation dynamics model and PFT of the CA model both written as Landlab data fields. Model B conceptualizes the implementation of simplistic CA models for PFTs adopted from Ravi and D'Odorico (2009). In Model B redistribution of soil resources (ie., sediments, nutrients) by erosion and deposition predisposes the establishment of shrubs, simulated by a set of CA plant establishment rules, and stochastic fires and prescribed grazing creates areas of bare soil by consuming grasses. Fires and grazing also interact with each other as they both update the PFT data field. Model C couples the fire and grazing processes of Model B with Model A, whereby the PFT data field is updated by these disturbances. In the next section of this paper we describe the components used in Figure 3-1.

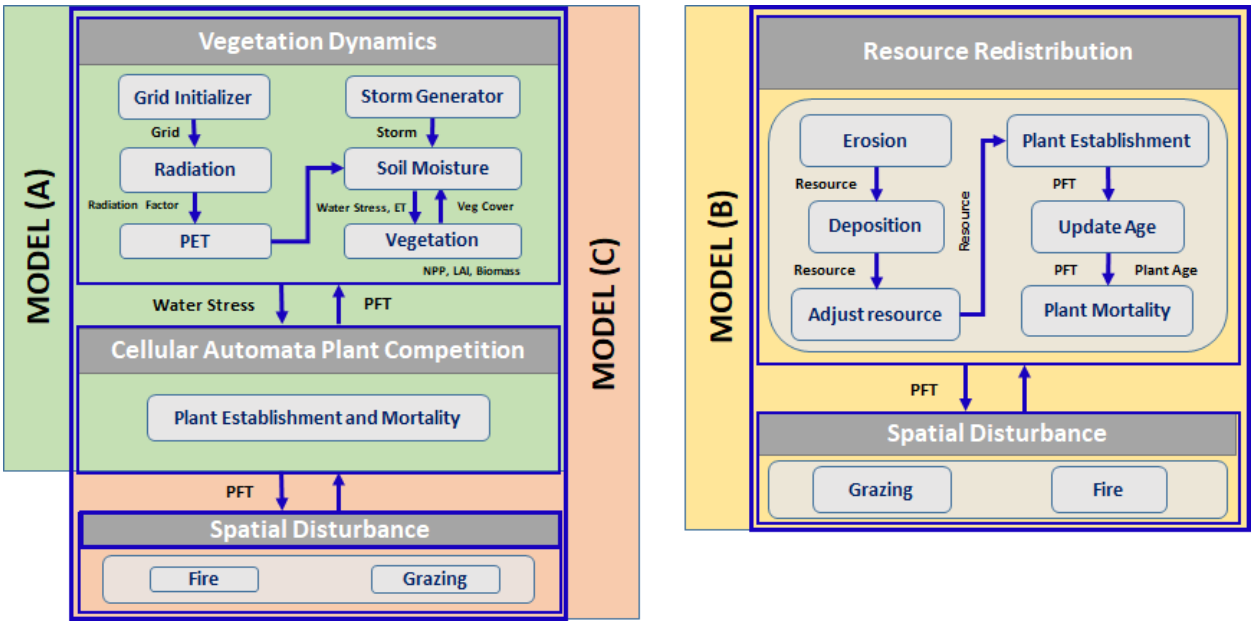


Figure 3-1: Examples of coupled ecohydrologic models that use Landlab ecohydrology components.

### 3.3.1 *Distributed soil moisture and plant growth*

The *SoilMoisture* component simulates a single-layer, depth-averaged root zone water balance at each cell of the raster model grid (e.g., Montaldo et al., 2005, Zhou et al., 2013). Moisture is added by individual storms and lateral runon input (if runon option is selected). Storm time series can be either obtained from daily observations or by stochastic storm generation (which is represented by the *PrecipitationDistribution* component). Potential evapotranspiration, estimated by *PotentialEvapotranspiration* and *Radiation* components, drives actual evapotranspiration. The continuity of soil water in the root-zone is modeled by

$$nZ_r \frac{ds}{dt} = I_a - ET_a(s) - D(s) \quad for \;\; I_a = \begin{cases} \min(r_{on},\, I_{max}), & P \le CI \\ \min(p + r_{on},\, I_{max}), & 0 \le s < 1;\; P > CI \\ \min(p + r_{on}, D), & s = 1; P > CI \end{cases} \quad (1)$$

$$r_{on} = \sum_{n_u} r_{off} \quad (1)$$

$$r_{off} = (p + r_{on}) - I_a \quad (2)$$

where $n$ is soil porosity, $Z_r$ (mm) is the effective root depth, s is relative saturation (volumetric soil moisture content normalized by n), $I_a$ and $I_{max}$ (mm/d) are actual and maximum rates of infiltration, $ET_a$ (mm/d) is the actual rate of evapotranspiration, D (mm/d) is the rate of root zone leakage, $r_{on}$ (mm/d) is runon into a cell calculated as the sum of runoff from neighboring upstream cells, $n_u$. $r_{off}$ (mm/d) is the runoff generated from the cell. The mean rate of net rainfall, p (mm/d), is defined as $p = (P\text{-}C_I)/T_r$, where P and $C_I$ are storm rainfall depth and canopy interception capacity (mm) respectively. $C_I$ is defined as $\min(I_{cmax}V_t, PV_t)$ where, $V_t$ ($m^2/m^2$) is the vegetation cover fraction and $I_{cmax}$ (mm/d) is the full canopy interception capacity. Tr (d) is the storm duration. All cells in the watershed are traversed in descending order of elevation, by adding rainfall in excess of interception and runoff from upstream (if any) to local water balance calculations. The water balance equation was solved using the analytical solution provided by Laio et al. (2001). Soil moisture decay depends on losses through transpiration by plants, evaporation from bare soil, and rootzone leakage following unsaturated hydraulic conductivity model under unit head loss gradient. Maximum unstressed evapotranspiration rate $ET_{max}$ sums transpiration from vegetation cover and evaporation from bare soil (mm/d) (Brolsma and Bierkens, 2007) according to:

$$ET_{max} = \begin{cases} T_{max} - CI & LAI_l = LAI_{max} \\ \left[T_{max}\frac{LAI_l}{LAI_{max}} + E_b\left(1 - \frac{LAI_l}{LAI_{max}}\right)\right] - CI & LAI_l < LAI_{max} \end{cases} \quad (3)$$

where, $T_{max}$ (mm/d) is daily maximum plant transpiration rate calculated from the Penman-Monteith equation based on full canopy cover of a PFT, CI (mm/d) is canopy interception, $LAI_l$ is the live LAI estimated from above ground live biomass using a specific leaf area multiplier ($m^2$/gr DM), $LAI_{max}$ is the PFT-specific maximum LAI used in the calculation of $T_{max}$.

The *PotentialEvapotranspiration* component provides options for *PriestleyTaylor*, *PenmanMonteith*, or prescribed sinusoidal function (*Cosine*) methods. For long-term simulations, in the absence of meteorologic forcing data, $T_{max}$ is approximated using a sinusoidal function, calibrated to modeled data [e.g., Small, 2005; Zhou et al., 2013]. *PotentialEvapotranspiration* is driven by net radiation from the *Radiation* component. The *Radiation* component uses the latitude, Day of the Year (DOY), and time of the day to calculate clear sky shortwave radiation, long wave radiation, and net radiation incident on a flat surface, following Bras (1990) and Eagleson (1970).

Net radiation is distributed across the landscape using the r*adiation_factor*, the ratio of incident solar radiation at a cell with certain slope and aspect to that of a flat surface, calculated by Sun's position (declination angle and hour angle) at each cell, and flat surface. For short-term simulations, in the presence of meteorologic forcing data, Tmax is calculated using Penman (Penman, 1948), or Priestley and Taylor (Priestley and Taylor, 1972) equation. $ET_{max}$ is distributed over the watershed by the *radiation_factor*. The rate of actual evapotranspiration $ET_a$ (mm/d) is a function of evapotranspiration efficiency β [0-1] that scales actual evapotranspiration $ET_a$ between $ET_{max}$ and 0, obtained as a linear function of soil moisture until it reaches the wilting point.

The *Vegetation* component simulates aboveground live $B_l$ (g DM $m^{-2}$) and dead biomass $B_d$ (g DM $m^2$) at each cell as a function of net primary productivity NPP (g DM $m^{-2}$ $d^{-1}$),

$$\frac{dB_l}{dt} = NPP \cdot \varphi_a - k_{sl}B_l - k_{sf}\xi B_l \quad (4)$$

$$\frac{dB_d}{dt} = k_{sl}B_l - k_{dd}\eta_{sd}B_d \quad (5)$$

where $k_{sl}$ (1/d) is the senescence coefficient for live biomass, $k_{sf}$ (1/d) is the maximum drought-induced foliage loss rate (Ivanov et al., 2008a), $k_{dd}$ is the rate of maximum decomposition of $B_d$, $\eta_{sd}$ is the adjustment coefficient for $B_d$ loss rate, and $\varphi_a$ is a coefficient that allocates PFT-specific NPP to $B_l$ (Istanbulluoglu, 2012; Williams and Albertson, 2005). LAI for live vegetation is estimated from its biomass. NPP is the rate at which an ecosystem accumulates biomass, excluding the energy it uses for the process of respiration calculated as the difference between gross primary productivity GPP and the plant autotrophic respiration $R_e$ (g DM $m^{-2}$ $d^{-1}$) and is simplified to the form (e.g., Sitch et al., 2003):

$$NPP = 0.75 \cdot (1 - \mu) \cdot ET_a \cdot WUE \cdot \rho_v \cdot w \quad (6)$$

where μ is the ratio of respiration required for maintenance $R_m$ and GPP, $\rho_v$ (kg $m^{-3}$) is water density, w (kg DM $kg^{-1}$ $CO_2$) converts $CO_2$ into dry matter, and WUE (kg $CO_2^{-1}$ $kg^{-1}$ $H_2O$) is the water use efficiency parameter. The SoilMoisture component also computes interstorm mean water stress ξ, which represents the stress experienced by the plant at the cell due to closed stomata.

NPP is partitioned into above and below ground biomass based on the LAI of grass and woody vegetation (Zhou et al., 2013).

### 3.3.2 *Ecohydrologic Cellular Automaton (CA) model for spatial vegetation dynamics*

In the current Landlab ecohydrology tools we provide two CA models. Of those, *VegCA* is an ecohydrology-driven CA adopted from CATGraSS (Zhou et al., 2013) that simulates spatial dynamics of PFTs driven by soil moisture. Each model grid is occupied by a single PFT (Grass, Shrub, Tree, Shrub Seedling, or Tree Seedling) or remains empty (ie., bare soil). Spatial dynamics of PFTs is driven by probabilities for plant establishment $P_E$, which decrease with plant water stress, and mortality $P_M$, which increases with plant water stress. For establishment, only the bare soil cells are considered. Shrubs can establish as new seedlings that increase the spatial frequency of shrubs, or established shrubs can expand radially by rhizomatous clonal stems (e.g. Ratajczak et al., 2014). The model we propose for establishment can be used to represent both expansion mechanisms for shrubs, however our examples focused on establishment by seed dispersal. Mature shrubs disperse seeds to the first ring neighbors (adjacent cells). Mature trees disperse seeds to both first and second ring neighbors. The CA algorithm checks all the bare cells in the model domain, and a PFT is randomly selected for establishment based on comparison of mean live indices of plants within the first ring (for shrubs) and first and second rings (for trees) of the selected empty cell. $P_E$ is assigned based on plant live index, ϕ, of each PFT in the domain, calculated from cumulative water stress within the growing season, WS:

$$\varphi = 1 - WS \tag{7}$$

where $WS = \frac{\sum_0^{N_{is}}(\xi . T_b)}{T_G}$. $N_{is}$ is the number of interstorm events in the year, $T_b$ (d) is the interstorm duration, and $T_G$ (d) is the length of the growing season. The mean live indices for shrubs and trees that neighbor a bare soil cell are:

$$\overline{\varphi_{SH}} = \frac{\sum \varphi_{SH}^{I}}{8} \tag{8}$$

$$\overline{\varphi_T} = \frac{\sum \varphi_T^{I}}{8} + \frac{\sum \varphi_T^{II}}{16} \tag{9}$$

where $\varphi_{SH}^{1}$is the live index of mature shrub neighbors in the first ring, and $\varphi_{T}^{1}$ and $\varphi_{T}^{11}$are live indices of mature trees in the first and second neighboring rings respectively. We assume that grass seeds are always available in the entire domain (Jeltsch et al., 1996; van Wijk and Rodriguez-Iturbe, 2002). Hence, we calculate mean live index for grass as the average of live indices of all grass cells present in the domain.

In CATGraSS, allelopathic effects of shrubs on grass (Knipe and Herbel, 1966) are implemented by inhibiting grass establishment by a factor $IN_G$. This inhibition is amplified by the presence of more shrubs in the first ring neighbors of the bare cell considered for establishment. Therefore, the aggregate plant establishment probabilities for grass ($P_{E\text{-}G}$), shrubs ($P_{E\text{-}SH}$), and trees ($P_{E\text{-}T}$) can be written as:

$$P_{E-G} = min\left(\frac{\overline{\varphi_G}}{IN_G.N^I}, P_{E-max-G}\right) \tag{10a}$$

$$P_{E-SH} = \min(\overline{\varphi_{SH}}, P_{E-max-SH}) \tag{11b}$$

$$P_{E-T} = \min(\overline{\varphi_T}, P_{E-max-T}) \tag{11c}$$

where $P_{E\text{-}max\text{-}G}$, $P_{E\text{-}max\text{-}SH}$, and $P_{E\text{-}max\text{-}T}$ are maximum (limit) establishment probabilities of grass, shrubs, and trees respectively. For every bare cell, a PFT is randomly selected, and its corresponding $P_E$ is calculated and compared to a uniformly distributed random number ~U(0, 1). If $P_E$ is greater than the generated number, the selected PFT is established at this bare cell. The selection process of the "winner" plant type when more than one PFT has a chance of establishing at an empty cell is a challenge in CA modeling, as nature does not list rules and execute in an order. A simple method to improve plant selection process was developed by Caracciolo et al. (2017) for selection among tree, shrub, and grass PFT, which may be tested in this component.

Probability of mortality $P_M$ comprises three parts: drought stress ($P_{Md}$), plant aging ($P_{Ma}$), and local disturbances such as fire and grazing ($P_{Mb}$). Thus, $P_M$ is defined as:

$$P_M = min(P_{Md} + P_{Ma} + P_{Mb}, 1) \tag{11}$$

Mortality probability due to drought stress is modeled as a function of *WS*-- and a PFT-specific water stress threshold $\theta_{PFT}$ (van Wijk and Rodriguez-Iturbe, 2002) defined as:

$$P_{Md} = max(WS - \theta_{PFT}, 0) \tag{12}$$

Mortality probability due to aging $P_{Ma}$ represents the susceptibility of a woody plant (tree or a shrub) to physiological changes due to disease and other environmental factors. It is defined as (Jeltsch et al., 1998):

$$P_{Ma} = \begin{cases} 0, & t_{PFT} < 0.5t_{PFT-max} \\ \frac{t_{PFT} - 0.5t_{PFT-max}}{0.5t_{PFT-max}}, & 0.5t_{PFT-max} < t_{PFT} < t_{PFT-max} \end{cases} \tag{13}$$

where $t_{PFT}$ (yr) is the age of the plant occupying a model grid cell and $t_{PFT\text{-}max}$ (yr) is the maximum age of the PFT at the cell. Mortality due to disturbance $P_{Mb}$ implicitly models the effects of disturbances such as fire and grazing and is input to the model. Total probability of mortality $P_M$ is now calculated for each cell and compared to a uniform random number ~U(0, 1). If $P_M$ is greater than the generated number, the plant is removed from the cell.

### 3.3.3 *Cellular Automaton (CA) for disturbances and resource redistribution*

In Landlab we represent two endogenous feedback mechanisms: grassland fuel-fire and vegetation-eolian sediment interactions and grazing as an exogenous driver for WPE based on algorithms adapted from Ravi and D'Odorico (2009) (Figure 3-1, Model B). The model couples categorical vegetation (V) states and soil resource level (R) updated by fire and grazing disturbances based on a set of rules governing the reorganization of *V* and *R*. *R* is conceptualized to represent a soil resource value relative to the mean resource level of a productive ecosystem in the range of -2 and 2. *R* accumulates by creep and trapping of aeolian sediments and subject to post-fire redistribution from local sediment mounts. Each cell in the domain can take an integer from 0 through 4 to represent the cell states for bare soil [0], grass [1], shrub [2], burnt grass [3], and burnt shrub [4]. Two components, *ResourceRedistribution* and *SpatialDisturbance* have been developed in Landlab to represent this model.

#### 3.3.3.1 Resource Redistribution:

The *ResourceRedistribution* component lumps coupled dynamics of resource redistribution and vegetation dynamics in space using four methods: *establish*(), *mortality*(), *erode*(), and *deposit*() (see flow charts in Appendix B). *establish*() and *mortality*() simulate state transitions of grass and shrub vegetation in a cell based on a one-step transition probability conditioned on resource availability, neighboring vegetation, and whether or not a plant is burnt. The *erode*() and *deposit*() methods redistribute the sediment based on current vegetation state to simulate sediment movement due to global aeolian sediment transport and local post-fire dissipation of sediment around shrubs to neighbors. State transition probabilities are configured for an annual timestep. We apply a periodic boundary condition, allowing sediment or seeds exiting the domain on one side to re-enter the domain from the opposite side.

*establish()* assigns grass and shrub vegetation only if the resource level $R$ in the cell exceeds PFT-specific thresholds, $R_{th\_gr}$ and $R_{th\_sh}$ for grass and shrubs (where $R_{th\_sh} > R_{th\_gr}$) respectively. This criterion makes a cell eligible for any of the three states: combined grass and shrub, only grass, or no vegetation establishment. The actual establishment process uses a series of rules detailed below, used in the order presented below in the component:

(1) When a cell is occupied by burnt shrubs and burnt grasses, probabilities of *P_sh_regrwth* and *P_gr_regrwth* are used respectively to regrow existing shrub and grass at the cell. This provides a legacy effect due to local seed/seedling availability for the regrowth of burnt vegetation.

(2) For the establishment of new shrub plants in empty cells, two seed dispersal mechanisms are used. At an empty cell the probability of shrub encroachment is *ns_sh*P_en*, where *ns_sh* is the number of shrub neighbors of an empty cell, and *P_en* is probability of shrub encroachment of a single shrub cell.

(3) Grazing herbivores carry seeds around as they browse across the landscape causing shrub encroachment with a probability of *Pgrz* on bare cells.

(4) Grass establishes in remaining bare cells with a probability of *P_gr*.

Plant mortality due to fire, aging, and water stress are incorporated with probabilities for shrub and grass individually in the *mortality()* component. Burnt shrubs and burnt grasses are converted to bare soil cells with a probability of *P_sh_fire_mor* and *P_gr_fire_mor* respectively. Shrubs die

due to probabilistic mortality by age, *Pmor_age*, following Jeltsch et al. (1998) (equation 14) We also added background mortality due to water stress, *Pmor_ws*, to account for PFT-specific drought resistance.

*erode()* removes resource *R* from a cell depending on the PFT occupying that cell in discrete units of *e* (e=0.1, Ravi and D'Odorico, 2009). Vegetated cells do not lose sediment unless they are burnt. If a cell is occupied by burnt shrub, *4e* resource is removed from that cell. If a cell is occupied by burnt grass, *0.2e* resource is removed. If a cell is occupied by bare cell, *e* resource is removed (Ravi and D'Odorico, 2009). All removed resources are accumulated for redistribution by the *deposit* method. These erosion and deposition parameters were reported for central New Mexico in Ravi and D'Odorico (2009), thus kept as default in our application.

The resource removed and accumulated from the domain for a year by the *erode()* method is deposited by the *deposit()* method. Deposition of aeolian sediment occurs locally, conditioned on the vegetation state of a cell, or through displacement of *R* from sediment mounds (e.g., islands of fertility) to adjacent neighbors that have smaller *R*. Firstly, neighbors of all burnt shrubs receive the sediment eroded from their burnt shrub neighbor, regardless of their vegetation state. Next, the cumulative resource collected across the domain from burnt grass and bare soil cells are distributed to cells occupying shrubs, grass, bare soil in the 3:2:1 ratio, respectively. This order is assumed to represent the relative canopy trapping efficiencies of shrub and grass canopies.

As sediment is redistributed by the methods *erode*() and *deposit*(), *re_adjust_resource*() maintains *R* within a prescribed range of -2 to 2. The upper limit can be considered as the amount of sediment that can be accumulated under shrub with a certain angle of repose. The lower limit can be considered to represent micro-topographic depressions. This method removes sediment from any cells with *R* in excess of 2 and distributes it to their neighbors with *R* less than 2 (ie., similar to sliding of sediment at the angle of repose). This method also adds sediment to cells where *R* is less than -2 , with sediment from surrounding cells (e.g., microtopographic trough filled by soil creep). Finally, the method *update_Veg_age()* increments the age at vegetated cells by a year.

#### 3.3.3.2 Spatial Disturbance

This component provides two methods, *initiate_fires()* and *graze()*, which can be used coupled to plant establishment models presented earlier. In arid and semiarid grasslands natural fires are generally initiated by lightning strikes (Parmenter, 2008). *initiate_fires()* simulates a desired number of lightning strikes by randomly placing them across the modeled domain. The number of lightning strikes is a fixed value input, based on the frequency of lightning strikes observed in a region, but it can be made a random number in the model driver. Fire starts if the struck cell is covered by grass and the fire vulnerability parameter of grass the PFT at the cell, *pft_vuln* [0-1], is greater than a generated uniformly distributed random number U[0, 1]. The fire spreads to the vegetated neighbors if the fire susceptibility parameter of each neighbor, *pft_susc*, is greater than a U[0,1], generated separately for each neighbor. We kept *pft_vuln* and *pft_susc* as two separate parameters, as the ease of vegetation catching fire could be lower during a fire than when lightning hits a plant. A fire, if started or spread to a cell, converts the PFT occupying the cell to either a bare soil (e.g. Models A & C) or a burnt PFT state (e.g. Model B) as these are two alternative states used by the plant establishment algorithms presented above. A periodic boundary condition is also assumed for the spread of fires. If a fire does not stop naturally as it spreads because of lack of vegetation to burn, it terminates when the fire size reaches a maximum fire area, randomly sampled from a uniform distribution. The range of the distribution is represented using the mean fire size and a deviation factor from the mean [(*fire_area_mean- fire_area_dev)*, (*fire_area_mean+ fire_area_dev)*]. Other distributions can be used in the model driver as desired by the user.

*graze()* removes grass from a cell where *grazing_pressure* at grass-occupied cell is greater than a uniformly distributed random number U[0, 1] generated at each grass cell. The influence of grazing is primarily on grass in arid and semiarid ecosystems as herbivores are known to graze herbaceous vegetation (Van Auken, 2000; Van Auken, 2009).

## 3.4 RESULTS

### 3.4.1 *Confirmation of coupled SoilMoisture and Vegetation model*

Here we present confirmation of a basic ecohydrologic model that predicts local soil moisture, plant biomass, and water balance dynamics for a given PFT by coupling *SoilMoisture* and *Vegetation* components (Figure 3-1, top box of Model A), driven by actual weather. Examples are from a grassland located in the Barta Brothers Ranch (BBR) of the Nebraska Sand Hills, NSH (Figure 3-3) and an aspect-controlled ecosystem in the Sevilleta National Wildlife Refuge (SNWR), New Mexico (Figure 3-3).

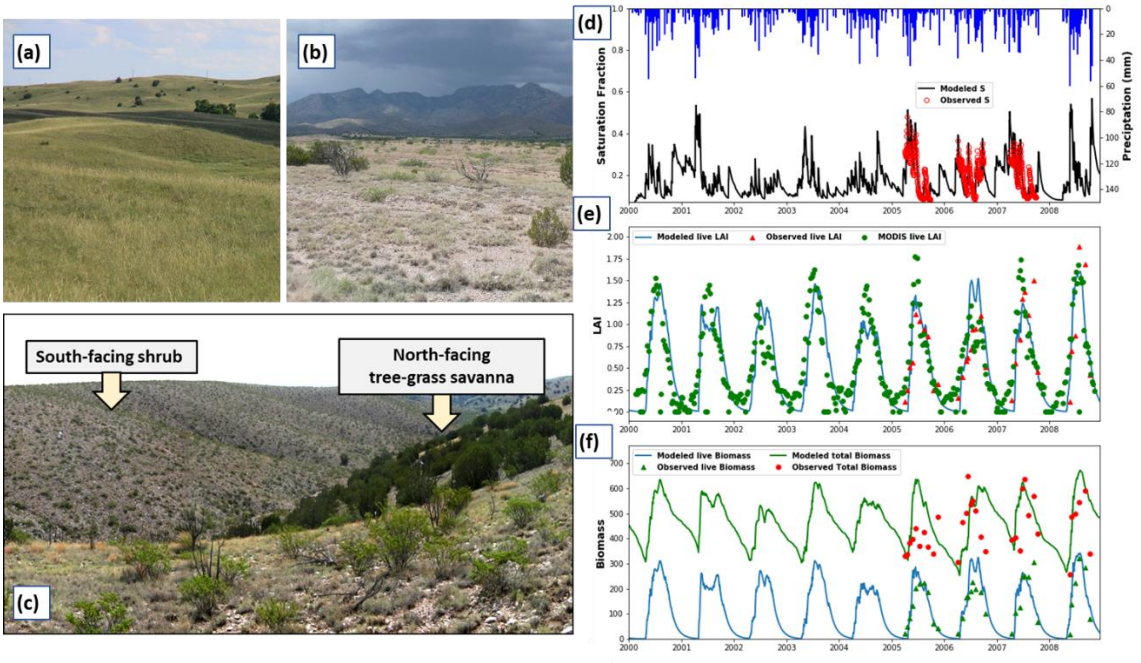


Figure 3-2: Left panel shows field sites used for model confirmation: a) Grassland in the Nebraska Sandhills, NE (Photo Credit: Jessin Hills); b) shrub-dominated flat landscape, and c) aspect-controlled shrub and tree-grass ecotones in central New Mexico, USA. Right panel shows modeled and observational-based data from grassland in the BBR: d) soil moisture; e) grass Leaf Area Index (LAI); f) grass total, live, and dead biomass [data from Istanbulluoglu et al., 2012].

The BBR-NSH site has continental climate, and the mean annual precipitation and temperature are 576 mm and 8.1 $^{o}$C, respectively. Half hourly growing season root-zone soil moisture (2005-2007), measured live and dead biomass (2005-2008), and MODIS-derived LAI (2000-200) data are used

for model confirmation (Istanbulluoglu et al., 2012; Sridhar and Wedin, 2009). Weather data at BBR were obtained from Automated Weather Data Network (ADWN) of weather stations as described by Istanbulluoglu et al., 2012. Reference grass equation is used for $T_{max}$ (Allen et al., 1998). The Nash-Sutcliffe $R^2$ values between modelled and observed data are 0.64, 0.47, and 0.52 for volumetric soil moisture saturation fraction, LAI, and live aboveground biomass respectively. Despite low NS-$R^2$ values, the model captures seasonal behavior and ranges of predictions realistically.

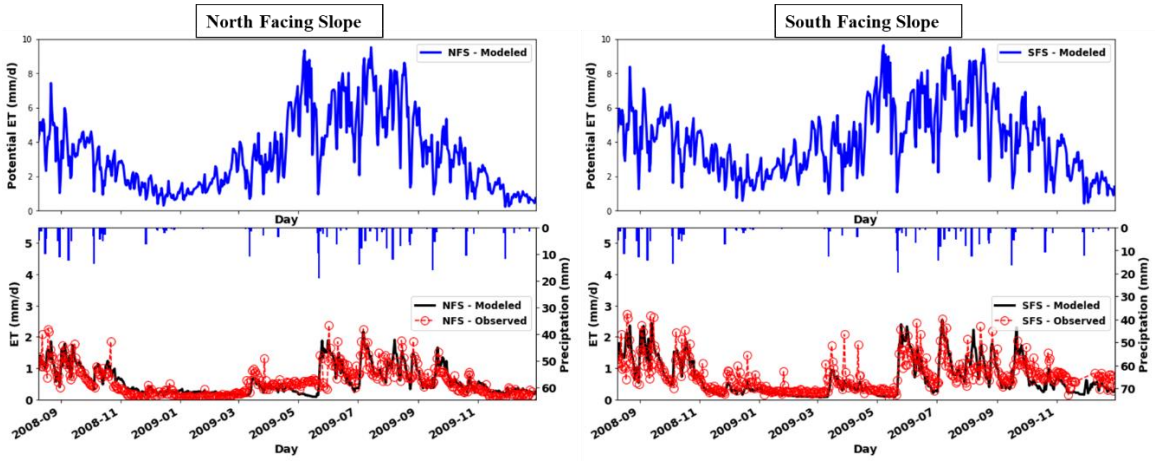


Figure 3-3: Time series of modeled potential Evapotranspiration (ET), modeled ET, and BREB-derived ET on North Facing Slope and South Facing Slope of the headwater basin shown in Figure 3-2c (data from Gutiérrez-Jurado et al., 2013).

Our model captures the dynamics of soil moisture, evapotranspiration, and LAI on a flat domain located in the SNWR (not shown, see Zhou et al., 2013), and aspect-dependent differences in observed evapotranspiration in a headwater catchment in the northwestern corner of the SNWR (Figure 3-3). In this headwater catchment one-seed Juniper (Juniperus mono-sperma) and dense black grama (*Bouteloa eriopoda*) coexist in North Facing Slopes (NFS), and creosotebush (*Larrea tridentate*) shrubs dominate South Facing Slopes (SFS, Figure 3-2c). In this semi-arid monsoonal climate, mean annual precipitation and temperature are ~250 mm and 20$^{o}$C, respectively (Gosz et al., 1995 Gutiérrez-Jurado et al.,2013; Zhou et al., 2013). To force the model in the aspect-controlled ecosystem, we used observations from a network of sensors deployed in transects along the NFS and SFS (Gutiérrez-Jurado et al., 2013). Data include observations of daily weather variables and ET obtained from a Bowen Ratio Energy Balance system (BREB) system on both

aspects (Gutiérrez-Jurado et al., 2013). The spatially-explicit model was run using a 10-m Lidar-derived DEM of the headwater catchment driven by spatially averaged weather data. Consistent with the state of the ecosystem in this region at the time of measurements (e.g., Gutiérrez-Jurado et al., 2013), we fixed PFTs with 50% trees and 20% grass randomly placed on NFS, and 100% shrub cover on SFS, while the model simulates biomass in response to climate. In fitting model predictions to observations, we used published model parameters in the literature for similar models, consistent with plant and soil properties of these sites (see Tables S1, S2, S3, & S4). For this study, we also considered runon in the *vegetation dynamics model*. Runoff ratio for the model period (Annual Runoff/Annual Precipitation) expressed in percent was 5% at the outlet, within a plausible range for this semiarid region (Gutierrez-Jurado et al., 2013; Yetemen et al., 2015). We spatially averaged the modeled evapotranspiration data over NFS and SFS to compare them with BREB-ET on respective slopes. The Nash-Sutcliffe $R^2$ values between modeled and observed ET are 0.62 and 0.47 for NFS and SFS respectively. There were several days in the ET data that showed increases unmatched by rainfall (and vice-versa), lowering the Nash-Sutcliffe $R^2$.

### 3.4.2 *Ecohydrology of aspect-dependent ecotones*

Aspect-dependent separation of soil moisture and plant conditions in xeric equator-facing slopes and mesic pole-facing slopes is common to mid latitude regions (e.g., Parson, 1976; Pelletier et al., 2016; Gutierrez-Jurado et al., 2013). Understanding the ecohydrologic controls of aspect-dependent ecotone formation is critical to forecast the future of such ecosystems under global change (e.g., Zhou et al., 2013; Caracciolo et al., 2016). *What roles do topography, local plant inhibitory effects, and runoff redistribution play in semiarid ecosystems*? We investigate this question at the headwater basin located in the SNWR using Landlab (Figure 3-2c).

Modeling the spatial dynamics of PFTs and their associated biomass requires the coupling of *SoilMoisture*, *Vegetation*, and *VegCA* components as illustrated in Figure 3-1 (Model A). We designed two options to configure the spatial implementation of the CA model with fully distributed, and binned representations of local ecohydrologic processes. In the distributed option soil moisture and vegetation growth are simulated in each cell individually. In the binned version slope and aspect ranges are lumped into representative slope-aspect classes within which representative soil moisture and local vegetation dynamics are simulated for each PFT and bare

soil and mapped across the watershed. The binned version is computationally more efficient and can be preferred when flow routing for runoff-runon calculations are not desired.

Using the parameter space that led to a realistic prediction of aspect-dependent evapotranspiration (Figure 3-3), we ran two sets of long-term simulations (Figure 3-4): with allelopathy, by reducing the live index of grass around shrubs by a factor of $IN_G$=2, and without allelopathy (ie., $IN_G$=1) for a flat 4 km by 1.4 km domain (5m grid size) and an actual watershed topography represented by a 5 m DEM. The actual watershed is a 3.3 $km^2$ catchment in the northwestern corner of the SNWR in central New Mexico (see photo taken from one of its headwater hollows in Figure 3-2c). It has a west-to-east flowing valley network, a 4.3 km long main channel, and approximately equal distributions of N and S aspects within an elevation range of 1,600 to 1,700 m. The lower NE section of the watershed (12% of its area) has moderate to flat topography. The 5-m topography is divided up into 108 slope-aspect bins, within which ecohydrologic dynamics for each of the six plant types are run separately. Grazing and fires are not explicitly simulated but their influences on mortality rates are incorporated within the probability of mortality, $P_M$ (from Zhou et al., 2013). Climate is divided into dry and wet (Monsoon) seasons with their corresponding statistics for storm duration, intensity and interstorm duration (Zhou et al., 2013). Model A is run for 20k years driven by individual storms (see Table S5 for parameters). As initial condition, equal proportions of tree, grass, shrub, and bare soil are used.

On flat surface shrubs and grasses outcompete Juniper pine within roughly the first 5k years (Figs. 3-4a to d). Regardless of the shrub-grass allelopathic influence, shrub vegetation is the dominant cover consistent with observations in the region. When shrubs inhibit grass growth ($IN_G$=2), shrub cover rose from 40% to 60% as grass cover diminished from >20% to <10%. When actual topography is used, Juniper pine tree permanently establishes on the landscape (Figs 3-4e, 3-4g), coexisting with blue grama, predominantly on northern aspects (N, NW, NE, ~27-20% tree cover on average) but also on E and W slopes (~10% tree cover) and some on flat land (~4%) (Figs. 3-4i-k).

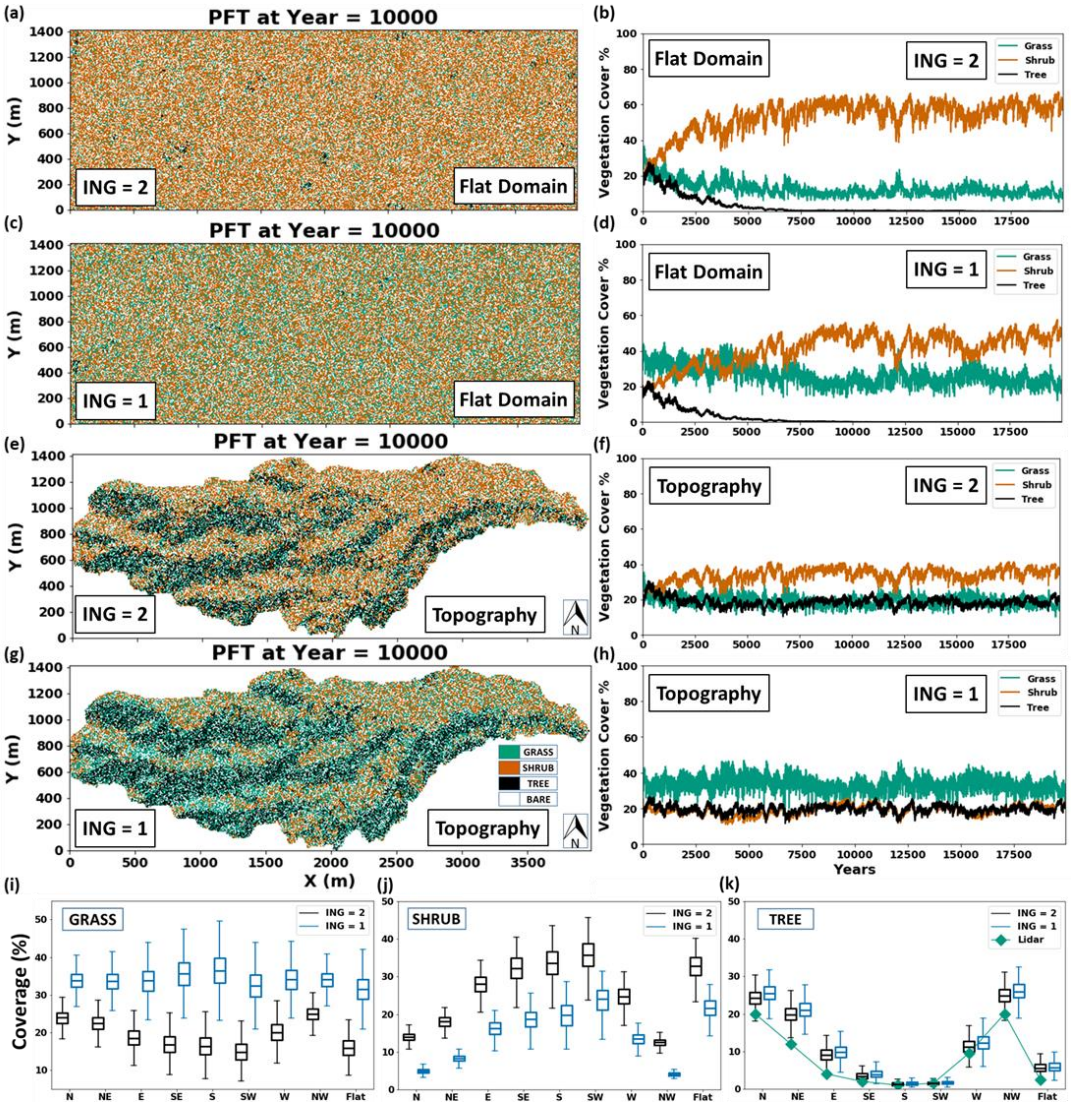


Figure 3-4: Modeled tree, grass, and shrub vegetation for central New Mexico USA climatology with (ING=2) and without (ING=1) shrub inhibitory effect on grass growth. Modeled vegetation cover map at year=10k and time series of vegetation cover (%) are presented for a flat domain (3-4a - 3-4d) and for an actual watershed (3-4e, 3-4h). Figs. 3-4i to 3-4k present whisker-box plots of percent cover of each PFT with respect to aspect with and without allelopathy based on spatial data from the last 10k year model results. LiDAR-derived tree cover (%) data from Zhou et al. (2013) are used for model comparison.

The influence of shrub-grass allelopathy is negligible on the Juniper tree cover, however it reduces the blue grama grass cover on all aspects where Juniper pine coexists with. Allelopathy clearly suppresses grasses and promotes shrubs in all aspects, but more profoundly on southern aspects

and flats (Figs. i, j). Interestingly while shrub is dominant on flat domain without allelopathy ($IN_G$=1), on the actual topography grass becomes the dominant under the same condition (Figure 3-4 g, h). Regardless of allelopathy a slight increase in proportion of the landscape occupied by vegetation (~5%) is predicted on actual watershed.

The model underscores the interplay between plant water stress and seed dispersal range as a mechanism responsible for the development of aspect-controlled arid to semiarid vegetation patterns. In all aspects modeled water stress is higher for juniper pine than creosotebush, while the highest water stress is modeled for grass due to its shallow root depth. Thus, on flat domain shrubs with the lowest water stress becomes the dominant plant, and trees only emerge through topographic niches of relatively higher soil moisture on NFS. Increase in the availability of seedlings in the ecosystem as trees establish on NFS, and the greater seed-dispersal range of trees enables them to spread rapidly, outcompeting shrubs on NFS. On drier SFS, seed dispersal advantage of juniper pine is not sufficient to maintain a population where shrubs have a greater ability to withstand water stress.

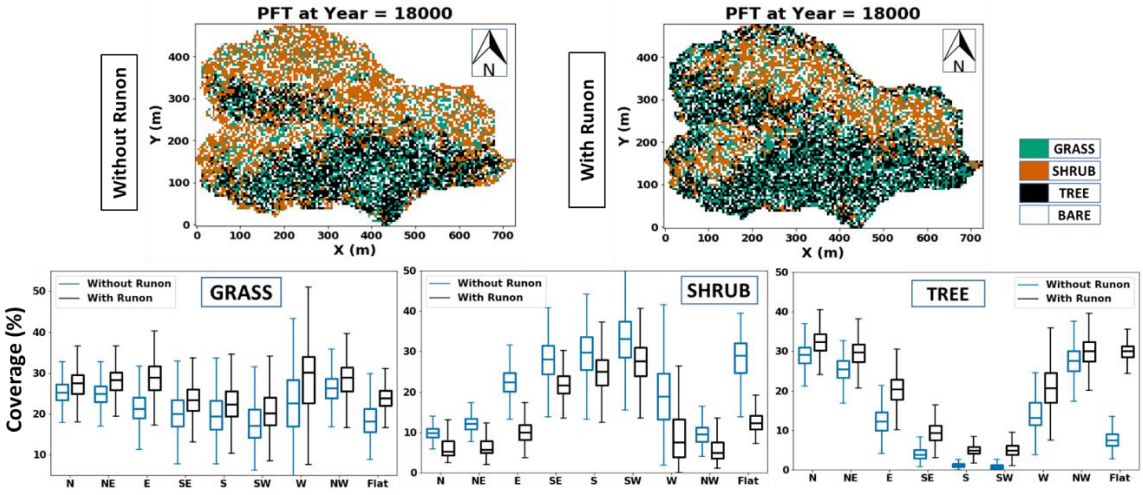


Figure 3-5: The influence of runon on aspect-dependent vegetation organization in a headwater watershed in the SNWR, central New Mexico USA illustrated by Landlab simulations run without and with runoff-runon exchange among model elements.

The use of runon water by downslope locations has been proposed as a process that leads to the development of banded vegetation patterns on planar hillslopes and organization of plants along topographic flow paths (Saco et al., 2007; Saco, and Moreno-de las Heras, 2013; Flores-Cervantes et al., 2014). We ran two simulations limited to the headwater catchment of the SNWR watershed for 20,000 years to investigate how runoff-runon contributes to ecosystem patterns in Model A (Figure 3-5). Overall there is more moisture available for the ecosystem to use for plant function in the runoff-runon simulation. Grass and Juniper pine trees benefit from runon in all aspect classes (based on the comparison of median values), with greater gains on east and west aspects. Interestingly in flats in the toe of hillslopes juniper cover increase as high as ~15%. Shrubs on the other hand lose cover in all aspects, with the greatest losses taking place over east and west facing slopes. Even though the drought resistant shrubs have a competitive advantage, when soil water increases incrementally through runon gains, trees and grasses outcompete shrubs, due to assumed longer dispersal lengths of trees and the infinite seed supply of grasses.

### 3.4.3 *Grazing-fire-resource distribution feedbacks control WPE*

Can the WPE be reversed? This question is critical for rangeland and environmental management globally. We examine how grazing-vegetation-fire-eolian sediment dynamics govern ecosystem response using Model B (Figure 3-1b) adapted from Ravi and D'Odorico (2009). In this model explicit soil moisture-plant feedback is neglected; static establishment and mortality probabilities govern plant state transition.

Three simulations are run with parameters from Ravi and D'Odorico (2009), proposed for central New Mexico, USA (Table S6), assuming shrub dominance (shrub, %40; grass 30%) in the initial plant cover. Plants are randomly distributed, and shrubs are initialized with a random age. A 2.5 km by 2.5 km domain constructed by 2.5m cell size is used. Each model is run for 300 years with an annual time step with no, moderate (10% cover/year) and intense (20% cover/year) grazing pressures (Wang et al., 2019; Ravi and D'Odorico, 2009). Every year either two or three lightning strikes are randomly placed within the domain. This lightning activity is based on calibration such that a realistic natural grassland fire regime (approximately 1 in 10 years) is obtained within the 6.25 $km^2$ modeled domain. Fire spreads cell by cell and usually stops before a maximum limit of

~9% of the domain is reached (~0.56 $km^2$). Mean fire size from the New Mexico wildfire map is 0.7 $km^2$ (Energy, Minerals, and Natural Resources, 2018).

*Pmor_age* in these simulations is set such that shrubs die only at their maximum age of 600 years. Regrowth probabilities at burnt sites are 0.5 for grass and 0.25 for shrub. A neighboring shrub adds a 5% chance to shrub establishment in unburnt cells (Pen). Naturally existing grazers only provide a small shrub establishment probability (Pgrz=0.001). When *Grazing* is considered, this probability is increased tenfold, Pgrz=0.01. Burnt shrubs (grasses) have a 75% (100%) chance of mortality.

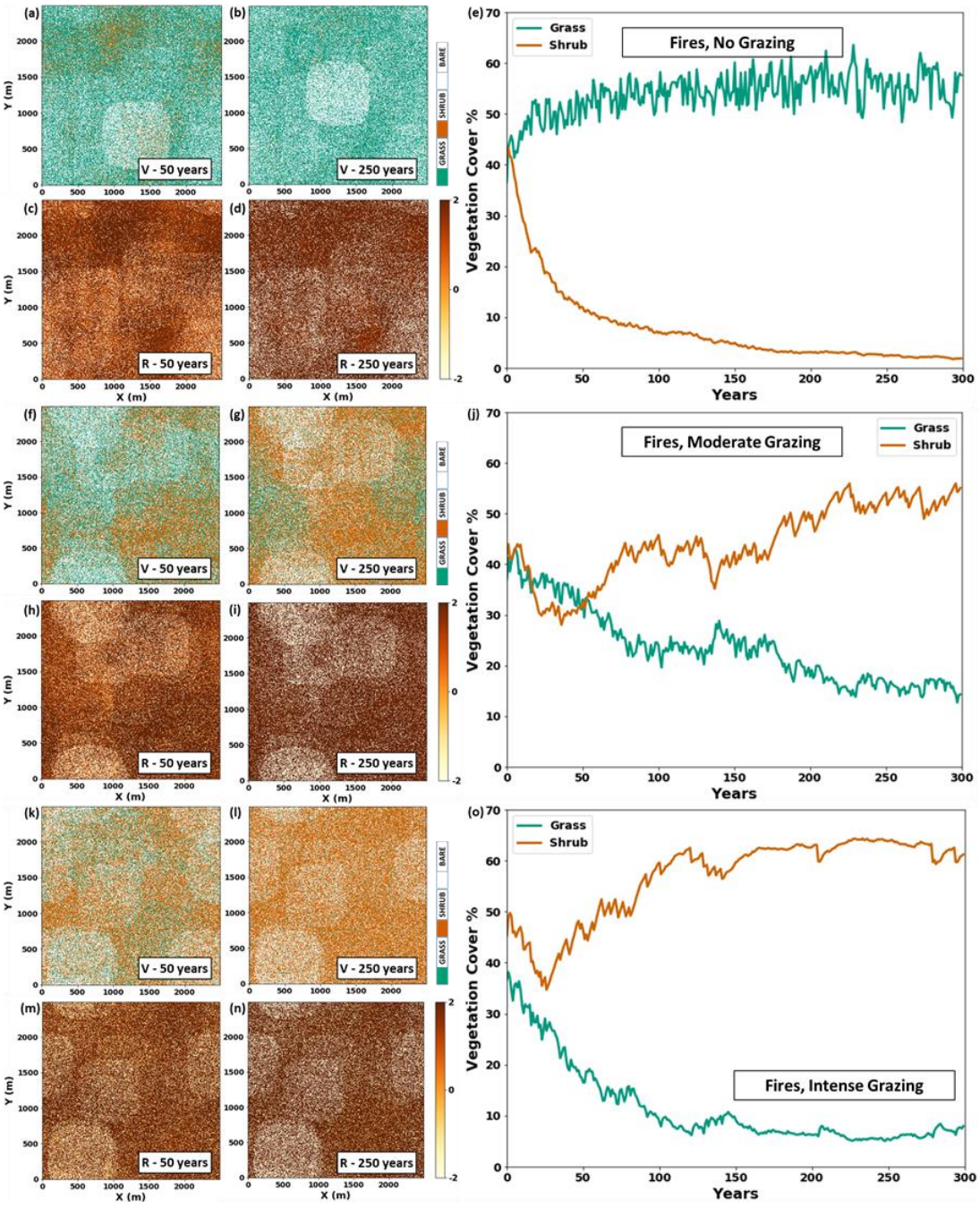


Figure 3-6: Influence of moderate and intense grazing on woody plant encroachment simulated with the rule-based model adapted from Ravi and D'Odorico (2009) (Model B in Fig. 3-1).

A stable grassland with a ~1 in 10 year fire return interval rapidly establishes in the absence of livestock grazing (Figure 3-6 a-e). The grassland maintains enough connectivity, as a result fires return due to high vulnerability of grasses to lightning fires and their high susceptibility to fire spread. Burnt grass patches have a higher probability of grass regrowth instead of shrub

establishment. This leads to an endogenous grass-fire feedback, reinforcing grass growth and preventing shrub establishment. Resources get depleted at sites visited by fires, lowering the chances of shrub establishment relative to grass as shrubs require a higher *R* (i.e., negative feedback).

With moderate grazing (*gr_pressure*=0.1) shrub cover begins to decline for a period of ~30 years, remains steady until around year 50 in a mixed shrub-grass ecosystem where grasses show a declining trend (Figure 3-6f), followed by a steady rise, dominating the ecosystem after 50 years. The key contribution of moderate grazing to shrub encroachment is the disruption of grass connectivity which leads to a gradual reduction in fire frequency. Shrubs are less susceptible to fires than grasses. Thus, loss of fire frequency and the opening of random patches by grazers creates a positive feedback for shrub expansion through seed dispersal, locally by neighboring shrubs, and globally by grazers. (Figure 3-6 h-i). With intense grazing (*gr_pressure*=0.2) shrubs become the dominant vegetation type within 30 years (Figure 3-6 k-o).

Two prominent features observed in the simulations are: 1) fires leave legacy on both vegetation and resource distribution, reinforced by grazing intensity; 2) as shrubs establish, resource-rich shrub patches form and grow due to the greater trapping efficiency of shrubs and local soil creep from neighbors. A rather permanent pattern of bi-modal resource distribution emerges. Resources within some burnt patches are depleted to the level below the threshold to support any vegetation type, causing local desertification, as other shrub patches get resourceful by trapping the wind-transported sediment eroded from bare patches. WPE may be reversed by no or low-intensity grazing unless a nutrient-rich spatial soil structure is developed, and a positive feedback for shrub establishment is established via the trapping of eolian sediments.

### 3.4.4 *Tempo of WPE investigated by coupled ecohydrologic and disturbance CA models*

In the application of the rule-based CA model of Ravi and D'Odorico (2009) in section 4.3. we used fixed state transition probabilities independent of climate and assumed that fires only start on grass cells. In this section we relaxed these limitations by coupling the climate-driven ecohydrologic CA model (e.g., Figure 3-4) with grazing and fire disturbance model (Figure 3-1,

Model C), and assuming that existing fires can burn trees and shrubs and new fires can start from their seedlings.

*How do grazing, plant establishment strategies, and grass-fire feedbacks interact and control the rate and spatial structure of woody plant encroachment, WPE?* This question is investigated here without vegetation-eolion process feedbacks. Our goal is not to reproduce any particular case of observed WPE, as rates and patterns of WPE vary across regions and types of species involved. We aim to gain some general insights by comparing and contrasting model results with real-world cases.

The model parameters used for simulations in Model A (Figures 3-4, 3-5) were selected to develop aspect-dependent patterns; the temporal dimension of pattern formation was not investigated. Here we use the same parameters, except for background mortality, $P_{Mb}$, used to lump annual chances of mortality due to fires, grazing, and diseases in the aspect simulations (Figures 3-4 and 3-5). When fire and grazing disturbances are simulated explicitly these $P_{Mb}$ values used earlier should be adjusted down. If a natural fire interval of 1 in 10 years and a grazing pressure of 0.1 are considered to act at a grassland site, the annual probability of disturbance adds up to a maximum of 0.2, but it could get much lower in reality as plants organise. This is 4 times larger than the $P_{Mb}$ of 0.05 used in the aspect simulations (Figures 3-4, 3-5). Tree and shrub disturbances would be less frequent than grass, considering their lower vulnerability and susceptibility to fire. Based on these arguments and minor calibration to obtain a grassland under a natural fire regime, we reduce $P_{Mb}$ values by a factor 2.5 ($P_{Mb}$=0.02) for grass and a factor of 5 for shrubs ($P_{Mb}$=0.002) and trees ($P_{Mb}$=0.005) with respect to the aspect simulations.

There are several differences in the implementation of the fire model of Ravi and D'Odorico (2009) in Model C: 1) fires start and spread from shrub and tree cells with probabilities nearly half that of grass; 2) grass vulnerability is reduced to 0.9 from 1.0 (i.e., 10% chance of a grass cell surviving a lightning strike); 3) both shrubs and trees have seedlings subject to fire initiation and spread with a 10% higher risk than mature plants as they are more vulnerable to disturbances (e.g., Hanan et al., 2008; Archer et al., 2017). Parameter values are presented in Table S7.

Prior to WPE, native woody plants were scattered across the semiarid landscapes of the western USA (<10% cover) (Laliberte et al., 2004). WPE has transformed grasslands to dense woodlands in less than a century (Archer et al., 2017). To establish a pre-WPE natural ecosystem, we first run Model C starting with initial conditions of randomly distributed 25% grass, shrub, and tree cover. Grass outcompetes shrub and tree PFTs and a stable grassland (~40% grass cover) with approximately 1 in 10 year fire return interval develops without livestock grazing (Figure 3-7a, 3-7b). This model result is consistent with the pre-encroachment grasslands in central New Mexico; some grasslands still exist where shrub encroachment was minimal (e.g., Mescalaro Sandsheet).

In the next simulation we start with the output of the grassland simulation (Figure 3-7a) and introduce grazing of grass with moderate grazing pressure (*gr_pressure*, of 0.1). Fixed boundaries of trees (top) and shrubs (bottom) are introduced to represent encroachment fronts into a native grassland. WPE does not take place and the grassland is maintained (Figure 3-7c, 3-7d). The same level of grazing pressure yields shrub dominance in Model B. A critical difference in this model compared to Model B is that only mature shrubs and trees disperse seedlings; shrubs and trees are considered mature when they are 18 and 20 years old, respectively. Even though some seedlings might establish after fires or with grazing, they are consumed by fires before they mature (Figure 3-7c, 3-7d).

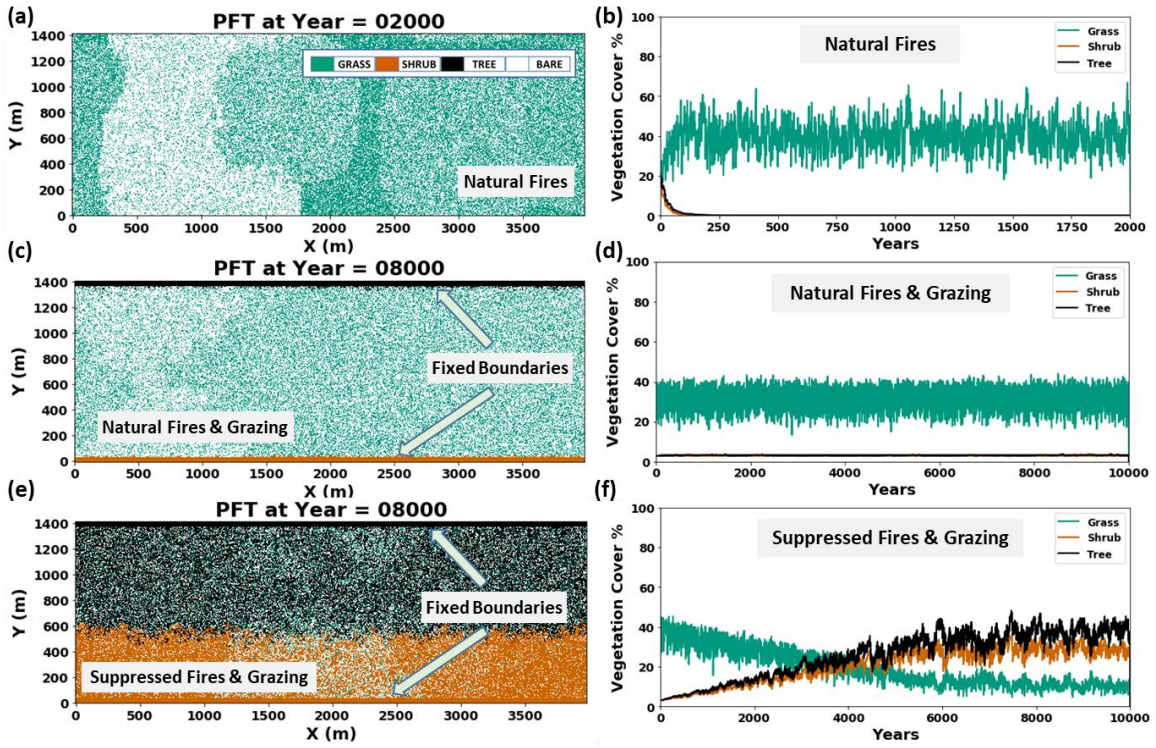


Figure 3-7: Influences of fire frequency and grazing on woody plant encroachment (tree and shrub) modeled for central New Mexico, USA, using Model C of Figure 3-1: a, b) natural fire regime without grazing, note circular fires cause patterns of low grass cover; c, d) moderate grazing with natural fires; e, f) reduced fire frequency and moderate grazing.

Next, we imposed "fire suppression" by reducing the fire frequency to 1 in 100 years (or more, as it naturally reduces by WPE) and kept *gr_pressure*=0.1 (Figures 3-7e, 3-7f). Our model predicts a slow rate of WPE (Figures 3-7e, 3-7f), more like long-term ecosystem shifts observed over the Holocene. The relatively steady rate of grass replacement by woody plants is controlled by the loss rate of grasses due to grazing, water-stress related mortality, and limited fire disturbance. Trees and shrubs march inward, and a battle for space establishes at the shrub-tree ecotone near the middle of the domain. Trees benefit slightly from their longer seed dispersal range over shrubs in the model.

The model clearly shows that fire suppression cause WPE, consistent with observational evidence (e.g., Van Auken, 2009), however it predicts much lower rates of woody plant increase (%0.0075

cover/year) than reported rates in the southwestern US (~0.35% cover/year) (Archer et al., 2017). There may be several reasons for the modeled low WPE rate (Figure 3-7e, f). First, an abrupt change to a tenfold lower fire frequency as a result of fire suppression may not be a realistic scenario for early Euro-American settlers in the southwest US. Thus, in the next simulation we allow the fires naturally initiate by lightning strikes and spread across the landscape without suppression, and the fire frequency adjust internally in the model as a result of grazing (as in Figures 3-7c, d). Second, the low rates of encroachment could also be due to limited seeds in the system. Considering introduced grazers and wind disperse seeds, we develop a simple non-local seed establishment rule by planting a percentage of the domain with the WP of interest (tree or shrub) using a linear relation to the cover fraction of WP in the domain. A base rate of seeding starts with an equivalent establishment rate of 0.025% (for 0 cover) and increases linearly up to a rate of 2% at 50% cover of the WP and stays fixed. Three simulations are run for tree (Figure 3-8a, b), shrub (Figure 3-8c, d), and a mixed tree-shrub-grass cover conditions (Figure 3-8e, f), all initiated with output of the grassland simulation (Figure 3-7a, b) and driven by moderate grazing. When grazing not included, no WPE developed in the models, thus not discussed here.

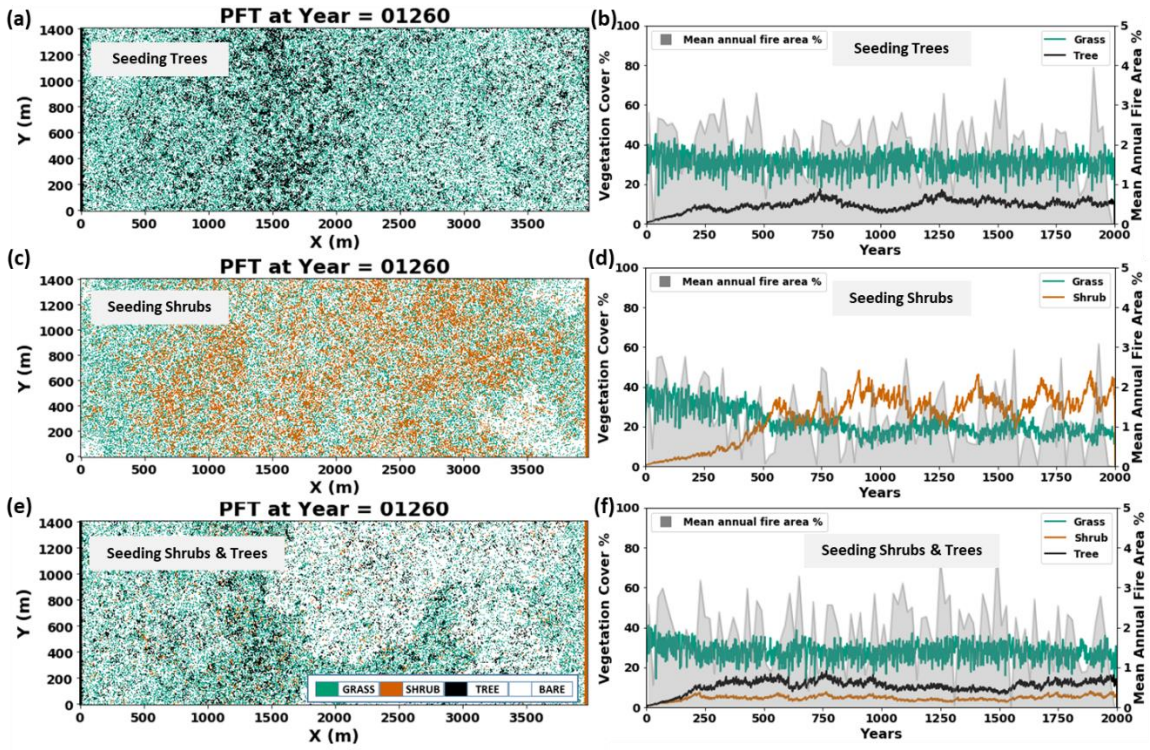


Figure 3-8: Vegetation model driven by natural fire regime, 10% grazing (moderate), and nonlocal plant establishment rule for central New Mexico, USA, conditions using Model C of Figure 3-1. Modeled maps of PFTs, and time series of PFT cover, 20-year average burnt area fractions for a, b) tree encroachment; c, d) shrub encroachment; and e, f) tree and shrub encroachment simulation experiments.

A clear outcome is that the proposed non-local plant seeding model significantly contributes to the establishment of new individual woody plants (Figure 3-8), while the natural fire regime prevents the propagation of ecotones established on the sides (similar to Figure 3-7c, d). A linear increase in tree and shrub cover is observed in all simulations until around model year 250 (Figure 3-8b, d, f). In the case of tree and tree-shrub simulations fairly stable grass-dominated savanna ecosystems are maintained by fires with low WP cover <15% (Figs. 3-8a, b and e, f). In the shrub simulation (Figs 3-8c, 3-8d), ~10% shrub cover emerges as a threshold beyond which a positive feedback process for shrub establishment initiates, accelerating the growth of its cover. What is this feedback mechanism and how does a cover threshold emerge?

In the shrub only experiment (Figs., 3-8c, 3-8d) we conceptualize the following phases in the emergence of a macro-scale cover threshold and rapid growth: (1) Initial establishment: starting from an initial small fraction, shrubs establish gradually at a nearly constant rate (~0.025% cover/year), and grass cover declines gradually. This phase ends when the critical shrub cover is attained (~10%) that is sufficient to alter the grassland's fire regime near year 350 (see loss of fire area, Fig. 3-8d). (2) Rapid expansion: loss of grass connectivity begins to reduce fire frequency and fire size; grazed grass cells are replaced at growing rates by shrub cells. As shrub cover grows so does the non-local seedling establishment rate. Individual shrubs establish and small clusters grow with local seed dispersal and inhibitory effects on grass, finally reaching 35% cover in year 570. Rapid expansion rate is ~0.15% cover/year. (3) Eco-climatic dynamic equilibrium: shrubs attain a cyclic equilibrium to the climate with a mean shrub cover of ~30%. A regime of less-frequent smaller-size fires establishes under a moderate grazing disturbance. Shrub cycles occur over periods of several decades to several centuries with amplitude of ~20% cover. Each upward trend in shrub expansion cycle (~0.15% cover/year) begins with a period when fires are absent or small scale and ends with the return of larger fires (Figure 3-8d). Years with large fires also follow periods of low fires during which shrubs colonize, and the cycle repeats.

In summary, in the case of fire suppression and local seedling dispersal strategy, shrub and tree encroachment rates are driven by seedling dispersal by mature plants mostly in the front line of the two ecotones (Figure 3-7e, f). The rate of expansion is limited by the rate of grass mortality right at the fringes of ecotones. Absence of any endogenous grass-fire feedback keeps the expansion rates very low (Figure 3-7e, f). Introducing non-local seed dispersal without fire suppression showed potential for woody plant dominance. When the endogenous grass-fire feedback remains intact, woody plant expansion is suppressed by fires and a stable savanna system emerges (Figure 3-8a, b and e, f). When woody plant expansion impairs the grass-fire feedback, causing less frequent fires, WPE rates increase nonlinearly that lead to shrub dominance in a three-phase process (Figure 3-8c, d). Findings show that WPE is related to low fire activity either by fire suppression or natural reduction. These findings lead to the following question. *Are savanna ecosystems stable over the long-term*?

### 3.4.5 *Focusing on the savanna question*

Savannas are mixed grass-woodland ecosystems, characterized by open grasslands with scattered trees. They contribute to about a quarter of the gross primary production (GPP) globally, and support diverse wildlife (Beer et al., 2010). *Are savanna ecosystems stable over the long-term, as opposed to drifting toward either grass or woodland*? Equilibrium and disequilibrium paradigms have been developed to address this question. The equilibrium paradigm suggests that savannas are in a long-term stable state maintained by climate variability and disturbances. The disequilibrium hypothesis argues that a savanna represents a transient state between grass and woodland end members, observable during times of disturbances (Archer, 1995; Scholes and Archer, 1997; Accatino et al., 2010). Fire is generally regarded as a key disturbance that maintain grass dominated savannas (Bond, 2008; Archer, 2017).

*Can fire frequency be sufficient for the transition of a savanna ecosystem to a woodland*? To isolate the role of fire in the model, grazing is turned off. Shrub vegetation is not included for simplicity and local seedling dispersal by mature trees is used. There are several fire parameters that can be used to address the question posed above. Here, we only use the fire susceptibility parameter for mature (*tr_susc*) and young (*tr_seed_susc*) trees that control the probability of cell-to-cell fire spread and ran a series of simulations. In order to make fires less frequent these parameters are lowered from the base values of the grassland simulation (*tr_susc*=0.4, *tr_seed_susc*=0.5) (Figure 3-7a, b) to the 0.4 - 0.1 range for *tr_susc*, and 0.5 - 0.2 range for *tr_seed_susc* in small decrements, while maintaining a difference of 0.1 between mature and young trees (*tr_seed_susc* > *tr_susc*). We assume that only grass cells can start a fire, with *gr_vuln* of 1.0. Tree mortality due to age and water stress remains, but the background mortality is eliminated. Simulations are started with 1% tree and 69% grass, and with lightning ignitions that maintain a natural grassland fire regime (1 in 10 years).

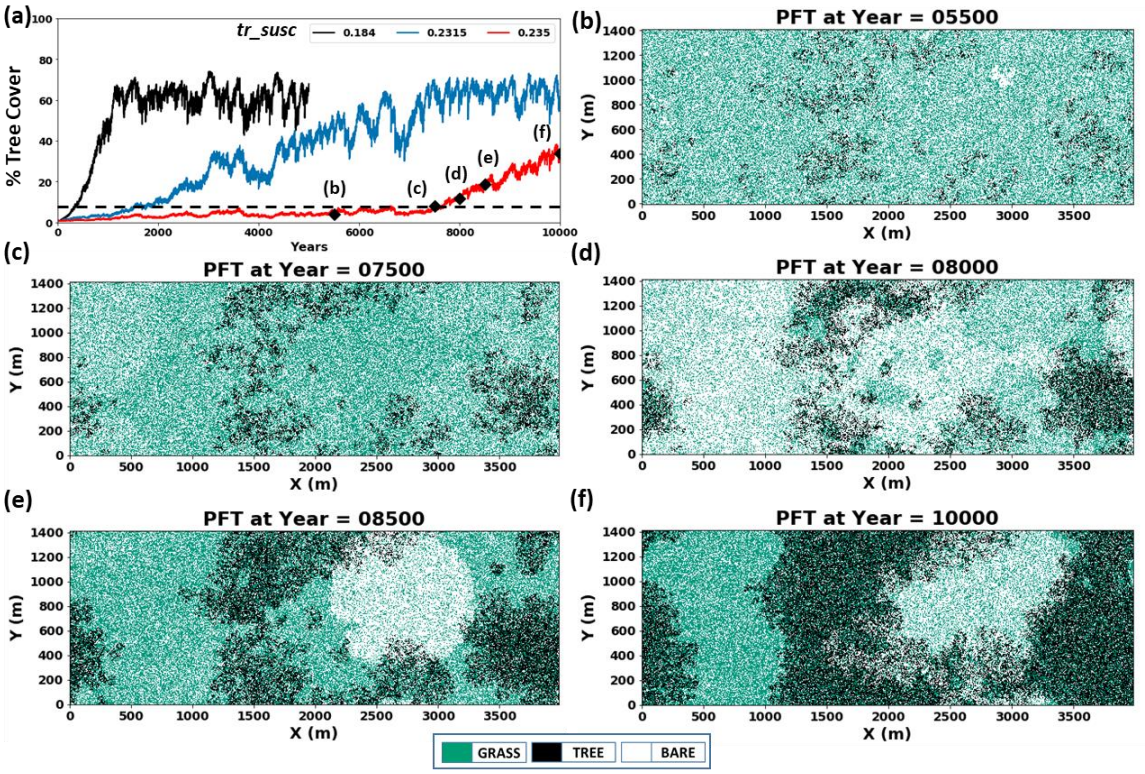


Figure 3-9: Sensitivity of the model to tr_susc: a) Times series of modeled tree cover (%) for tr_susc values of 0.184, 0.2315, and 0.235; b, c, d, e, & f) spatial organization of grass and trees with tr_susc = 0.235 at different years as indicated on 9a. Impacts of irregularly shaped and circular grassland fires on vegetation can be viewed (d, e, & f).

In all simulations that use *tr_susc* < 0.3 (i.e., 30% risk of catching fire when a neighbor burns), trees eventually attain a carrying capacity of 60% when simulations are run long enough. Examples of tree cover trajectories illustrate the highly sensitive model response to fire susceptibility in relation to time (Figure 3-9a). A threshold-dependent rapid expansion phase of tree cover emerges. As trees become more fire resistant (from left to right), the model predicts: a slightly larger critical cover threshold required for the initiation of rapid expansion (phase 2 of WPE); a much longer time to the exceedance of the critical cover; and lower rates of expansion in phase 2 with the exceedance of the cover threshold (Figure 3-9a).

A marked feature of the simulation is that there is a nonlinear increase in the time of exceedance of the critical tree cover threshold before the onset of rapid expansion as *tr_susc* grows close to 0.3. Compare the last two trajectories with *tr_susc*=0.2315 (moderate expansion, blue) and

*tr_susc*=0.235 (slow expansion, red) simulations. Slightly higher probability of fire susceptibility of each tree (i.e., 0.0035) delays the development of spatial conditions that facilitate the transition to the rapid expansion phase for thousands of years in the slow expansion simulation (red) (Fig. 3-9a).

Cluster formation due to local seedling dispersal by trees and the coalescence of small clusters into larger clusters drives tree expansion (Figure 3-9b – 3-9f). The macro-scale horseshoe-shape structure made up of small tree clusters is established in the model, much before the phase of rapid expansion (Figure 3-9b). For nearly two thousand years, the ecosystem shows small rates of change and the change occurs largely around the clusters (Figure 3-9b, c). For an observer over several centuries, this ecosystem would look like a typical equilibrium savanna. However, this period of stability is disrupted with the arrival of a few large grassland fires that open space for tree establishment (Figures 3-9c, d), resulting in rapid growth and coalescence of clusters, impairing the grass-fire feedback without livestock grazing (Figure 3-9e and f).

In the previous simulations we have seen grazing and natural increase in woody plants as mechanisms that impair the endogenous grass-fire feedback that maintains grassland savannas. Plant drought resistance to water stress is another parameter that controls mortality. We will investigate the grass-fire feedback with the tree-grass savanna system here, as we ask the following additional question: *Does plant water stress play any role in the space-time dynamics of savanna response*? In the previous experiments, the drought resistance of trees, $\Theta_{tr}$, was kept constant at 0.71 (as used in Figures 3-4, 3-9). The higher the drought resistance value, the greater the chance of the plant to survive a drought. By experimenting with the model we find that when $\Theta_{tr}$ is less than 0.66, the modeled ecosystem in Figure 3-9 transitions into a grassland. We rerun the simulation *tr_susc*=0.2315 (blue line) in Fig 3-9a, for 20 kyr with the same parameters but randomly selecting a value of $\Theta_{tr}$ between 0.66 and 0.76 every year (Figure 3-10). This simulation still has a mean $\Theta_{tr}$=0.71, but in some years trees are less drought resistant, thus there is a higher risk for the ecosystem to experience greater drought-induced tree mortality and in other years trees experience a smaller drought-induced mortality risk.

A reciprocal time series can be clearly seen between fire size and tree expansion, with a marked three-phase tree encroachment process over time (Fig. 3-10a). A natural grassland fire regime continues in phase I. Tree cover grows at very slow rates (<0.001% per year) until a cluster structure that lower the size of fires forms (Figure 3-10b), and creates a feedback between loss of fire size and tree encroachment (phase II), until a carrying capacity with closed tree canopy is reached (phase III). We can clearly see the spatial memory of the initial structure on the landscape similar to Fig 3-9. Randomizing the water stress threshold extends phase 1 for about 4,500 yrs longer, and shortens phase II ~1,000 years (compare tree covers in Fig 3-9a, blue line and Fig. 3-10a). The longer duration of phase I can be related to the variable nature of $\Theta_{tr}$, as half of the time there is a larger risk of drought-related mortality.

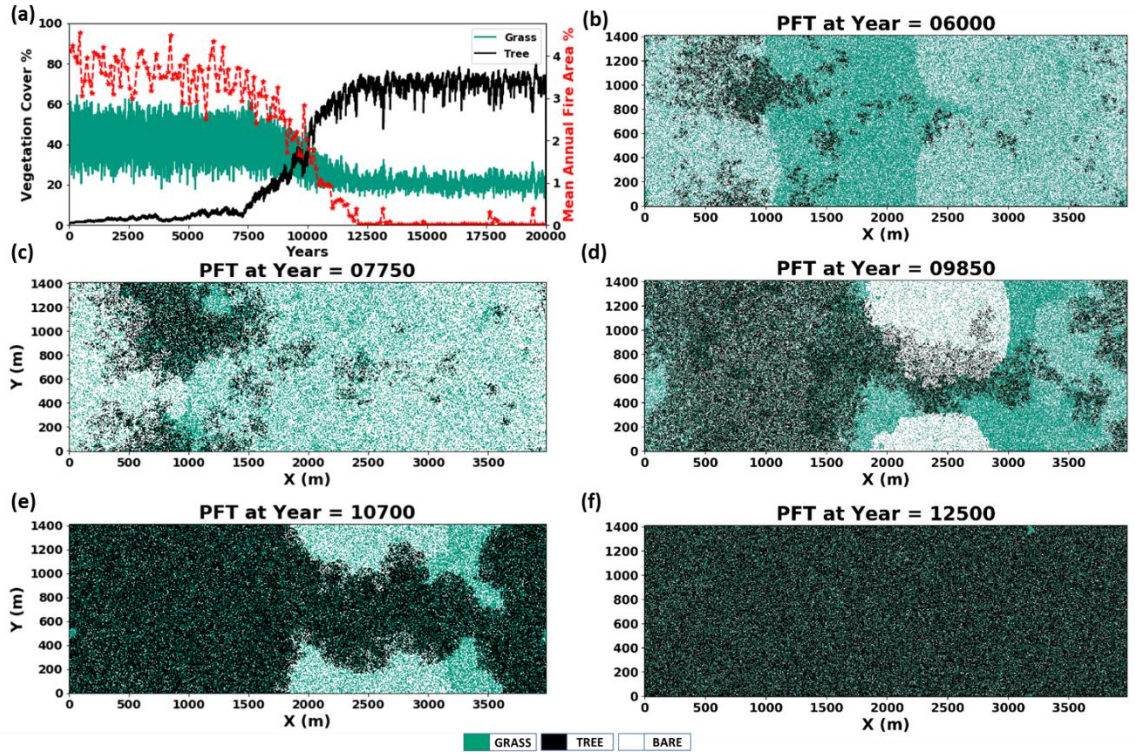


Figure 3-10: The role of temporally varying tree water stress threshold on tree encroachment: (a) time series of tree and grass cover (%) and the average burnt area (%) over a moving time window of 20 years; (b to f) maps of vegetation type at different time slices.

## 3.5 DISCUSSION

The alternative stable states (or attractors) theory (ASST) postulates that alternative states in ecosystems can exist under the same exogenous conditions if states are governed by stabilizing endogenous feedbacks, and state shifts can occur when such feedbacks are weakened (Bowman et al., 2015). ASST was initially proposed through conceptual (Jackson, 1968; Holling, 1973) and analytical (May, 1977; Walker et al., 1981) models, and it now receives growing observational and experimental support across a range of ecosystems including lakes, coral reefs, oceans, forests and arid lands (Scheffer et al., 2001, 2012; Anderies et al., 2002; Carpenter et al., 2011; Ratajczak et al., 2014; Wilcox et al., 2018).

Based on observational evidence it has been hypothesized that large changes in vegetation structure from grassland to woodland requires a perturbation to an exogenous driver and/or to an endogenous feedback mechanism (Van Auken, 2009; Scheffer et al., 2001; D'Odorico et al., 2012). Changes in vegetation structure may be gradual and reversible, threshold-dependent nonlinear and reversible, or threshold-dependent nonlinear and catastrophic, as in the ASST, with a critical transition from one attractor (state) to another often with hysteresis (see reviews by Ratajczak et al., 2014a, 2014b; Wilcox et al., 2018). Threshold states could emerge with demographic bottlenecks (establishment barriers or low growth conditions for species) and strong feedback mechanisms. For example, a positive grass-fire feedback that maintains a grassland acts as a demographic bottleneck for the establishment of new shrub seedlings (Van Auken, 2000). Similarly, increased grazing is a demographic bottleneck for grasses as it impairs grass-fire feedback, reduces grass cover and promotes WPE (Anderies et al., 2002; Ravi and D'Odorico, 2009; Wilcox et al., 2018).

There are relatively few models that represent, to a limited level, some of the key endogenous feedback mechanics (e.g., grass-fire, and grazing-erosion) in mixed grass and woodland systems. Besides the cellular automaton models we adapt in Landlab (e.g., Ravi and D'Odorico, 2009; Zhou et al., 2013; Caracciolo et al., 2016, 2017), dynamical system models based on ordinary differential equations (ODE) (e.g., Lotka–Volterra type) have been used to evolve spatially lumped fractional covers (and/or biomass) of grass, shrub, and/or tree functional types. ODE models have

been formulated using minimal ecological assumptions drawn from specific ecosystem observations and related hypothesis of competition and disturbances (Tilman, 1994; Anderies et al., 2002; Fernandez-Illescas and Rodriguez-Iturbe, 2003; Hanan et al., 2008; Okin et al., 2009; D'Odorico et al. 2012; Touboul et al., 2018). These models aim to develop a qualitative understanding of dynamical system behavior of mixed vegetation, rather than predictions for environmental management.

A rich array of behaviors emerge in ODE models over the time domain including bistable states, diverse cyclicity, reversible and catastrophic transitions, not only as a result of perturbations to exogenic drivers or noise but sometimes also due to endogenous feedbacks (e.g., Touboul et al., 2018). Various classes of ODE model behaviors arise from differences in plant colonization and mortality rates, factors that control ecosystem carrying capacity, selection of superior and inferior competitors, and rules used in the implicit representations of vegetation-fire and vegetation-erosion feedbacks, without considering any spatial structure. Simple ODE-based models have repeatedly shown that if shrubs are in competitive advantage the modeled system exhibits bistable vegetation dynamics due to either vegetation-fire or vegetation-microclimate feedbacks but when grasses are superior over shrubs or trees bi-stability is an outcome of vegetation-erosion feedbacks (D'Odorico et al., 2006a; Okin et al., 2009; Accatino et al., 2010; D'Odorico et al., 2012). In ecosystems where woody plants (WPs) are superior competitors models emphasize the strength of vegetation-fire feedback (i.e., decrease of fire pressure on WP as WP cover increases) on state shifts. When the vegetation-fire feedback is weak, stable savannas may persist. Increase in the strength of feedback gives rise to a sharp catastrophic transition from grassland to woodland occurs (D'Odorico et al., 2012).

Landlab modeling applications present a rich set of model responses without the need for making critical assumptions such as a competitive ranking (superior or inferior) of PFTs. In our simulations the vegetation-fire feedback establishes naturally driven by the random positioning of lightnings, spatial pattern of PFTs and their susceptibility to fire. In Model C a naturally evolved strong grass-fire feedback under moderate levels of grazing acts as a bottleneck for tree and shrub establishment when their seedling sources are limited to mature plants (Fig 3-7a to d) as commonly observed in grasslands (e.g., Roques et al., 2001). When fire is suppressed, both tree and shrub encroached into

the domain at constant rates until the space is filled, without the emergence of any thresholds. This gradual change response can be attributed to the sudden loss of vegetation-fire feedback, and the slow WP response is largely due to limited local seed dispersal at ecosystem front lines. Gradual WPE without abrupt expansion rates have been reported in areas with complete fire suppression and without introduced grazers where shrubs and trees attain their new spatial carrying capacity (Walker et al. 1981; Roques et al. 2001; Hoh et al., 2002; Briggs et al., 2002; Ratajczak et al., 2014).

When a global seedling establishment is introduced stable grassland savannas with coexisting grass-tree (Fig. 3-8 a,b) and grass-tree-shrub (Fig 3-8 e, f) savannas form. This model outcome supports the disequilibrium savanna hypothesis that coexistence of PFTs is maintained by disturbances rather than plant competition (e.g., Sankaran et al. 2004). In these simulations woody plant cover was not sufficient to impair the grass-fire feedback, which caused a persistent bottleneck of WPE. However, when shrub and grass were the two PFTs modeled, a threshold for shrub cover (~10%) that separates slow and rapid expansion phases of WPE emerged (Fig. 3-8c, d). Gradual increase in the spatial frequency of shrub establishment with non-local seedling, local seedling dispersal from newly established plants when they mature, and the inhibitory effects of shrubs on neighboring grass establishment collectively increased the shrub cover to a threshold that slightly perturbed the grass-fire feedback, causing smaller/less frequent fires and more rapid rates of shrub expansion (Fig 3-8 c, d). This illustrates a case where woody plant competition capacity overwhelms the natural disturbance regime of a mixed ecosystem.

Phases (stages) of WPE have been proposed earlier, based on observations that relate the rate of WP establishment to population density and various plant and environmental factors including the roles of seed dispersal, grazing, and fires (e.g., Miller et al., 2000; Miller et al., 2005; Archer et al., 2017; D'Odorico et al., 2012). Rates of WPE have been reported in the range of 0.1 to 3.3% cover/year, that vary depending on ecoregion (Archer et al., 2017). In hot, dry regions like the Chihuahuan and Sonoran deserts, shrub encroachment rates vary from <0.1% up to 0.4% cover/year (Barger et al., 2011). During the expansion phase of shrubs in Model C (Figure 3-8 c, d) the rate of encroachment is ~0.15%, close to the low end of Chihuahuan and Sonoran deserts, without detailed calibration for specific site conditions.

Changes in exogenic drivers trigger state shifts in simple mathematical models (see review of D'Odorico et al., 2012). Time-dependent spatially explicit processes we simulated in this paper seem to suggest that state shifts may take place without an exogenous trigger. In the case of Figure (3-8c, d), shrub encroachment was triggered by grazing, but accelerated and sustained due to diminished fire activity with loss of grass cover once a threshold shrub cover is exceeded. In the case of the tree-grass savanna experiments (Figs. 3-9, 3-10) the transformation of the landscape to trees takes place solely from an internal feedback process of the gradual expansion of trees in grassland that result in loss of fire probability, and over time a complete elimination of fires. A striking difference is the formation of resilient plant clusters that grew laterally over time in the tree-grass simulations (Figs 3-9, 3-10) compared the increase in the spatial frequency of grasses in the shrub-grass (Fig 3-8c, d). In the tree-grass savanna simulations a catastrophic shift is clear, the system won't return to a grassland because the fire regime is completely turned down. The shrub dominated system in Fig (3-8c, d) still maintains a relatively frequent fire regime and bares a higher chance for a grassland shift in case of a perturbation on climate and fire regime.

Our model based findings are closely related to the ~30-year observational study of Ratajczak et al. (2014a, 2014b) who reported shrub-grass dynamics in grazed, ungrazed, and varying fire regime treatments in the Konza Prairie Biological Station, Kansas, USA (precipitation 835 mm/yr). In the plots with fire return periods of 4 and 20 years, shrub cover first increases gradually for the first 17 years (0.5% cover/year). A rapid increase in shrub cover (5% to 10% cover/yr) begins with a ~5% shrub cover threshold, continues for 1 to 3 years, followed by a decade-long moderate expansion (1.4% to 2.7% cover/year) in both grazed and ungrazed plots. The increase in shrub cover was correlated with a size index that quantifies the radial expansion of individual clonal shrub patches, rather than spatial frequency of shrubs. Spatial growth rates of non-clonal shrubs were ~8-fold slower than the clonal shrubs. Size expansion allows the plant cluster to be more resilient to fire pressure, circumventing a bottleneck for their encroachment (Ratajczak et al., 2014a, 2014b). A longer fire interval >15 years was found sufficient for tree (*Juniperus virginiana,* Eastern Red Cedar) establishment to grasslands while this threshold dropped to 6-10 under heavy grazing.

## 3.6 CONCLUSIONS

A major challenge facing ecosystem and hydrosystem scientists in the face of global change is to provide long-term predictions to aid decision making for sustainable nations. This task is particularly difficult in heterogeneous and transient ecosystems over complex terrain. Landlab offers a platform for coupling models of varying sophistications with respect to spatial and temporal processes. In response to the questions raised in the introduction we briefly list our conclusions with respect to arid-to-semiarid mixed grass-woody plant context:

- The model underscores the interplay between plant water stress and seed dispersal range as a mechanism responsible for the development of aspect-controlled vegetation patterns, and how additional run-on input can make species with deeper roots and longer seed dispersal capacity more competitive.
- Coupling vegetation-disturbances-eolian sediment dynamics (Figure 3-1, Model B) provided insights that relate WPE to a regime of grazing disturbance (Figure 3-6), and the development of ecosystem memory to fires and grazing.
- Coupling grazing and grass-fire interactions in an ecohydrologic cellular automaton model reveals linear and nonlinear response patterns of woody plants and their causes. Fire suppression causes gradual expansion of woody plants that further reduce fire frequency. Natural grass-fire feedback outcompetes woody plants if their seedlings are limited.
- Providing non-local seedlings into the domain enhance WP spatial frequency. Depending on the competitive nature of woody plants a threshold cover that alters the grass-fire feedback could emerge, triggering a nonlinear woody plant expansion. A grass-dominated is maintained if the grass-fire feedback remains largely intact.
- Threshold woody plant covers, and catastrophic shifts are related to the formation of fire-resistant woody plant clusters and their coalition that completely impairs the natural grass-fire feedbacks in the beginning of the simulations.
- Our final model experiment illustrates a major impact of the role of parameter uncertainty on the temporal dynamics of the grass-woodland transition, but not the final outcome.

- Modeling of spatial plant interactions and competition processes would require monitoring earth surface and plant changes in long-term field experiments as well as high resolution imagery for time scales of ecosystem significance.

## ACKNOWLEDGEMENTS

This research was supported by the US National Science Foundation through the following grant contracts: ACI-1148305 and OAC-1450412 (Istanbulluoglu), OAC-1147454, OAC-1450409 (Tucker, Hobley), OAC-1450338, EAR-1082 1349375, The Oliver Fund of Tulane University (Gasparini, Hutton), and EAR-1725774 (Barnhart). Landlab version 1.12.0 (https://doi.org/10.5281/zenodo.3753854) was used for the experiments presented in this manuscript. Example driver scripts (Python software and supporting files) used to generate figures are available in the github repository 'pub_nudurupati_etal_wrr' (https://doi.org/10.5281/zenodo.3762947).

## REFERENCES

Anderies, J. M., Janssen, M. A., & Walker, B. H. (2002). Grazing management, resilience, and the dynamics of a fire-driven rangeland system. Ecosystems, 5(1), 23-44.

Archer, S. R., Andersen, E. M., Predick, K. I., Schwinning, S., Steidl, R. J., & Woods, S. R. (2017). Woody plant encroachment: causes and consequences. In Rangeland systems (pp. 25-84). Springer, Cham..

Beer, C., Reichstein, M., Tomelleri, E., Ciais, P., Jung, M., Carvalhais, N., ... & Bondeau, A. (2010). Terrestrial gross carbon dioxide uptake: global distribution and covariation with climate. Science, 329(5993), 834-838.

Berenstein, I. (2012). Pattern formation in a reaction-diffusion-advection system with wave instability. Chaos: An Interdisciplinary Journal of Nonlinear Science, 22(2), 023112.

Bonan, G. B., Williams, M., Fisher, R. A., & Oleson, K. W. (2014). Modeling stomatal conductance in the earth system: linking leaf water-use efficiency and water transport along the soil–plant–atmosphere continuum. Geoscientific Model Development, 7(5), 2193-2222.

Bond, W. J. (2008). What limits trees in C4 grasslands and savannas?. Annual review of ecology, evolution, and systematics, 39, 641-659.

Borgogno, F., D'Odorico, P., Laio, F., & Ridolfi, L. (2009). Mathematical models of vegetation pattern formation in ecohydrology. Reviews of Geophysics, 47(1).

Bohrer, G., Mourad, H., Laursen, T. A., Drewry, D., Avissar, R., Poggi, D., ... & Katul, G. G. (2005). Finite element tree crown hydrodynamics model (FETCH) using porous media flow within branching elements: A new representation of tree hydrodynamics. Water Resources Research, 41(11).

Bowman, D. M., Perry, G. L., & Marston, J. B. (2015). Feedbacks and landscape-level vegetation dynamics. Trends in ecology & evolution, 30(5), 255-260.

Briggs, J. M., Hoch, G. A., & Johnson, L. C. (2002). Assessing the rate, mechanisms, and consequences of the conversion of tallgrass prairie to Juniperus virginiana forest. Ecosystems, 5(6), 578-586.

Briggs, J. M., Knapp, A. K., Blair, J. M., Heisler, J. L., Hoch, G. A., Lett, M. S., & McCarron, J. K. (2005). An ecosystem in transition: causes and consequences of the conversion of mesic grassland to shrubland. BioScience, 55(3), 243-254.

Brown, J. H., Valone, T. J., & Curtin, C. G. (1997). Reorganization of an arid ecosystem in response to recent climate change. Proceedings of the National Academy of Sciences, 94(18), 9729-9733.

Caracciolo, D., Noto, L. V., Istanbulluoglu, E., Fatichi, S., & Zhou, X. (2014). Climate change and Ecotone boundaries: Insights from a cellular automata ecohydrology model in a Mediterranean catchment with topography controlled vegetation patterns. Advances in water resources, 73, 159-175.

Caracciolo, D., Istanbulluoglu, E., Noto, L. V., & Collins, S. L. (2016). Mechanisms of shrub encroachment into Northern Chihuahuan Desert grasslands and impacts of climate change investigated using a cellular automata model. Advances in water resources, 91, 46-62.

Caracciolo, D., Istanbulluoglu, E., & Noto, L. V. (2017). An ecohydrological cellular automata model investigation of juniper tree encroachment in a western North American landscape. Ecosystems, 20(6), 1104-1123.

Carpenter, S. R., Cole, J. J., Pace, M. L., Batt, R., Brock, W. A., Cline, T., ... & Smith, L. (2011). Early warnings of regime shifts: a whole-ecosystem experiment. Science, 332(6033), 1079-1082.

Charley, J. L., & West, N. E. (1975). Plant-induced soil chemical patterns in some shrub-dominated semi-desert ecosystems of Utah. The Journal of Ecology, 945-963.

Colasanti, R. L., Hunt, R., & Watrud, L. (2007). A simple cellular automaton model for high-level vegetation dynamics. Ecological Modelling, 203(3-4), 363-374.

Crampin, E. J., & Maini, P. K. (2001). Reaction-diffusion models for biological pattern formation.

De Gennaro, S., Russo, L., Giannino, F., Pier, L. M., Mazzoleni, S., & Siettos, C. (2018). Analysis of Catastrophic Shifts between Different Moving Vegetation Patterns. Chemical Engineering Transactions, 67, 343-348.

Dunbabin, V. M., Postma, J. A., Schnepf, A., Pagès, L., Javaux, M., Wu, L., ... & Diggle, A. J. (2013). Modelling root–soil interactions using three–dimensional models of root growth, architecture and function. Plant and soil, 372(1-2), 93-124.

D'Odorico, P., Laio, F., & Ridolfi, L. (2006a). A probabilistic analysis of fire-induced tree-grass coexistence in savannas. The American Naturalist, 167(3), E79-E87.

D'Odorico, P., Laio, F., & Ridolfi, L. (2006b). Patterns as indicators of productivity enhancement by facilitation and competition in dryland vegetation. Journal of Geophysical Research: Biogeosciences, 111(G3).

D'Odorico, P., Bhattachan, A., Davis, K. F., Ravi, S., & Runyan, C. W. (2013). Global desertification: drivers and feedbacks. Advances in water resources, 51, 326-344.

D'Odorico, P., Okin, G. S., & Bestelmeyer, B. T. (2012). A synthetic review of feedbacks and drivers of shrub encroachment in arid grasslands. Ecohydrology, 5(5), 520-530.

Donohue, I., Petchey, O. L., Montoya, J. M., Jackson, A. L., McNally, L., Viana, M., ... & Emmerson, M. C. (2013). On the dimensionality of ecological stability. Ecology letters, 16(4), 421-429.

Dormann, S., Deutsch, A., & Lawniczak, A. T. (2001). Fourier analysis of Turing-like pattern formation in cellular automaton models. Future Generation Computer Systems, 17(7), 901-909.

Eagleson, P. S. (2005). Ecohydrology: Darwinian expression of vegetation form and function. Cambridge University Press.

Emanuel, W. R., Shugart, H. H., & Stevenson, M. P. (1985). Climatic change and the broad-scale distribution of terrestrial ecosystem complexes. Climatic change, 7(1), 29-43.

Energy, Minerals, and Natural Resources (2018). 2018 annual report of New Mexico's Energy, Minerals, and Natural Resources annual report. Retreived from http://www.emnrd.state.nm.us/ADMIN/documents/bw2018AR30Feb.pdf.

Fatichi, S., Ivanov, V. Y., & Caporali, E. (2012). A mechanistic ecohydrological model to investigate complex interactions in cold and warm water-controlled environments: 1. Theoretical framework and plot-scale analysis. Journal of Advances in Modeling Earth Systems, 4(2).

Pilar Fernandez-Illescas, C., & Rodriguez-Iturbe, I. (2003). Hydrologically driven hierarchical competition–colonization models: the impact of interannual climate fluctuations. Ecological monographs, 73(2), 207-222.

Flores Cervantes, J. H., Istanbulluoglu, E., Vivoni, E. R., Holifield Collins, C. D., & Bras, R. L. (2014). A geomorphic perspective on terrain-modulated organization of vegetation productivity: Analysis in two semiarid grassland ecosystems in southwestern United States. Ecohydrology, 7(2), 242-257.

Fritz, S. C. (2013). The climate of the Holocene and its landscape and biotic impacts. Tellus B: Chemical and Physical Meteorology, 65(1), 20602.

Finzi, A. C., Austin, A. T., Cleland, E. E., Frey, S. D., Houlton, B. Z., & Wallenstein, M. D. (2011). Responses and feedbacks of coupled biogeochemical cycles to climate change: examples from terrestrial ecosystems. Frontiers in Ecology and the Environment, 9(1), 61-67.

Foster, A. C., Shuman, J. K., Shugart, H. H., Dwire, K. A., Fornwalt, P. J., Sibold, J., & Negron, J. (2017). Validation and application of a forest gap model to the southern Rocky Mountains. Ecological Modelling, 351, 109-128.

Furbish, D. J., Childs, E. M., Haff, P. K., & Schmeeckle, M. W. (2009). Rain splash of soil grains as a stochastic advection-dispersion process, with implications for desert plant-soil interactions and land-surface evolution. Journal of Geophysical Research: Earth Surface, 114(F3).

Greig-Smith, P. (1979). Pattern in vegetation. The Journal of Ecology, 755-779.

Grimm, N. B., Chapin III, F. S., Bierwagen, B., Gonzalez, P., Groffman, P. M., Luo, Y., ... & Schimel, J. (2013). The impacts of climate change on ecosystem structure and function. Frontiers in Ecology and the Environment, 11(9), 474-482.

Grosjean, M., Santoro, C. M., Thompson, L. G., Núñez, L., & Standen, V. G. (2007). Mid-Holocene climate and culture change in the South Central Andes. In Climate Change and Cultural Dynamics (pp. 51-115). Academic Press.

Hanan, N. P., Sea, W. B., Dangelmayr, G., & Govender, N. (2008). Do fires in savannas consume woody biomass? A comment on approaches to modeling savanna dynamics. The American Naturalist, 171(6), 851-856.

HilleRisLambers, R., Rietkerk, M., van den Bosch, F., Prins, H. H., & de Kroon, H. (2001). Vegetation pattern formation in semi-arid grazing systems. Ecology, 82(1), 50-61.

Holling, C. S. (1973). Resilience and stability of ecological systems. Annual review of ecology and systematics, 4(1), 1-23.

Holmgren, C. A., Norris, J., & Betancourt, J. L. (2007). Inferences about winter temperatures and summer rains from the late Quaternary record of C4 perennial grasses and C3 desert shrubs in the northern Chihuahuan Desert. Journal of Quaternary Science: Published for the Quaternary Research Association, 22(2), 141-161.

Ivanov, V. Y., Bras, R. L., & Vivoni, E. R. (2008). Vegetation-hydrology dynamics in complex terrain of semiarid areas: 1. A mechanistic approach to modeling dynamic feedbacks. Water Resources Research, 44(3).

Jackson, W. D. (1968). Fire, air, water and earth–an elemental ecology of Tasmania. In Proceedings of the ecological society of Australia (Vol. 3, No. 9, p. 16).

Javaux, M., Couvreur, V., Vanderborght, J., & Vereecken, H. Root Water Uptake: From 3D Biophysical Processes to Macroscopic Modeling Approaches. Vadose Zone J.

Kidron, G. J., & Aloni, I. (2018). The contrasting effect of biocrusts on shallow-rooted perennial plants (hemicryptophytes): Increasing mortality (through evaporation) or survival (through runoff). Ecohydrology, 11(6), e1912.

Kirschbaum, M. U., Keith, H., Leuning, R., Cleugh, H. A., Jacobsen, K. L., van Gorsel, E., & Raison, R. J. (2007). Modelling net ecosystem carbon and water exchange of a temperate Eucalyptus delegatensis forest using multiple constraints. Agricultural and Forest Meteorology, 145(1-2), 48-68.

Kröpelin, S., Verschuren, D., Lézine, A. M., Eggermont, H., Cocquyt, C., Francus, P., ... & Darius, F. (2008). Climate-driven ecosystem succession in the Sahara: the past 6000 years. science, 320(5877), 765-768.

Laliberte, A. S., Rango, A., Havstad, K. M., Paris, J. F., Beck, R. F., McNeely, R., & Gonzalez, A. L. (2004). Object-oriented image analysis for mapping shrub encroachment from 1937 to 2003 in southern New Mexico. Remote sensing of Environment, 93(1-2), 198-210.

Lanzer, A. T. S., & Pillar, V. D. (2002). Probabilistic cellular automaton: model and application to vegetation dynamics. Community Ecology, 3(2), 159-167.

Lefever, R., & Lejeune, O. (1997). On the origin of tiger bush. Bulletin of Mathematical biology, 59(2), 263-294.

Li, J., Wang, G., Allison, S. D., Mayes, M. A., & Luo, Y. (2014). Soil carbon sensitivity to temperature and carbon use efficiency compared across microbial-ecosystem models of varying complexity. Biogeochemistry, 119(1-3), 67-84.

Littell, J. S., McKenzie, D., Peterson, D. L., & Westerling, A. L. (2009). Climate and wildfire area burned in western US ecoprovinces, 1916–2003. Ecological Applications, 19(4), 1003-1021.

Competition for light between individual trees lowers reference canopy stomatal conductance: results from a model.

Machadoa, K. S., & Froehnerb, S. (2016). Effect of the Little Ice Age on Climate and Vegetation Recorded by n-Alkanes and Glycerol Dialkyl Glycerol Tetraether Proxies. 7: 331. doi: 10.4172/2157-7617.1000331 Page 2 of 8 Volume 7• Issue 2• 1000331 J Earth Sci Clim Change ISSN: 2157-7617 JESCC, an open access journal Tamandare, Curitiba, and Araucaria (Figure 1). The river is, 67.

Mackay, D. S., Roberts, D. E., Ewers, B. E., Sperry, J. S., McDowell, N. G., & Pockman, W. T. (2015). Interdependence of chronic hydraulic dysfunction and canopy processes can improve integrated models of tree response to drought. Water Resources Research, 51(8), 6156-6176.

Martínez-García, R., Calabrese, J. M., Hernández-García, E., & López, C. (2014). Minimal mechanisms for vegetation patterns in semiarid regions. Philosophical Transactions of the Royal Society A: Mathematical, Physical and Engineering Sciences, 372(2027), 20140068.

May, R. M. (1977). Thresholds and breakpoints in ecosystems with a multiplicity of stable states. Nature, 269(5628), 471-477.

Machadoa, K. S., & Froehnerb, S. (2016). Effect of the Little Ice Age on Climate and Vegetation Recorded by n-Alkanes and Glycerol Dialkyl Glycerol Tetraether Proxies. 7: 331. doi: 10.4172/2157-7617.1000331 Page 2 of 8 Volume 7, Issue 2, 1000331 J Earth Sci Clim Change ISSN: 2157-7617 JESCC, an open access journal Tamandare, Curitiba, and Araucaria (Figure 1). The river is, 67.

Miller, R. F., & Rose, J. A. (1999). Fire history and western juniper encroachment in sagebrush steppe. Journal of Range Management, 550-559.

Miller, R. F., Svejcar, T. J., & Rose, J. A. (2000). Impacts of western juniper on plant community composition and structure. Rangeland Ecology & Management/Journal of Range Management Archives, 53(6), 574-585.

Miller, R. F., Bates, J. D., Svejcar, T. J., Pierson, F. B., & Eddleman, L. E. (2005). Biology, ecology, and management of western juniper. Tech. Bull, 152.

Montaldo, N., Rondena, R., Albertson, J. D., & Mancini, M. (2005). Parsimonious modeling of vegetation dynamics for ecohydrologic studies of water-limited ecosystems. Water Resources Research, 41(10).

Murray, J. D. (2002). Mathematical Biology, Volume I, An Introduction.

Murray, J. D., & Maini, P. K. (1989). Pattern formation mechanisms–a comparison of reaction-diffusion and mechanochemical models. In Cell to Cell Signalling (pp. 159-170). Academic Press.

Myers-Smith, I. H., Forbes, B. C., Wilmking, M., Hallinger, M., Lantz, T., Blok, D., ... & Boudreau, S. (2011). Shrub expansion in tundra ecosystems: dynamics, impacts and research priorities. Environmental Research Letters, 6(4), 045509.

Nikinmaa, E., Sievänen, R., & Hölttä, T. (2014). Dynamics of leaf gas exchange, xylem and phloem transport, water potential and carbohydrate concentration in a realistic 3-D model tree crown. Annals of botany, 114(4), 653-666.

Okin, G. S., D'Odorico, P., & Archer, S. R. (2009). Impact of feedbacks on Chihuahuan desert grasslands: transience and metastability. Journal of Geophysical Research: Biogeosciences, 114(G1).

Okin, G. S., & Gillette, D. A. (2001). Distribution of vegetation in wind-dominated landscapes: Implications for wind erosion modeling and landscape processes. Journal of Geophysical Research: Atmospheres, 106(D9), 9673-9683.

Parsons, D. J. (1976). Vegetation structure in the mediterranean scrub communities of California and Chile. The Journal of Ecology, 435-447.

Pelletier, J. D., Barron-Gafford, G. A., Gutiérrez-Jurado, H., Hinckley, E. L. S., Istanbulluoglu, E., McGuire, L. A., ... & Swetnam, T. L. (2018). Which way do you lean? Using slope aspect variations to understand Critical Zone processes and feedbacks. Earth Surface Processes and Landforms, 43(5), 1133-1154.

Pelletier, J. D., Nichols, M. H., & Nearing, M. A. (2016). The influence of Holocene vegetation changes on topography and erosion rates: A case study at Walnut Gulch Experimental Watershed, Arizona.

Puttock, A., Dungait, J. A., Macleod, C. J., Bol, R., & Brazier, R. E. (2014). Woody plant encroachment into grasslands leads to accelerated erosion of previously stable organic carbon from dryland soils. Journal of Geophysical Research: Biogeosciences, 119(12), 2345-2357.

Quillet, A., Peng, C., & Garneau, M. (2010). Toward dynamic global vegetation models for simulating vegetation–climate interactions and feedbacks: recent developments, limitations, and future challenges. Environmental Reviews, 18(NA), 333-353.

Ratajczak, Z., Nippert, J. B., Briggs, J. M., & Blair, J. M. (2014). Fire dynamics distinguish grasslands, shrublands and woodlands as alternative attractors in the Central Great Plains of North America. Journal of Ecology, 102(6), 1374-1385.

Ratajczak, Z., Nippert, J. B., & Ocheltree, T. W. (2014). Abrupt transition of mesic grassland to shrubland: evidence for thresholds, alternative attractors, and regime shifts. Ecology, 95(9), 2633-2645.

Ravi, S., D'Odorico, P., Herbert, B., Zobeck, T., & Over, T. M. (2006). Enhancement of wind erosion by fire-induced water repellency. Water Resources Research, 42(11).

Ravi, S., D'Odorico, P., & Okin, G. S. (2007). Hydrologic and aeolian controls on vegetation patterns in arid landscapes. Geophysical Research Letters, 34(24).

Ravi, S., & D'Odorico, P. (2009). Post-fire resource redistribution and fertility island dynamics in shrub encroached desert grasslands: a modeling approach. Landscape Ecology, 24(3), 325-335.

Rietkerk, M., Boerlijst, M. C., van Langevelde, F., HilleRisLambers, R., de Koppel, J. V., Kumar, L., ... & de Roos, A. M. (2002). Self-organization of vegetation in arid ecosystems. The American Naturalist, 160(4), 524-530.

Rodríguez-Iturbe, I., & Porporato, A. (2007). Ecohydrology of water-controlled ecosystems: soil moisture and plant dynamics. Cambridge University Press.

Saco, P.M, Willgoose, G.R, and G.R. Hancock (2007). Eco-geomorphology of banded vegetation patterns in arid and semi-arid regions. Hydrology and Earth System Sciences 11, 1717–1730.

Saco, P. M., & Moreno-de las Heras, M. (2013). Ecogeomorphic coevolution of semiarid hillslopes: Emergence of banded and striped vegetation patterns through interaction of biotic and abiotic processes. Water Resources Research, 49(1), 115-126.

Sagués, F., Sancho, J. M., & García-Ojalvo, J. (2007). Spatiotemporal order out of noise. Reviews of Modern Physics, 79(3), 829.

Sankaran, M., Hanan, N. P., Scholes, R. J., Ratnam, J., Augustine, D. J., Cade, B. S., ... & Ardo, J. (2005). Determinants of woody cover in African savannas. Nature, 438(7069), 846-849.

Scanlon, T. M., Caylor, K. K., Levin, S. A., & Rodriguez-Iturbe, I. (2007). Positive feedbacks promote power-law clustering of Kalahari vegetation. Nature, 449(7159), 209-212.

Scheffer, M., Carpenter, S., Foley, J. A., Folke, C., & Walker, B. (2001). Catastrophic shifts in ecosystems. Nature, 413(6856), 591-596.

Schlesinger, W. H., Reynolds, J. F., Cunningham, G. L., Huenneke, L. F., Jarrell, W. M., Virginia, R. A., & Whitford, W. G. (1990). Biological feedbacks in global desertification. Science, 247(4946), 1043-1048.

Sherratt, J. A. (2005). An analysis of vegetation stripe formation in semi-arid landscapes. Journal of mathematical biology, 51(2), 183-197.

Shugart, H. H., Wang, B., Fischer, R., Ma, J., Fang, J., Yan, X., ... & Armstrong, A. H. (2018). Gap models and their individual-based relatives in the assessment of the consequences of global change. Environmental Research Letters, 13(3), 033001.

Stewart, J., Parsons, A. J., Wainwright, J., Okin, G. S., Bestelmeyer, B. T., Fredrickson, E. L., & Schlesinger, W. H. (2014). Modeling emergent patterns of dynamic desert ecosystems. Ecological Monographs, 84(3), 373-410.

Stevens, N., Lehmann, C. E., Murphy, B. P., & Durigan, G. (2017). Savanna woody encroachment is widespread across three continents. Global change biology, 23(1), 235-244. Symstad, A. J., & Leis, S. A. (2017). Woody encroachment in northern great plains grasslands: perceptions, actions, and needs. Natural areas journal, 37(1), 118-127.

Tague, C. L., & Band, L. E. (2004). RHESSys: Regional Hydro-Ecologic Simulation System—An object-oriented approach to spatially distributed modeling of carbon, water, and nutrient cycling. Earth interactions, 8(19), 1-42.

Tague, C. L., McDowell, N. G., & Allen, C. D. (2013). An integrated model of environmental effects on growth, carbohydrate balance, and mortality of Pinus ponderosa forests in the southern Rocky Mountains. PLoS One, 8(11).

Thompson, S. E., Assouline, S., Chen, L., Trahktenbrot, A., Svoray, T., & Katul, G. G. (2014). Secondary dispersal driven by overland flow in drylands: Review and mechanistic model development. Movement ecology, 2(1), 7.

Thompson, S., Katul, G., & McMahon, S. M. (2008). Role of biomass spread in vegetation pattern formation within arid ecosystems. Water Resources Research, 44(10).

Tilman, D. (1994). Competition and biodiversity in spatially structured habitats. Ecology, 75(1), 2-16.

Touboul, J. D., Staver, A. C., & Levin, S. A. (2018). On the complex dynamics of savanna landscapes. Proceedings of the National Academy of Sciences, 115(7), E1336-E1345.

Turing, A. M. (1990). The chemical basis of morphogenesis. Bulletin of mathematical biology, 52(1-2), 153-197.

Van Wijk, M. T., & Rodriguez-Iturbe, I. (2002). Tree-grass competition in space and time: Insights from a simple cellular automata model based on ecohydrological dynamics. Water Resources Research, 38(9), 18-1.

Venter, Z. S., Cramer, M. D., & Hawkins, H. J. (2018). Drivers of woody plant encroachment over Africa. Nature communications, 9(1), 1-7.

Vincenot, C. E., Carteni, F., Mazzoleni, S., Rietkerk, M., & Giannino, F. (2016). Spatial self-organization of vegetation subject to climatic stress—insights from a system dynamics—individual-based hybrid model. Frontiers in plant science, 7, 636.

Wang, G., Li, J., & Ravi, S. (2019). A combined grazing and fire management may reverse woody shrub encroachment in desert grasslands. Landscape Ecology, 34(8), 2017-2031.

Waters, M. R., & Haynes, C. V. (2001). Late Quaternary arroyo formation and climate change in the American Southwest. Geology, 29(5), 399-402.

Watt, A. S. (1947). Pattern and process in the plant community. Journal of ecology, 35(1/2), 1-22.

Wenzel, S., Cox, P. M., Eyring, V., & Friedlingstein, P. (2014). Emergent constraints on climate-carbon cycle feedbacks in the CMIP5 Earth system models. Journal of Geophysical Research: Biogeosciences, 119(5), 794-807.

Wieder, W. R., Bonan, G. B., & Allison, S. D. (2013). Global soil carbon projections are improved by modelling microbial processes. Nature Climate Change, 3(10), 909-912.

Whitlock, C., Shafer, S. L., & Marlon, J. (2003). The role of climate and vegetation change in shaping past and future fire regimes in the northwestern US and the implications for ecosystem management. Forest ecology and management, 178(1-2), 5-21.

Worman, S. L., & Furbish, D. J. (2019). A probabilistic, biologically informed model of desert shrub population dynamics with the granularity appropriate for geomorphic simulations. Earth Surface Processes and Landforms, 44(6), 1221-1232..

Woodward, F. I., Lomas, M. R., & Kelly, C. K. (2004). Global climate and the distribution of plant biomes. Philosophical Transactions of the Royal Society of London. Series B: Biological Sciences, 359(1450), 1465-1476.

Wu, L., McGechan, M. B., McRoberts, N., Baddeley, J. A., & Watson, C. A. (2007). SPACSYS: integration of a 3D root architecture component to carbon, nitrogen and water cycling—model description. Ecological Modelling, 200(3-4), 343-359.

Zhou, X., Istanbulluoglu, E., & Vivoni, E. R. (2013). Modeling the ecohydrological role of aspect-controlled radiation on tree-grass-shrub coexistence in a semiarid climate. Water Resources Research, 49(5), 2872-2895.

SUPPORTING INFORMATION

# On Transient semi-arid ecosystem dynamics using Landlab

**Sai S. Nudurupati[1], Erkan Istanbulluoglu[1], Gregory E. Tucker[2,3,4], Nicole M. Gasparini[4], Daniel E. J. Hobley[6], Eric W. H. Hutton[3], Katherine R. Barnhart[2,3], and Jordan M. Adams[7]**

[1]Department of Civil & Environmental Engineering, University of Washington, Seattle, WA, USA

[2]Department of Geological Sciences, University of Colorado, Boulder, CO, USA

[3]Community Surface Dynamics Modeling System (CSDMS), University of Colorado, Boulder, USA

[4]Cooperative Institute for Research in Environmental Sciences (CIRES), University of Colorado, Boulder, USA

[5]Department of Earth and Environmental Sciences, Tulane University, New Orleans, USA

[6]School of Earth and Ocean Sciences, Cardiff University, Cardiff, UK

[7]Division of Science & Math, Delgado Community College, New Orleans, USA

## Introduction

Input parameters used for models used in the simulations presented in the manuscript are provided here as supplementary information in Tables S1 through S7. Algorithms used for selected methods used in the components *ResourceRedistribution* and *SpatialDisturbance* are presented in Figures S1 through S7.

Table S 1: Plant parameters used as inputs for Model A.

| Parameter | Description | units | Grass | Shrub | Tree |
|---|---|---|---|---|---|
| VEGTYPE_(pft) | Zhou et al. 2013 PFT | | 0 | 1 | 2 |
| percent_(pft)_initial | Initial vegetation cover | % | 25 | 25 | 25 |
| intercept_cap_(pft) | Full canopy interception | mm | 0 | 0 | 0 |
| zr_(pft) | Root depth | m | 0.3 | 0.6 | 1.3 |
| I_V_(pft) | Infiltration capacity of vegetated soil | mm/h | 24 | 40 | 40 |
| sc_(pft) | Saturation degree at stomata closure | - | 0.33 | 0.33 | 0.33 |
| wp_(pft) | Saturation degree at wilting point | - | 0.13 | 0.13 | 0.15 |
| hgw_(pft) | Saturation degree at hydgroscopic point | - | 0.1 | 0.1 | 0.1 |
| GT, DT | Growth and Dormancy thresholds | mm/d | 3.8, 6.8 | N/A | N/A |
| w | conversion factor of CO2 to dry biomass | Kg DM/Kg CO2 | 0.55 | | |
| Tdmax | Constant for dead biomass loss adjustment | mm/d | 10 | | |
| WUE_(pft) | Water use efficiency | KgCO2/KgH2O | 0.01 | 0.0025 | 0.0045 |
| cb_(pft) | Specific leaf area for green/live biomass | m2 leaf/g DM | 0.0047 | 0.004 | 0.004 |
| cd_(pft) | Specific leaf area for dead biomass | m2 leaf/g DM | 0.009 | 0.01 | 0.01 |
| ksg_(pft) | Senescence coefficient of green/live biomass | d^-1 | 0.012 | 0.002 | 0.002 |
| kdd_(pft) | Decay coefficient of aboveground dead biomass | d^-1 | 0.013 | 0.013 | 0.013 |
| kws_(pft) | Maximum drought induced foliage loss rate | d^-1 | 0.02 | 0.02 | 0.01 |
| LAI_max_(pft) | Maximum leaf area index | m2/m2 | 2 | 2 | 4 |
| LAIR_max_(pft) | Reference leaf area index | m2/m2 | 2 | 2 | 4 |

Table S 2: Plant establishment and mortality parameters used as inputs for Model A.

| Description | units | Grass | Shrub | Tree | Shrub Seedling | Tree Seedling |
|---|---|---|---|---|---|---|
| Maximum establishment probability | - | 0.35 | 0.16 | 0.21 | N/A | N/A |
| Allelopathic effect of shrubs on grass | - | 2 | N/A | N/A | N/A | N/A |
| Drought resistance threshold | - | 0.65 | 0.76 | 0.71 | 0.63 | 0.6 |
| Probability of background mortality | - | 0.05 | 0.01 | 0.011 | 0.03 | 0.03 |
| Maximum age | yr | N/A | 600 | 350 | 18 | 20 |

Table S 3: Potential evapotranspiration parameters used as inputs for Model A.

| Parameter | Description | units | Value |
|---|---|---|---|
| PET_method | PET method | | Cosine |
| LT | Lag between peak TmaxF and solar forcing | days | 0 |
| Δd | Calibrated difference between max & min daily TmaxF | mm/d | 7 |
| Nd | Number of days in year | days | 365 |
| Mean TmaxF_grass | Plant maximum transpiration rate for Grass | mm/d | 4.96 |
| Mean TmaxF_shrub | Plant maximum transpiration rate for Shrubs | mm/d | 3.77 |
| Mean TmaxF_tree | Plant maximum transpiration rate for Trees | mm/d | 5.15 |
| f_bare | fraction of maximum transpiration rate | | 0.7 |

Table S 4: Soil parameters used as inputs for Model A.

| Parameter | Description | units | Value |
|---|---|---|---|
| Soil type | Sandy loam | | |
| I_B | Infiltration capacity of bare soil | mm/h | 20 |
| K_s | Hydraulic conductivity | mm/h | 42 |
| pc | Soil Porosity | - | 0.43 |
| fc | Soil Field Capacity | - | 0.56 |
| b | Water retention parameter | - | 4.9 |

Table S 5: Input parameters for stochastic rainfall simulator for simulations presented in Figures 4 & 5.

| Parameter | Description | units | dry | wet |
|---|---|---|---|---|
| mean_storm_(season) | storm duration | hours | 0.48 | 0.46 |
| mean_interstorm_(season) | interstorm duration | hours | 159.36 | 84.24 |
| mean_storm_depth_(season) | storm depth | mm | 3.07 | 4.79 |
| doy__start_of_monsoon | | | | 182 |
| doy__end_of_monsoon | | | | 273 |

Table S 6: Model inputs for Model B.

| Parameter | Description | No Grazing | Grazing |
|---|---|---|---|
| VEGTYPE | Ravi et al. 2013 PFT | | |
| percent_grass | initial grass vegetation cover (%) | 30 | |
| percent_shrub | initial shrub vegetation cover (%) | 40 | |
| e | soil erosion at bare soil cell (-) | 0.1 | |
| R_low_threshold | Minimum value of R (-) | -2 | |
| R_threshold | Maximum value of R (-) | 2 | |
| R_dep_threshold | threshold for deposition during adjustment (-) | 2 | |
| Rth_gr | Minimum R for establishment of Grass (-) | 0.4 | |
| Rth_sh | Minimum R for establishment of Shrub (-) | 0.8 | |
| P_gr_regrwth | Probability of grass regrowth in burnt grass patches (-) | 0.5 | |
| P_sh_regrwth | Probability of shrub regrowth in burnt shrub patches (-) | 0.25 | |
| Pen | Probability of shrub establishment (neighborhood) (-) | 0.05 | |
| Pgrz | Probability of shrub establishment (seed dispersal due to herbivores) (-) | 0.001 | 0.01 |
| P_gr | Probability of grass establishment (-) | 0.5 | |
| sh_max_age | Maximum age of shrubs (yr) | 600 | |
| sh_seedling_max_age | Maximum age of shrub seedlings (yr) | 18 | |
| sh_seedling_mor_dis | Probability of mortality of shrub seedlings due to disease (-) | 0 | |
| sh_mor_dis_low_thresh_age | Age at which shrubs start experiencing disease (yr) | 600 | |
| sh_mor_dis_low_slp | Probability of mortality of shrubs due to disease at sh_mor_dis_low_thresh_age (-) | 0.01 | |
| sh_mor_dis_high_slp | Probability of mortality of shrubs due to disease at sh_max_age (-) | 0.99 | |
| P_sh_fire_mor | Probability of shrub mortality due to fire (-) | 0.75 | |
| P_gr_fire_mor | Probability of grass mortality due to fire (-) | 1 | |
| sh_mor_ws_thresh | Background mortality probability of shrubs due to waterstress (P_mor_ws) (-) | 0.01 | |
| gr_mor_ws_thresh | Background mortality probability of grass due to waterstress (-) | 0.08 | |
| stoc_fire_extent_min | Mininum area of the sample for fire (m^2/m^2) | 0.089 | |
| stoc_fire_extent_max | Maximum area of the sample for fire (m^2/m^2) | 0.09 | |
| | resultant maximum fire area for each fire | ~9% | |
| no_fires_per_year_min | | 2 | |
| no_fires_per_year_max | | 3 | |
| P1 | Grazing Pressure (-) | 0% | 20% |
| sh_susc | probability of shrubs catching fire from a neighbor (-) | 0.5 | |
| gr_susc | probability of grass catching fire from a neighbor (-) | 1 | |

Table S 7: Model C input parameters for simulations presented in Figures 7 & 8.

| Parameter | Description | units | Value |
|---|---|---|---|
| n_fires | number of fires | - | 1 or 2 per year |
| fire_area_mean | mean area of uniform distribution to sample fire size w.r.t to watershed area | $m^2/m^2$ | 0.1-0.2 |
| gr_susc | susceptibility of grass to fire | - | 0.9 |
| sh_susc | susceptibility of shrub to fire | - | 0.5 |
| tr_susc | susceptibility of tree to fire | - | 0.4 |
| sh_seed_susc | susceptibility of shrub seedling to fire | - | 0.6 |
| tr_seed_susc | susceptibility of tree seedling to fire | - | 0.5 |
| gr_vuln | probability of grass cell to catch fire due to lightning | - | 0.9 |
| sh_vuln | probability of shrub cell to catch fire due to lightning | - | 0.5 |
| tr_vuln | probability of tree cell to catch fire due to lightning | - | 0.4 |
| sh_seed_vuln | probability of shrub seedling cell to catch fire due to lightning | - | 0.6 |
| tr_seed_vuln | probability of tree seedling cell to catch fire due to lightning | - | 0.5 |

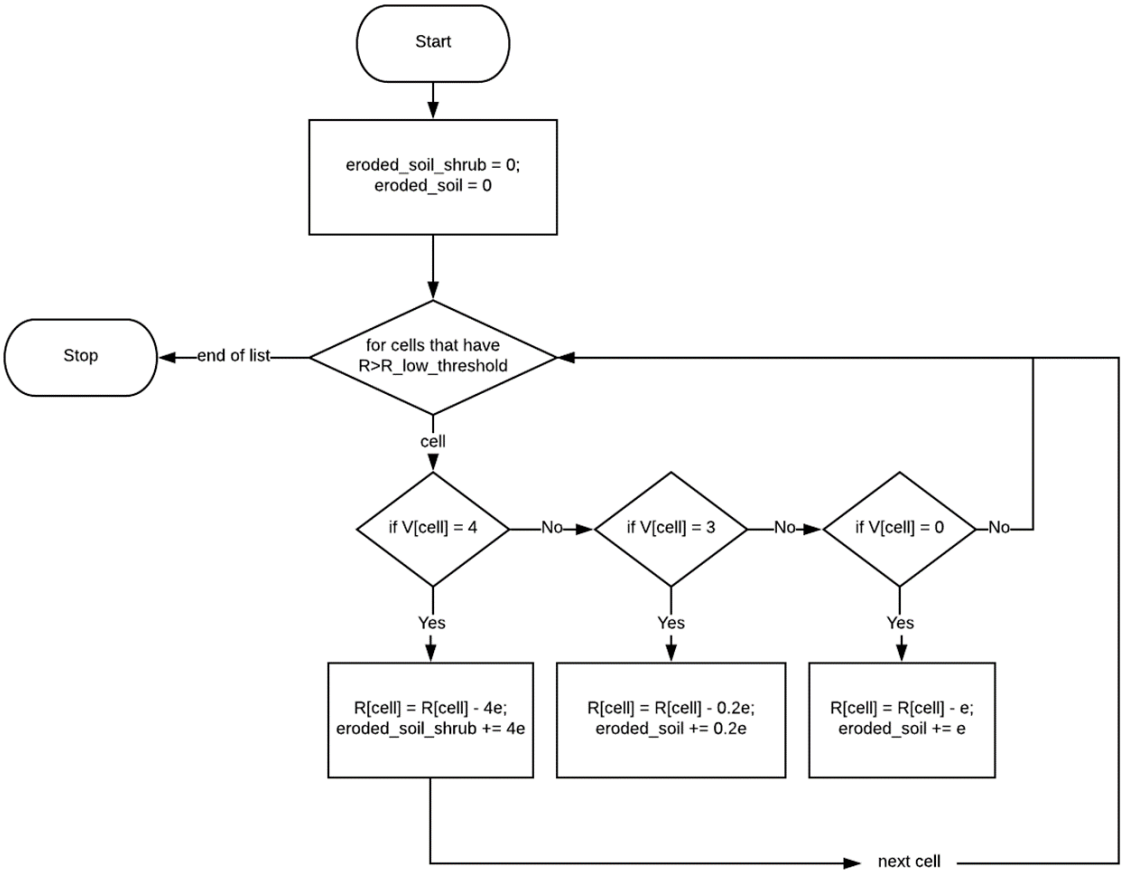


Figure S 1: Algorithm for the method ResourceRedistribution.erode()

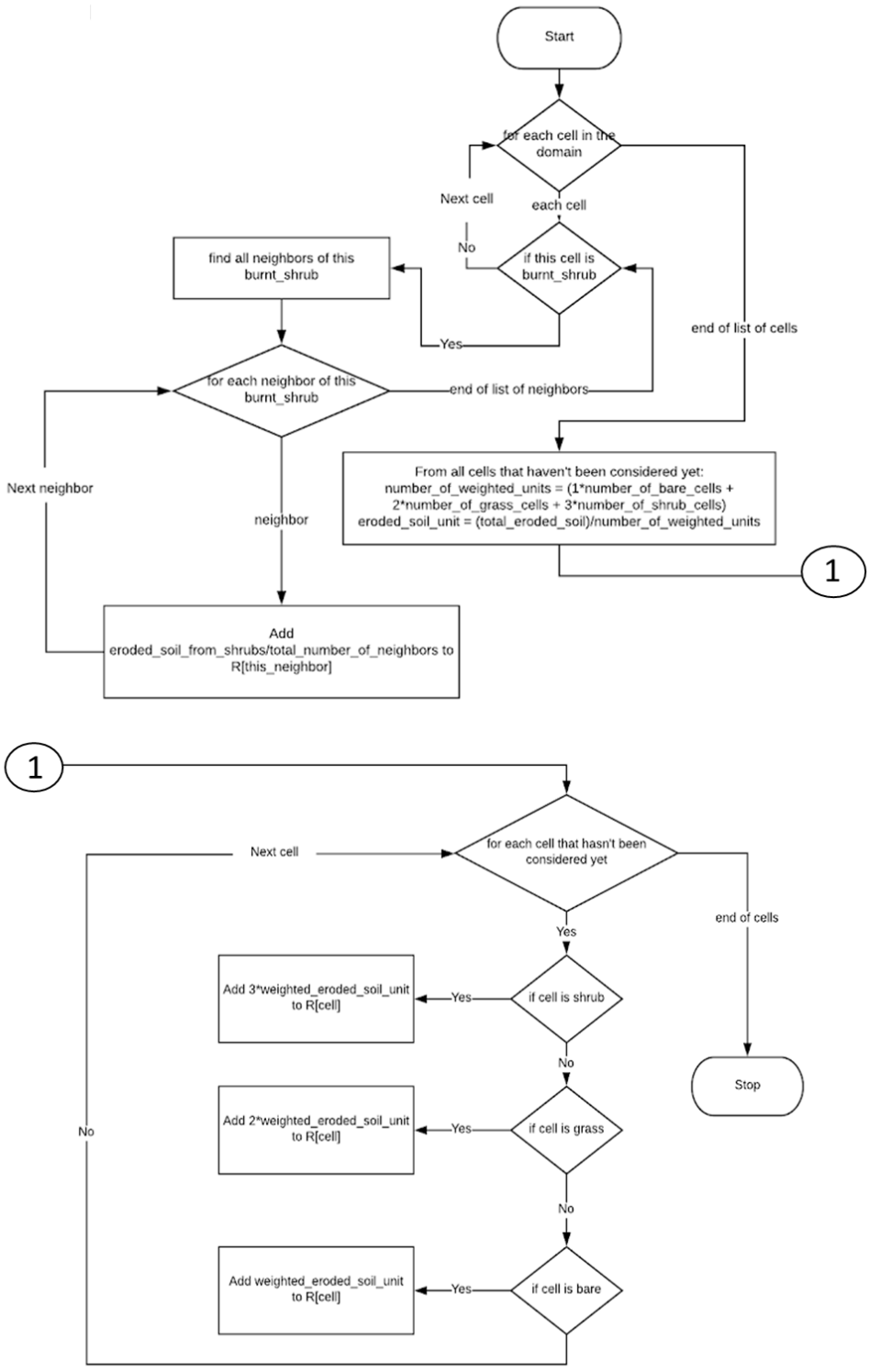


Figure S 2: Algorithm for the method ResourceRedistribution.deposit()

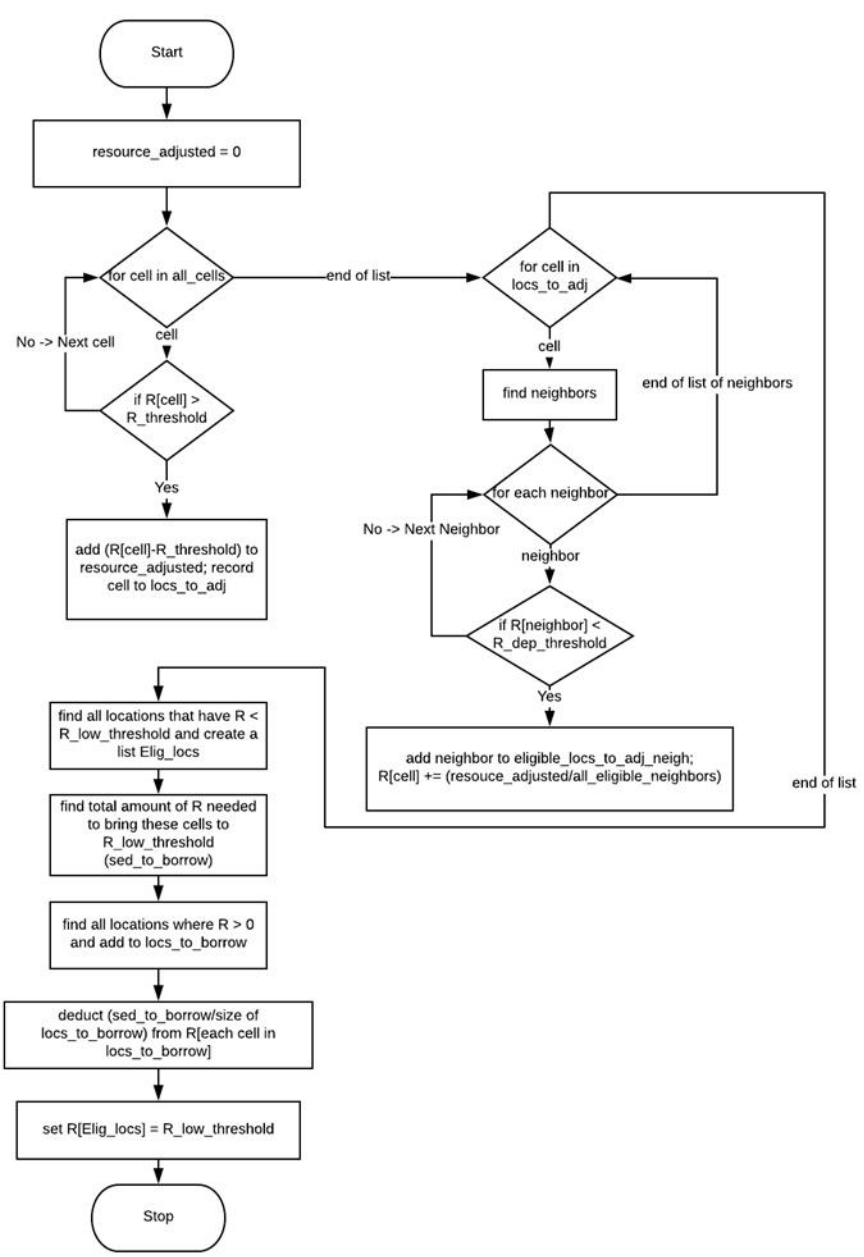


Figure S 3: Algorithm for the method ResourceRedistribution.re_adjust_resource().

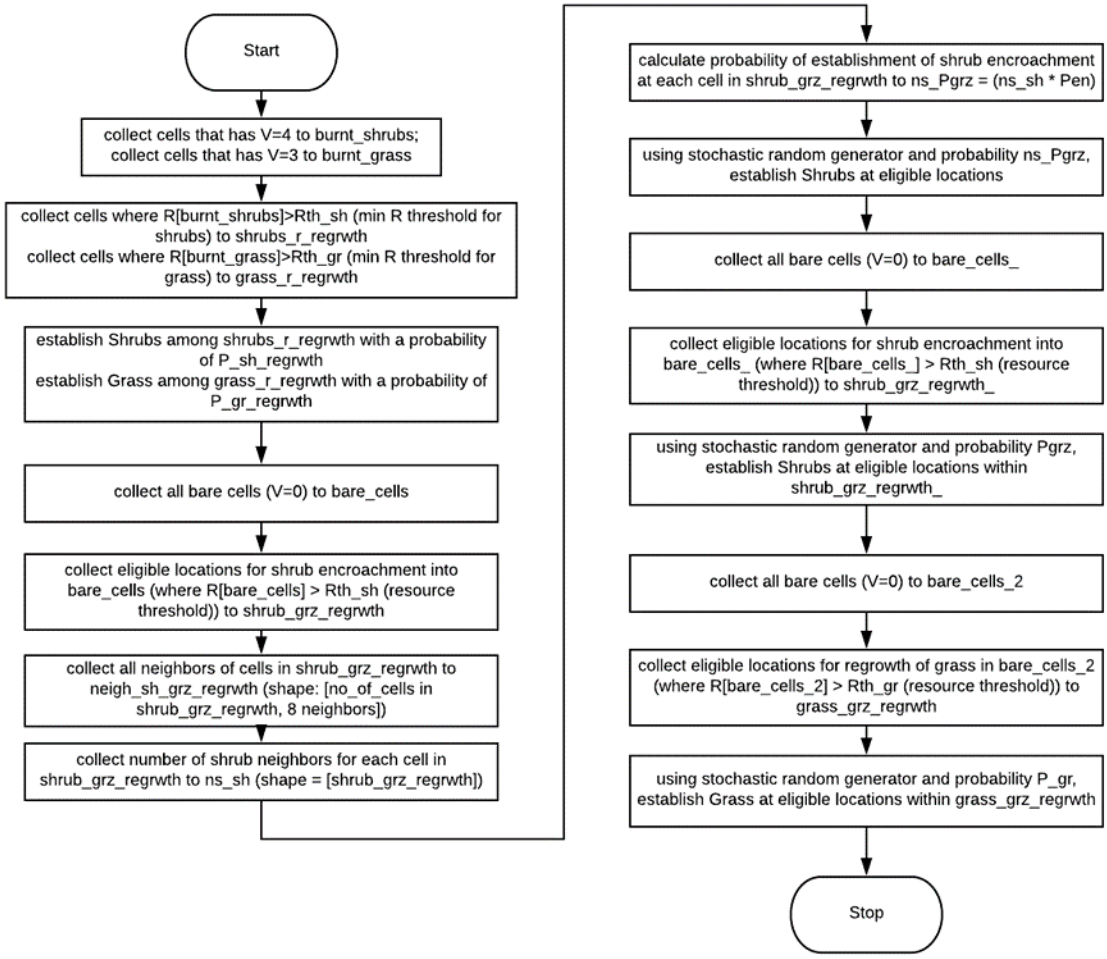


Figure S 4: Algorithm for ResourceRedistribution.establish().

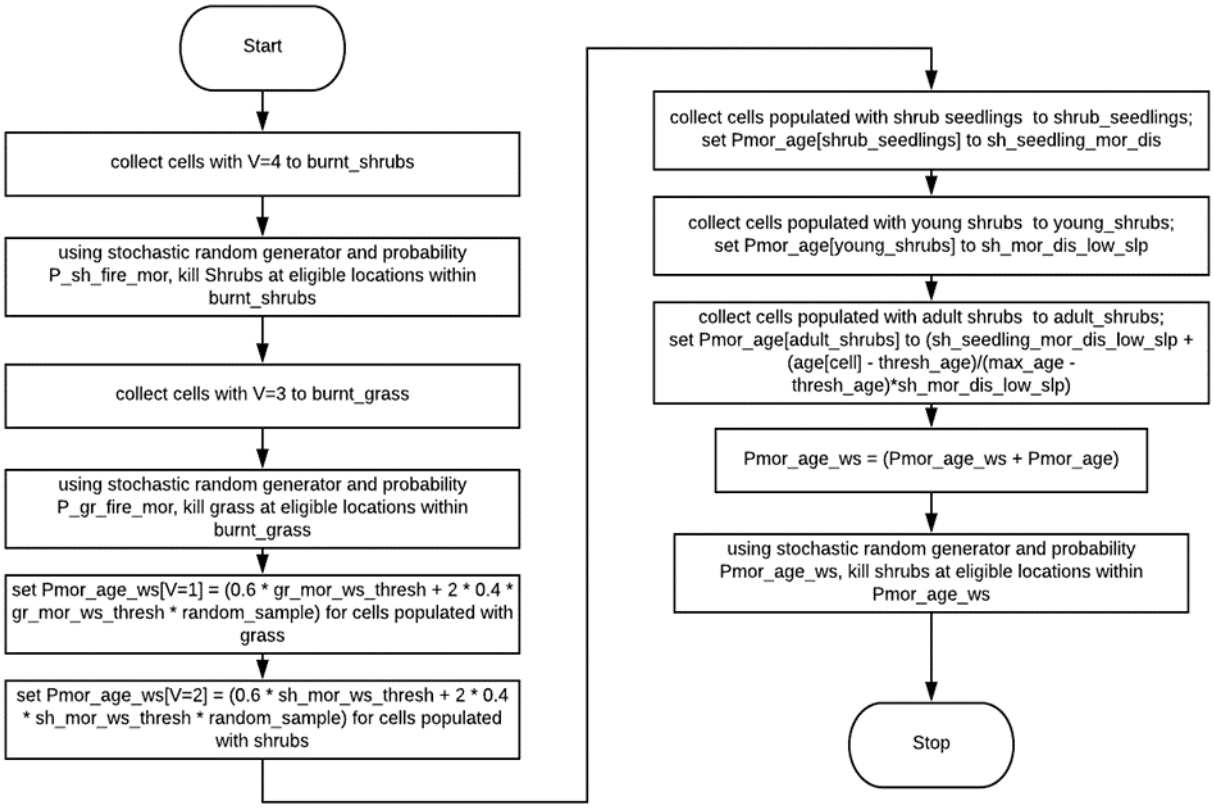


Figure S 5: Algorithm for ResourceRedistribution.mortality().

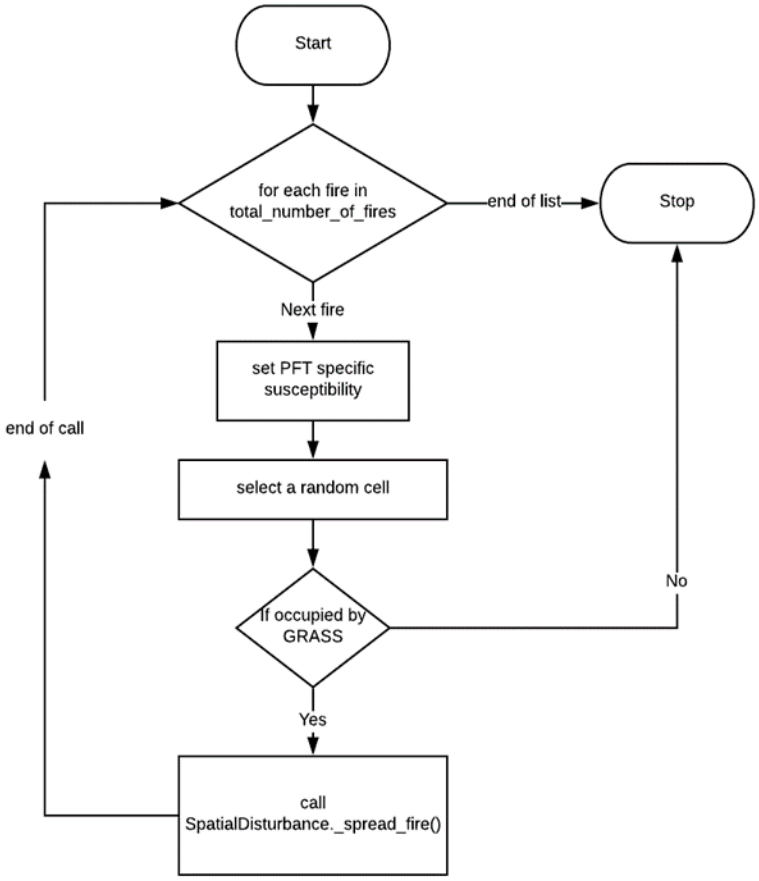


Figure S 6: Algorithm for SpatialDisturbance.initiate_fires().

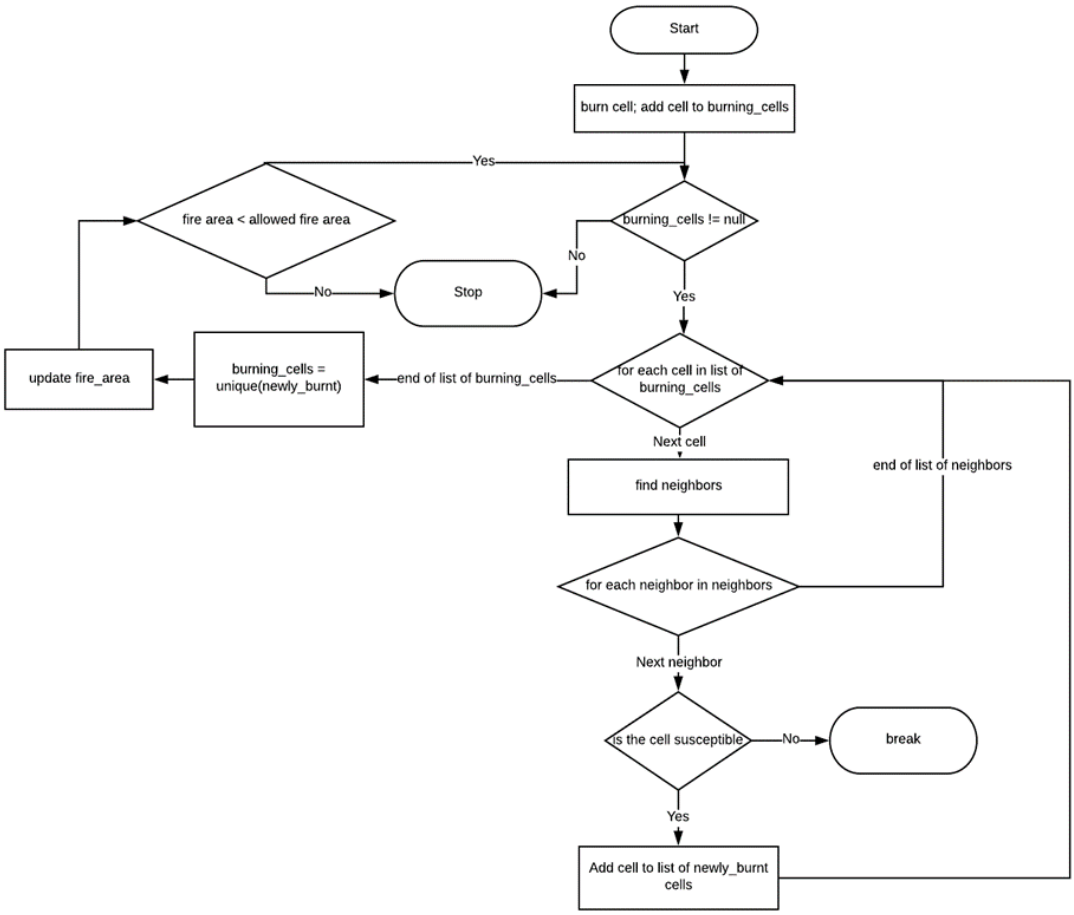


Figure S 7: Algorithm for SpatialDisturbance._spread_fire().

# Chapter 4. PREDICTING TRANSIENT ECOSYSTEM RESPONSE TO CLIMATE VARIABILITY SINCE LATE PLEISTOCENE

This chapter is currently under preparation for submittal to a journal.

Coauthor: Erkan Istanbulluoglu

## 4.1 INTRODUCTION

During last glacial cycle that peaked ~18,000 years (B.P.) in the Late Pleistocene, the southwestern United States was much wetter and cooler than in the Holocene (last 11,000 years) and today. In the arid interior of North America, the remains of plant and animals preserved for tens of thousands of years in urine-cemented and fossilized packrat (Neotoma spp.) middens have been used with radiocarbon dating and analyzed to reconstruct vegetation type and species history of the past climates (e.g., Betancourt et al., 1990).

Southwestern landscapes have changed dramatically since the end of the last ice age, 12,000 years ago. During the last ice age, desert vegetation was restricted to the lower elevations (<300 m) in Death Valley and the mouth of the Colorado River. Sonoran Desert plants such as the giant cactus, saguaro (Carnegiea gigantea) and the palo verde (Cercidium) were located far south into Mexico. Creosotebush (Larrea tridentata), currently the dominant shrub of the Chihuahuan, Sonoran and Mojave deserts, had its northernmost populations along the Arizona-Sonora border. Current desert elevations of the Southwestern US (300-1700 m) were extensively covered by piñon-juniper-oak woodlands, which are now only restricted to cooler highland, while higher elevations were dominated by spruce–fir, mixed-conifer, and subalpine forests (Betancourt et al., 1990; Thompson et al., 1993). The modern climate regime was developed ~4000 years ago, which led to creosote bush establishment in the Sevilleta National Wildlife Refuge (SNWR) and a mix of shrubs and grasses in desert elevations (Holmgren et al., 2007). Strong evidence shows that this climate transition and vegetation change enhanced erosion activity in the region. For example, arroyo formation and cut and fill cycles first began around 8000 yr BP, and intensified in the past 4000 years (Waters and Haynes, 2001).

Reconstruction of past climates is necessary to develop quantitative analysis of ecosystem response to climate change. Hydroclimatic change studies that focus large regions to continents have used an array of methods, combining paleoclimate proxy records from lakes (Fritz et al., 1991; 2013), speleothems, groundwater deposits, packrat middens (Betancourt et al., 1990: Holmgren et al., 2007), change in glaciers thicknesses and an ensemble of climate simulations (e.g., Oster et al., 2015). Such studies provide broader predictions of a general trends and

regional variations in the past climate in relation to historical vegetation change. A growing number of studies in the semiarid and arid regions of the Western US have combined several lines of information including dependence between July temperatures and C4 species proportion (e.g., Terri and Stowe, 1976), and the signature of C4 species on carbon-13 (δ13C: isotopic signature of 13C/12C) in soils and sedimentary deposits, and correlations between annual temperature and precipitation, such that a proxy estimate of one can be used to estimate the other (Nordt et al., 2007, 2008; Hall and Penner, 2013).

Paleo-ecological records show emergence of shrub PFT in Middle Holocene and their establishment around 4,000 – 5,000 yr BP in the Southwestern USA, while C3 Juniper trees and C4 grasses have been present in the region through the Pleistocene and Holocene. Emergence of shrubs is attributed to warm and dry conditions as well as the northward migration of shrub plants, making seeds and seedlings available for establishment. Since around 1850 around the time of Euro-America settlements, extensive observations have been reported on conversion of grasslands into woodlands. *Can vegetation change be attributed to climate variability since the Late Pleistocene?*

Predicting transient ecosystem response is difficult as the rate of change in species composition is tightly related to the spatial dynamics of plant mortality, establishment, and plant competition which have not been adequately represented in distributed ecohydrology models (e.g., Fatichi et al., 2017). Most recently developed ecohydrology models are fairly sophisticated in their handling of water, energy, and carbon balance and thus not suitable for long-term simulations over Paleoclimatic epochs. In this study we use ecohydrology components of the Landlab earth surface modeling toolkit (Hobley et al., 2017; Nudurupati et al., 2020) to investigate the role of historical climate variability on ecosystem change since late Pleistocene in central New Mexico, USA. Landlab is suitable for Paleoclimatic time-scale simulations due to its analytical handling of water and carbon balance following each storm. The model is driven by reconstructed time series of precipitation and temperature from Hall and Penner (2013).

## 4.2 METHODS

The configuration of Landlab components used to construct our model is given in the model workflow diagram (Figure 4-1). We couple daily local soil moisture and carbon balance (Net Primary Productivity) for different plant functional types (PFT: grass, shrub, and trees), driven by potential evapotranspiration (PET) and storm sequences (Figure 4-1). The cellular-automaton fire component generates random ignitions on the modeled domain; if a fire breaks the fire are expand cell by cell until low fire susceptibility cells dominate the domain or an upper fire area threshold is reached. Simulations experiments are conducted using both reconstructed historical storm time series and a stochastic weather generator that vary mean values of storm intensity, duration, and time between storm over the wet (Monsson) and dry seasons of the regional climatology.

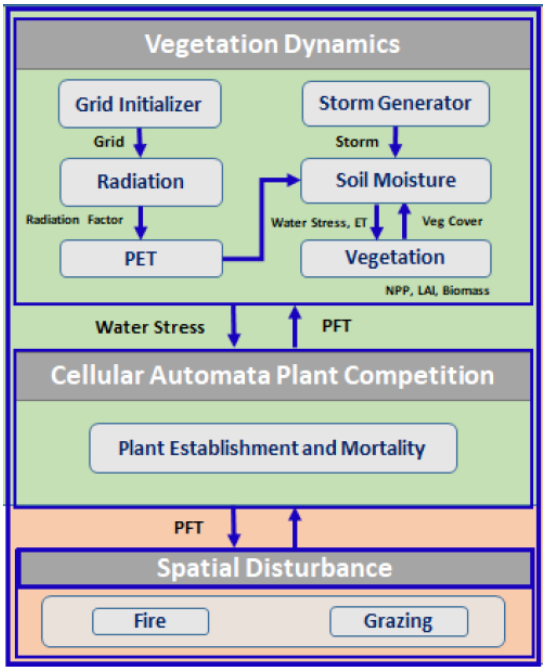


Figure 4-1: Landlab components used to develop a coupled model for local ecohydrologic water and carbon balance, and cellular automaton-based spatial establishment driven by plant competition for space, mortality and disturbance processes.

The model is not calibrated for this climate change study; all parameters are used from Chapter 3. In our model grass vegetation represent C4 warm season grass, shrub is C3 creosotebush (L. tridentate) and tree is C3 one-seed Juniper (J. monosperma). Grasses have the highest

susceptibility to fires followed by trees and shrubs. Trees are more susceptible to fires by a factor of 2.5 compared to shrubs. Grasses are more susceptible to fires by an order of magnitude compared to shrubs. Establishment of shrub and tree PFTs is based on local and non-local seeding rules. The non-local rule uses a base rate of seeding for woody plants with an equivalent establishment rate of 0.025% (for 0 cover) and increases linearly as the woody plant cover grows (i.e. more seedlings become available) up to a rate of 2% at 50% cover fraction of tree or shrub and stays fixed. The base rate represents the arrival of seedlings from the boundaries of the modeled domain (e.g. grass-shrub ecotone). The rules of local establishment provide seeds to the neighbors of shrub (first ring) and neighbors of tree (two-rings) individuals as earlier described in Chapter 3 (also see Zhou et al., 2013).

## 4.3 STUDY SITE

Our study site is a semiarid ecosystem in the northwestern corner of the Sevilleta National Wildlife Refuge (SNWR) within the Chihuahuan desert in New Mexico. The coupled Landlab ecohydrology components used in this study were calibrated and tested for this region (Chapter 3). To investigate the effects of climate variability on ecosystem change we used a flat domain and an actual 3.3 km2 catchment that has an elevation range of 1600 m to 1700 m, a west-to-east flowing main channel of 4.3 km and distinct polar (north) and equatorial (south) facing slopes. The climate shows distinct seasonality: a high-intensity summer monsoon season (July to September) during which approximately 50% of the ~250 mm of mean annual precipitation falls, and low-intensity winter rainfalls, controlled by broad-scale frontal systems (Gutierrez-Jurado et al., 2007, Zhou et al., 2013). Within the watershed plant distribution is strongly controlled by topographic aspect, with mesic one-seed juniper (Juniperus monosperma) and dense black grama (Bouteloua eriopoda) coexisting in the north facing slopes, and xeric Creosotebush (Larrea tridentata) dominating the south facing slopes. Vegetation type on the flat surfaces within the SNWR vary, as the Chihuahuan desert has witnessed an active transition of grasslands into shrublands within the last 150 years (e.g., Moreno-de las Heras et al., 2015). In the McKenzie flats region, the north-eastern quadrant of the SNWR, an active shrub-grass ecotone can be observed with nearly monospecific Black Grama grass (~ 30% cover) in the NE of the domain

with a sharp transition to Creosotebush shrub (~60% cover) in the SE of the domain (e.g., Kurc and Small, 2007; Moreno-de las Heras et al., 2015).

In Chapter 3 local ecohydrologic soil moisture and vegetation dynamics components of Landlab were calibrated at the Deep Well site, located in the McKenzie Flats region of the SNWR (Figure 4-2c). Meteorological data (precipitation, solar radiation, air temperature, relative humidity) from the Deep Well meteorological station were used to drive Landlab. Modeled soil moisture and daily evapotranspiration were compared to observations at the Deep Well site and predicted leaf area index for grass was compared against MODIS-LAI. Thus, in this study we used Landlab calibrated for Deep Well site conditions to investigate the role of long-term variability in the climate on ecosystem dynamics.

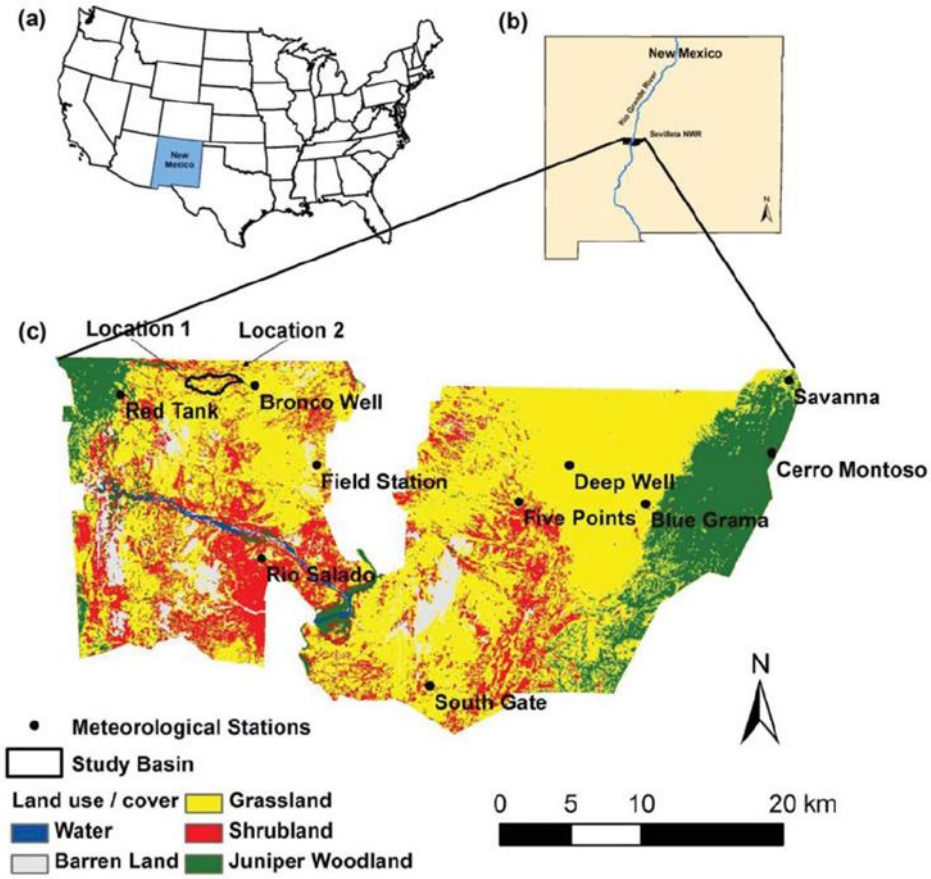


Figure 4-2: (a, b, c) Location map of the study watershed within the Sevilleta National Wildlife Refuge (SNWR) in New Mexico, USA (Zhou et al., 2013, reproduction of their Fig. 2 with permission)

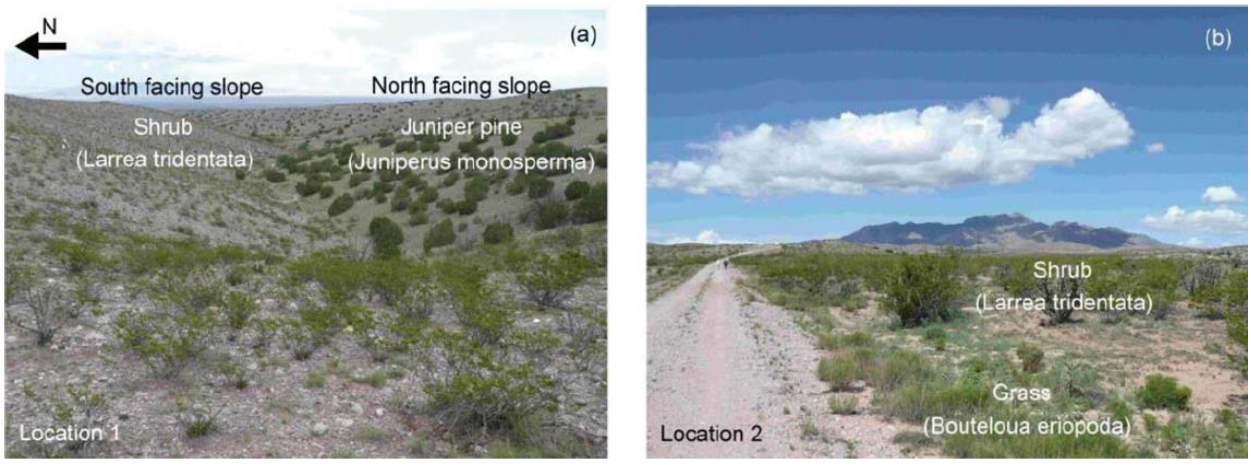


Figure 4-3: Distribution of PFTs in relation to topography: (a) photograph taken at Location 1 of Figure 4-2 looking eastward from the headwater of the study basin. Southern aspects are

covered by Creosotebush. Northern aspects are covered by mixed Juniper Pine and Grass. (b) photograph taken at Location 2 of Figure 4-2, looking in the northwest direction. Dominant vegetation is shrub. Scattered trees and limited grass clumps also exist (Zhou et al., 2013, reproduction of their Fig. 3 with permission).

## 4.4 PALEO-ECO-CLIMATE CHANGE

### 4.4.1 *Reconstruction of Late Pleistocene Climate and Biome*

In the North American desert biomes climate-driven vegetation change revolves around C3 cool season grasses and trees (e.g., Pinion-Juniper woodlands), desert shrubs (e.g., Creosotebush), and warm season C4 grasses such as black grama and blue grama (Waller and Lewis, 1979). Here we review vegetation change in the desert elevations of the Southwestern USA in reference to the Paleoclimatic and Paleoecologic data reported by Hall and Penner (2013) as well as other broader studies (e.g., Van Devender, 1997; Holmgren et al., 2007) (Figures 4-4a and 4-4b).

Hall and Penner (2013) reported reconstructed annual precipitation and temperature since the late Pleistocene from 38 sediment samples obtained from the walls along 14-km stretch of the Abo Arroyo, NM (mean elevation, 1,430 m at head ~1,980 m). This elevation range overlaps with the range of the study basin (1,600 m – 1,700 m) as well as the Deep Well weather station (1,600 m). The measured radiocarbon age of samples ranged from 905-1,053 (yr BP) to 12,617-12,968 yr BP. The average temporal resolution of the data was 422 years for the late Pleistocene (12,800 to 9,000 yr BP), while the late Holocene was represented with a much finer resolution of ~90 years. The general trend shows switches between cool-wet and warm-dry conditions (Figure 4-4a).

Several lines of information are used to reconstruct annual average precipitation and temperature (Hall and Penner, 2013). These include a widely reported correlation between July temperatures and C4 plant species in the flora across North America (e.g., Terri and Stowe, 1976) and correlation between the proportion of C4 species and carbon-13 ($\delta$13C: isotopic signature of 13C/12C) in soils and sedimentary deposits. Thus, using observed $\delta$13C, July temperatures are obtained ($r^2$=0.67) (Nordt et al., 2007). Using empirical relationships between July temperatures

and annual temperatures (r2=0.94), and between annual precipitation and annual temperature (r2=-0.81) in modern climate records from a large number of stations within 100 km of Abo Arroyo, annual temperature and precipitation of the past are reconstructed (Nordt et al., 2007, 2008; Hall and Penner, 2013). Their reconstruction model estimates annual temperature and precipitation for Abo Arroyo consistent with the modern means at the closest weather station to Abo Arroyo (360 mm annual precipitation and 10.8 ºC annual temperature) (Hall and Penner, 2013) (Figure 4-4a).

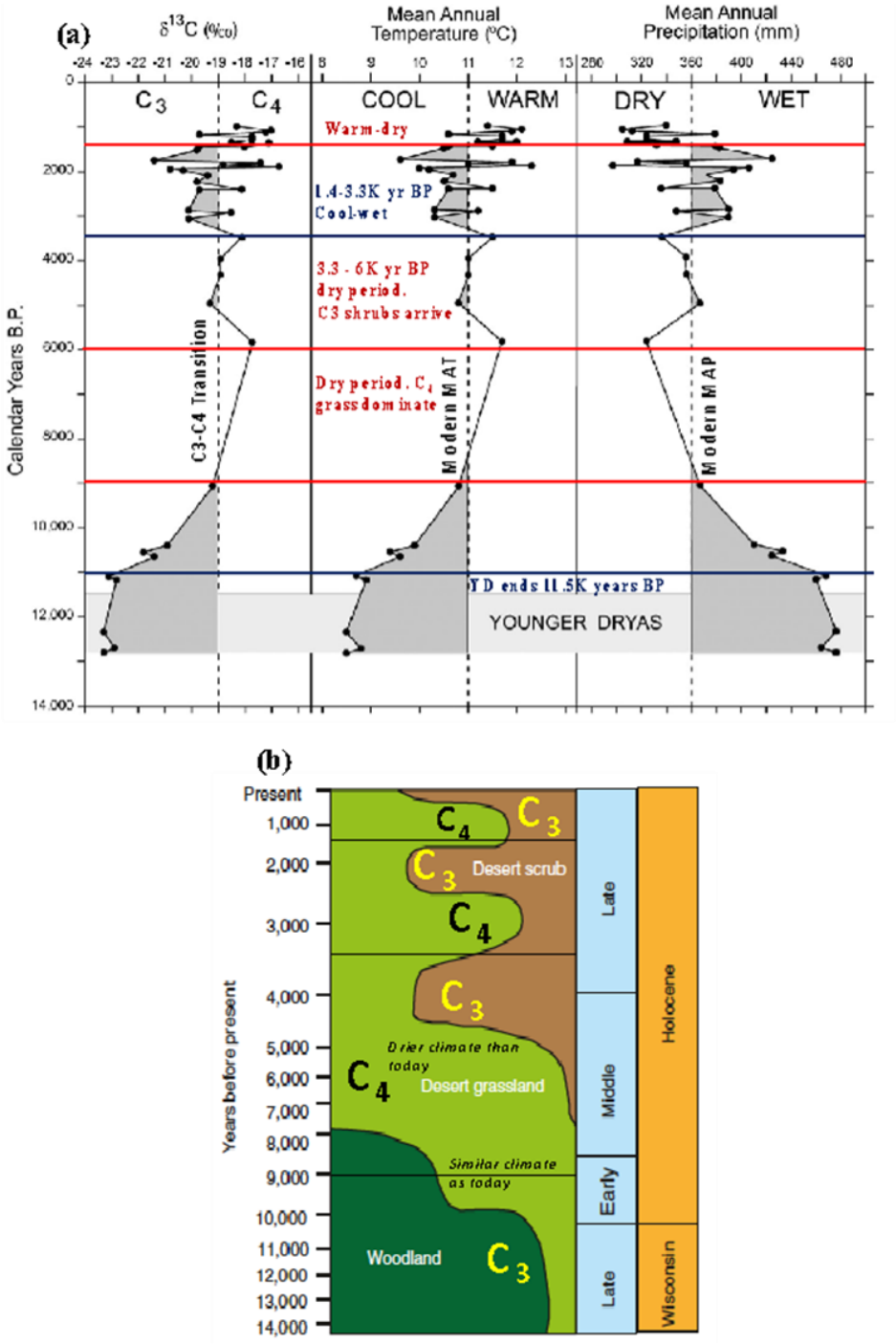


Figure 4-4: (a) Abo Arroyo stable carbon isotope record; C3-C4 vegetation, mean annual temperature, and mean annual precipitation on during the past 12,800 years (Hall and Penner, 2013, Modification of their Fig. 4 with permission). (b) Changes of the desert biomes of the Southwestern USA during Late Pleistocene and Holocene (Archer et al. (2017), original from Van Devender (1997), reproduction of their Fig. 2.1a).

The late Pleistocene record starts with the cool and wet Younger Dryas (~13K yr BP – 11K yr BP), during which the warming trend since the Last Glacial Maximum (LGM) reversed globally (Alley, 2000), and the Southwest USA has experienced cooler and wetter climate than any later time during the Holocene. At the Abo arroyo site, evidence from sediment samples show the formation of wet meadows (Hall et al., 2012b). With plenty of moisture, current desert elevations (300-1700 m) were dominated by C3 trees (piñon-juniper-oak woodlands) that coexist with C4 grasses (black grama, B. eriopoda; blue grama, B. gracilis) as secondary vegetation. Conditions were too cold for C4 grasses to compete with trees. Similarly, cold and wet winters and cool summers prevented the northward expansion of C3 desert shrubs (e.g., Creosotebush, L. tridentata); they remained further South in Mexico and elevations lower than 300 m (Betancourt et al., 1990; Thompson et al., 1993; Holmgren et al., 2007) (Figure 4-4).

Around 9K yr BP, warming climate since the late Pleistocene became similar to the modern climate averages in the region. An array of other evidence including packrat mittens (Van Devender, 1990; McAuliffe and Van Devender, 1998), and climate model output (Kutzbach, 1998) suggest greater-than modern summer temperatures and precipitation during the mid-Holocene (8K – 6 K yr BP). This period is marked by increase in the dominance of C4 grasses and the migration of C3 trees to higher elevations (Holmgren et al., 2007). Toward the end of the middle of Holocene (5K yr BP- 4K yr BP) C3 shrubs (e.g., L. tridentate) arrived and rapidly expanded in the region and the modern biomes of the low desert elevations are established (Van Devender et al., 1997). Warmer and drier conditions continued until a wetter and cooler period has reached around ~3.3 K yr BP. Since ~3.3 K yr BP low elevation have witnessed a coexistence of C3 shrubs and C4 grasses, with alternating dominance as climate more frequently vary between wet-cool and warm-dry periods.

Following the wet-cool period (3.3 K yr BP – 1.4 K yr BP) the climate turned warmer and drier in late Holocene at the Abo arroyo site, earlier than several other neighboring sites that report onset of warming around 800-1000 yr BP (Polyak et al., 2001; Rasmussen et al., 2006). The Medieval Warm Period (MWP) corresponds to this period in 900 AD - 1300 AD during which C3 shrubs outcompete C4 grasses in low desert elevations. Hall and Penner (2013) data misses the Little Ice Age (LIA) (1300 – 1850 AD) that marked the end of the MWP. LIA might have

marginally supported grasslands during the time of Euro-American settlers and the rate of woody-plant expansion began to increase since then (Archer et al., 2017). In this paper between 1,000 BP and 2015 is considered as the modern climate.

### 4.4.2 *Representation of the past climate in Landlab*

The mean annual precipitation and mean annual temperature at the Abo Arroyo site (Figure 4-4a, dashed lines) are used to calculate relative annual changes at each Paleoclimate data point. Precipitation change is estimated as the ratio of annual precipitation at a Paleoclimate data point divided by the modern mean. Temperature change is estimated as the difference between a past temperature to the modern mean annual temperature. These correction factors are used to scale the modern climate at the Deep Well site to obtain precipitation and temperature change since the Late Pleistocene as:

$$\overline{P_{DW_i}} = \overline{P_{DW}} \frac{\overline{P_{AA_i}}}{\overline{P_{AA}}} \quad (1)$$

$$T_{DW_i} = T_{DW} + \left(\overline{T_{AA_i}} - T_{AA}\right) \quad (2)$$

where, DW indicates Deep Well site, AA indicates Abo Arroyo site, i is the time represented by each of the 38 Paleoclimate data point (Figure 4-4a). $\bar{P}$ is mean annual precipitation (mm), $\bar{T}$ mean annual temperature (ºC), T is daily temperature. Note that in (2) the mean annual temperature difference is applied daily to simulate a uniform change across seasons. This is a limiting assumption. More Paleo-climatologic approximations can be developed using seasonal reconstructions or Paleoclimate model runs.

We used the Penman-Monteith (P-M) equation for transpiration for each PFT (grass, shrub, tree). The P-M equation requires daily temperature and surface resistance, rs (s/m). We used the simple model of Yang et al (2019) to incorporate changes in atmospheric CO2 on transpiration:

$$r_{s_i} = r_s + 0.05\,\Delta\,CO_2 \quad (3)$$

This equation reflects results from across 16 CMIP 5 model outputs.

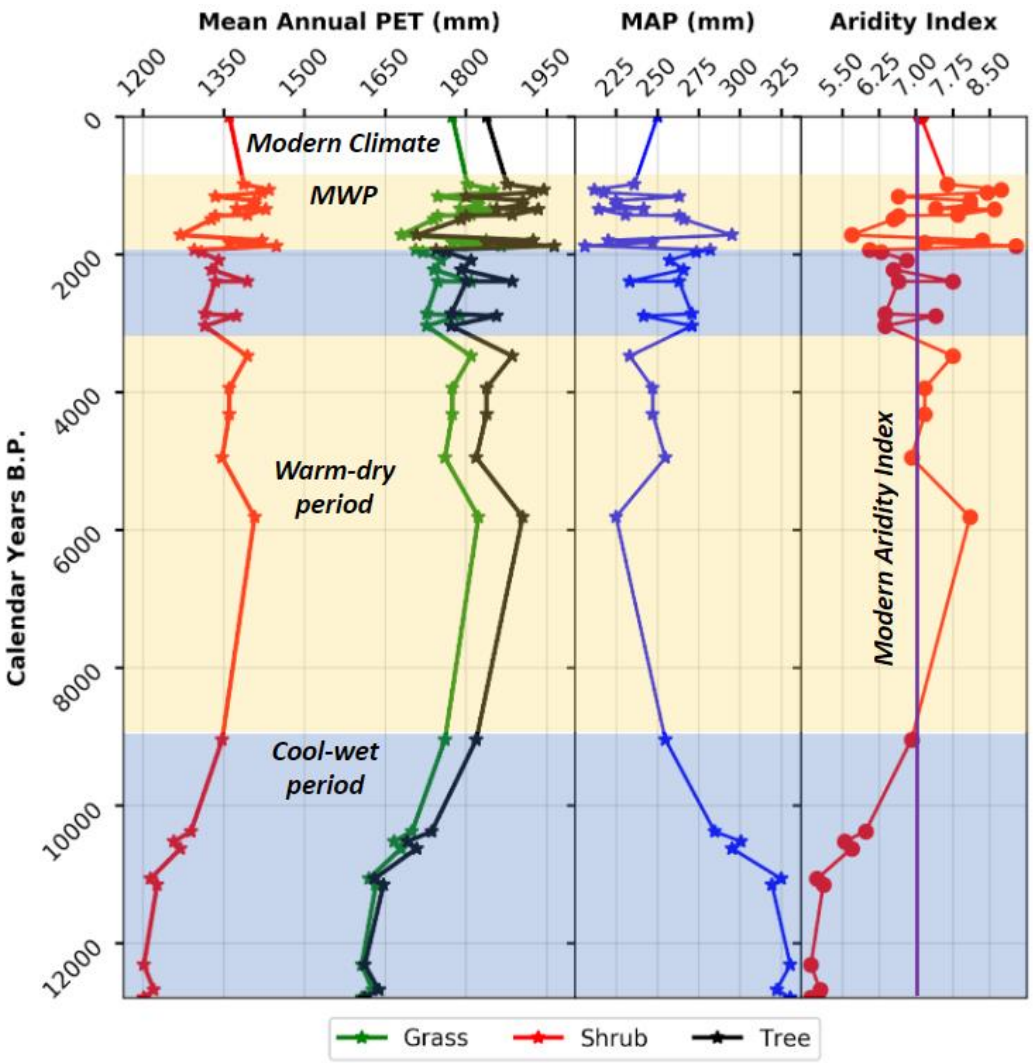


Figure 4-5: Reconstructed annual potential transpiration, mean annual precipitation, and aridity index for the climatology of the Deep Well meteorological station site in McKenzie Flats, SNWR, NM, USA.

Reconstructed Paleoclimatic averages are reported in Figure 4-5. Mean annual potential transpiration (P-T) grows in the order of shrub (creosotebush), grass (blue/black grama) and tree (one-seed Juniper) PFTs. Representative biophysical parameters of the P-M equation for these PFTs are used from Zhou et al. (2013) and Chapter 3. Shrub's lower PT is largely because of their higher surface resistance to transpiration, as they are more drought tolerant than tree and grass PFT. Mean annual precipitation ranges between 200 mm and 325 mm. Aridity index (ratio of mean annual precipitation to mean annual grass P-T) are in the approximate range of 5.0 to

9.0 that correspond to a borderline semiarid to arid. Given that the modern mean of the precipitation is 250 mm/yr at the Deep Well site, in Late Pleistocene our estimates gives ~30% more precipitation and 20% less rainfall during the MWP broadly.

Landlab requires storm depth and time between storms, and potential transpiration and bare soil evaporation between two subsequent storms (Figure 4-1). In each of the reconstructed Paleoclimatic record MAP is divided equally to wet (Monsoon, JJA) and dry (rest of the year) seasons. Time between storms are set identical to the modern storm statistics, and mean storm depth is estimated for wet and dry seasons. In each of the reconstructed Paleoclimatic record mean daily PT is estimated and its daily variability is assumed to follow a sinusoidal function consistent with the temporal distribution of solar radiation over a year (e.g., Zhou et al., 2013). The influence of aspect on PT is represented using the fraction of pre-calculated daily ratios of incoming solar radiation on sloped surface to that of flat surface. Bare soil evaporation is assumed 75% of reference grass transpiration (Zhou et al., 2013; Yetemen et al., 2015; Nudurupati et al., 2020). Starting with the parameters obtained by the modern climate, we varied parameters in the middle of the two Paleoclimatic data points.

## 4.5 RESULTS

### 4.5.1 *Ecosystem response of flat landscape*

*Can vegetation change be attributed to climate variability since the Late Pleistocene?*
In the first set of simulations we investigate the role of seedling availability of woody plants as climate transitions from Late Pleistocene to today's condition. A flat landscape (4 km by 1.4 km) at 5m grid cell resolution is used. Four simulations are run: a) no seeding; b) seeding shrubs; c) seeding trees; d) seeding shrubs and trees. Here seeding is used to represent the availability of tree and shrub seeds and seedlings such that when and if climatic conditions improve individual PFTs can grow. For each of these cases, an initial vegetation map is developed by running the climate of the Late Pleistocene for 3,000 years.

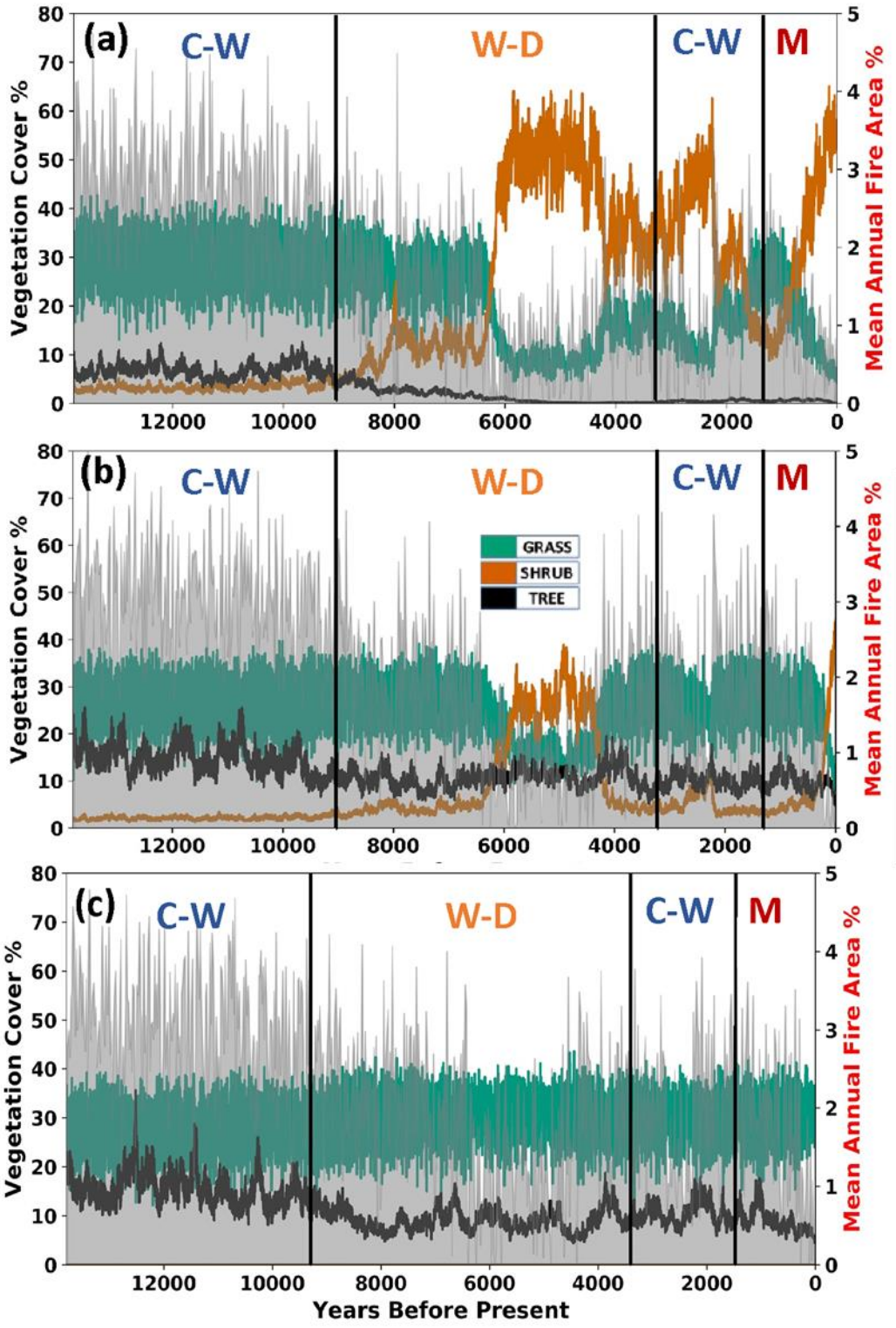


Figure 4-6 Pale-ecologic simulation using Landlab for a flat domain representative of central New Mexico conditions with seeding of: a) shrubs, b) shrubs and trees, c) trees. C-W: cool-wet period, W-D warm-dry period, M modern climate. Fire impact area is plotted in gray.

In all three simulations presented in Figure 4-6 the cool-wet (C-W) late Pleistocene ecosystem is composed of trees and grasses. Shrubs stay at a relatively constant level only when maintained by continuous seeding. Even in the extreme condition when shrubs are seeded throughout the simulation and trees are not, C-W late Pleistocene ecosystem is dominated by a mixture of C3 trees and C4 grasses. Here a key component of the model is the arrival of fires, driven by lightning strike. In this simulation we used the fire model that provides realistic fire frequency and area for the modern climate conditions (Chapter 3). It can be argued that fires were less frequent in the C-W late Pleistocene, which would potentially reduce the fire arrival and promote more tree cover. While this can be investigated in future research, the main prediction of our model here is the dominance of trees compared to shrubs during the late Pleistocene, consistent with the literature (Figure 4-4).

After 9K yr BP the climate becomes gradually warmer and drier (W-D) than today; drought conditions peak in the 5K yr BP – 6K yr BP range in Middle Holocene (Figure 4-4a, 4-4b). Modeled shrubs expand during this period by outcompeting trees and grasses, supported by Paleo-ecologic evidence (Figure 4-4a, 4-4b) (Van Devender, 1997; Holmgren et al., 2007; Archer et al., 2017). The model shows interesting outcomes of fire-vegetation feedback in the Mid-Holocene period when shrubs coexist with grasses (Figure 4-6a) and when all three PFTs coexist (Figure 4-6b). Intensification of the W-D conditions between 9K yr BP and 6K yr BP is marked by gradual increase in shrub cover until ~ 6.5 K yr BP followed by a rapid expansion until ~4.5 K yr BP (Figures 4-6a, 4-6b).

The sparsity of the Paleoclimatic data limit our predictions during the W-D to C-W transition in the 4K yr BP and 3K yr BP period. More frequent Paleoclimatic observations (~70%) fall between 4K yr BP- 900 yr BP, that includes highly variable C-W period and the MWP. The model predicts a dynamic interplay between grass and shrub cover that compete for space under the influence of varying climate and fire size in absence of trees (Figure 4-6a). When tree seedlings are available trees suppress the shrub dominance during the C-W period (~ 3.3K yr BP – 1.4K yr BP). Thus, our model clearly shows that shrubs in the Southwestern USA establish in response to shifts to a warmer and drier climate. Importantly, model runs suggest that even though ecosystems could have seen grass domination in certain parts of the Southwest USA

where tree seedlings are available during the LIA and the time of Euro-American settlement (Figure 4-6b, M period), shrubs could rebound in response to climate without the need for extensive grazing and fire suppression.

*How do fire-grass feedbacks and climate trends interact to reinforce shrub expansion?* To examine this question, we identified periods of rapid shrub expansion and contraction and investigate the distributions of grass connectivity for select PFT maps for shrub-seeding (Figure 4-7) and tree- and shrub-seeding simulations (Figure 4-8). Connectivity of grass cover in arid ecosystems is regarded as a key attribute of sustained grasslands, and loss of connectivity is often associated with the reduction of fire frequency and size (e.g., Ravi and D'Odorico, 2009; Archer et al., 2017). Distribution of grass connectivity gives % of the landscape where a grass cell is connected to no or up to 8 neighboring grass cells (Figures 4-7a, 4-8a). Zero connectivity can indicate a burnt area or a grass cell surrounded by woody plants.

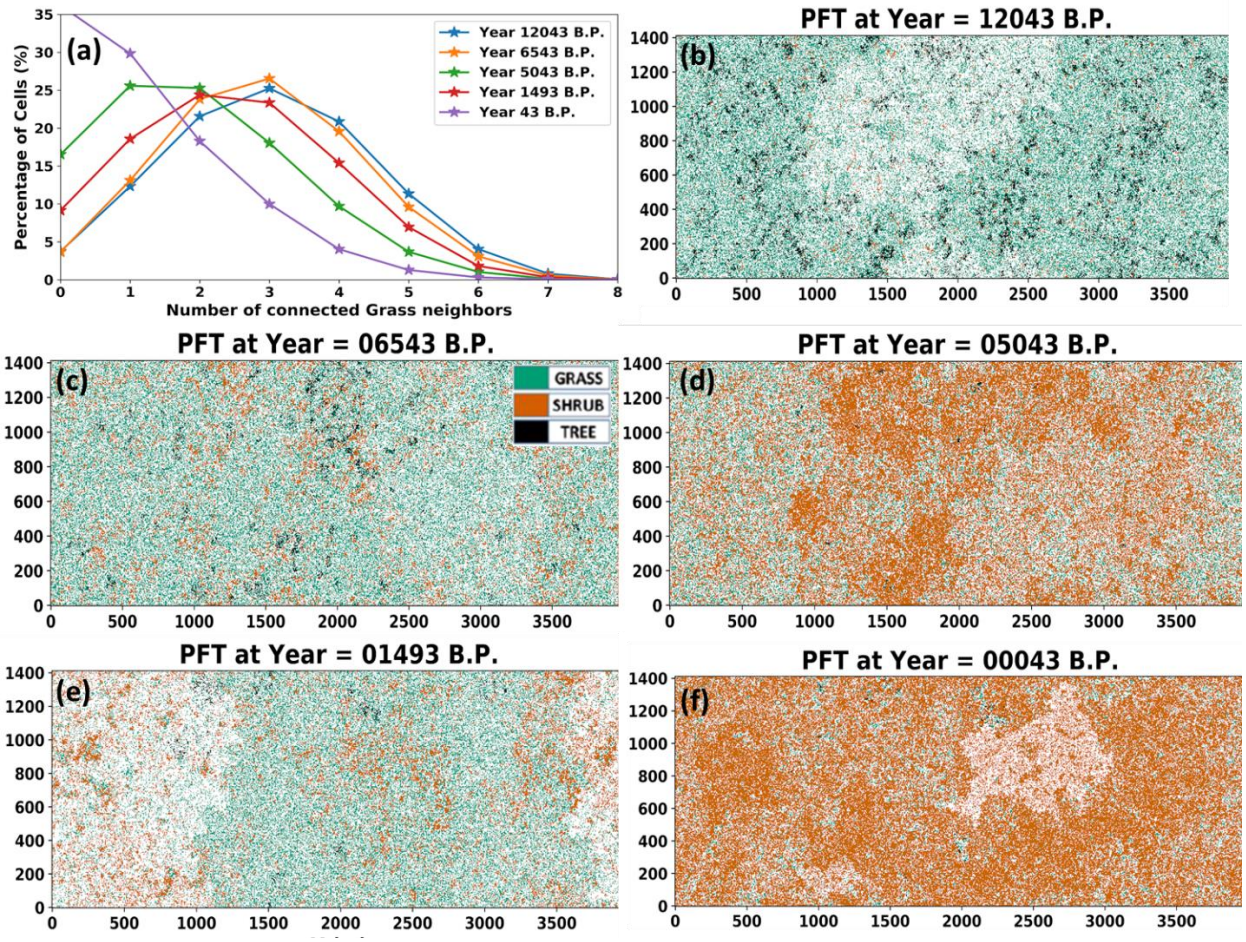


Figure 4-7 Modeled ecosystem response to reconstructed climate variability since the Late Pleistocene in a flat landscape representative of central New Mexico, USA ecosystem with non-local seeding of shrubs. Distribution of connectivity of grass cells are plotted (a) for modeled PFT maps at select pivotal times for ecosystem change since the Late Pleistocene (b to f).

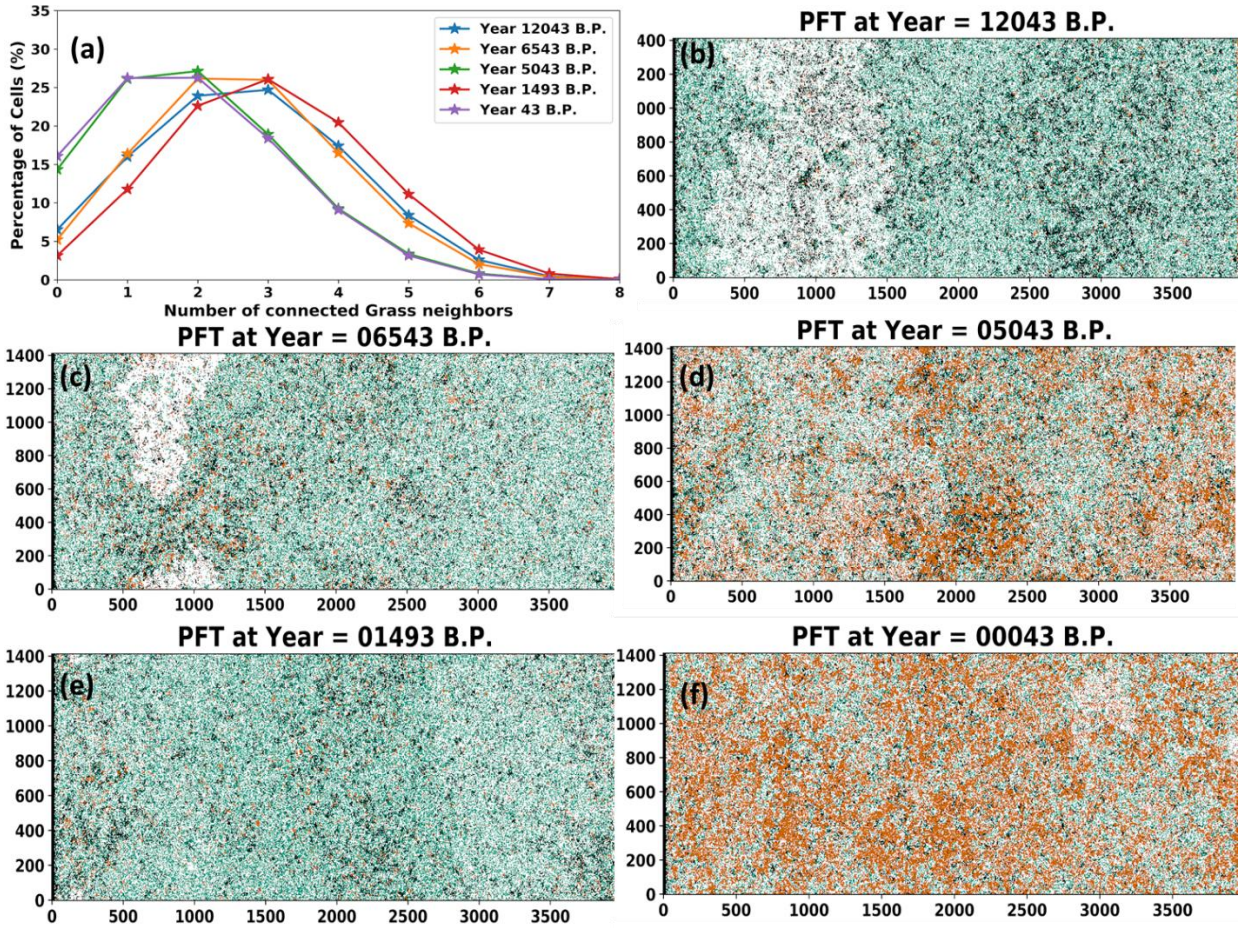


Figure 4-8 Modeled ecosystem response to reconstructed climate variability since the Late Pleistocene in a flat landscape representative of central New Mexico, USA ecosystem with non-local seeding of shrubs and tree. Distribution of connectivity of grass cells are plotted (a) for modeled PFT maps at select pivotal times for ecosystem change since the Late Pleistocene (b to f).

In both cases cooler and wetter Late Pleistocene climate (MAP=~360 mm, AI=5.0) supports highly connective mixed grass-tree ecosystems with a nearly bell-shape connectivity distribution with a peak at 3 neighbors (Figures 4-7a, 4-8a). Footprints of relatively large fires can be observed (Figures 4-7b, 4-8b). At ~6.5 K yr BP, before the rapid Mid-Holocene shrub expansion (Figure 4-6a, 4-6b), small shrub clusters are formed (Figures 4-7c, 4-8c) and within the next ~500 years shrub cover becomes dominant (Figure 4-7d, 4-8d), as both grass cover and mean annual fire area get smaller (Figure 4-6a, 4-6b). The connectivity distribution for grass cells shift to the left (peaks at 2 cells) owing to the increase in woody plant cover (Figures 4-7a, 4-8a).

Toward the end of the cool and wet period (3.3 K yr BP – 1.4 K yrBP) shrubs have retreated to levels similar to Early-Mid Holocene (Figures 4-7e, 4-8e). The cooler-wetter climate also shifted the distribution for grass connectivity to the right, improving grass cell connectivity. In the modern period, warmer and drier conditions enable a fast shrub come back, and shift the connectivity distribution to the left once again (Figure 4-7a, 4-7f; 4-8a, 4-8f), and lower the size of fires (Figures 4-6a, 4-6b). In the case where tree and shrub seeds were sustained non-locally shrub expansion did not occur during the MWP. In the last 4,000 years ecosystem was composed of a relatively stable mixture of tree, shrub and grass. Fast shrub expansion occurred in the last 150 years of the model, consistent with the woody plant encroachment observations in the Southwest USA that started in mid to late 1800s and continued throughout most of the 1900s and today (e.g., Van Auken, 2009).

### 4.5.2 *Aspect-dependent ecosystem response*

Topography mediates local climatology; forms micro climatic niches and creates refugia for plants during prolonged droughts and disturbance such as wildfires. This enables saplings of many grassland and savanna species to regenerate when the conditions improve (e.g., Archer et al., 2017). *What is the role of moderate topography on ecosystem change?* To address this question, we first ran two simulations on an actual watershed (Figure 4-2c) for an extreme cool-wet (Late Pleistocene, MAP=325 mm) and a warm-dry period (MWP, MAP=205 mm) for 5,000 years. The intent of these experiments is to identify steady-state end-member ecosystems. Both shrub and trees seeds were introduced by non-local and local seed dispersal. The initial condition for these simulations were identical vegetation maps obtained by a Late Pleistocene spin-up model run. Thus, the warm-dry simulation will illustrate an ecosystem response to an abrupt climate change and will give us some indication of ecosystem relaxation time.

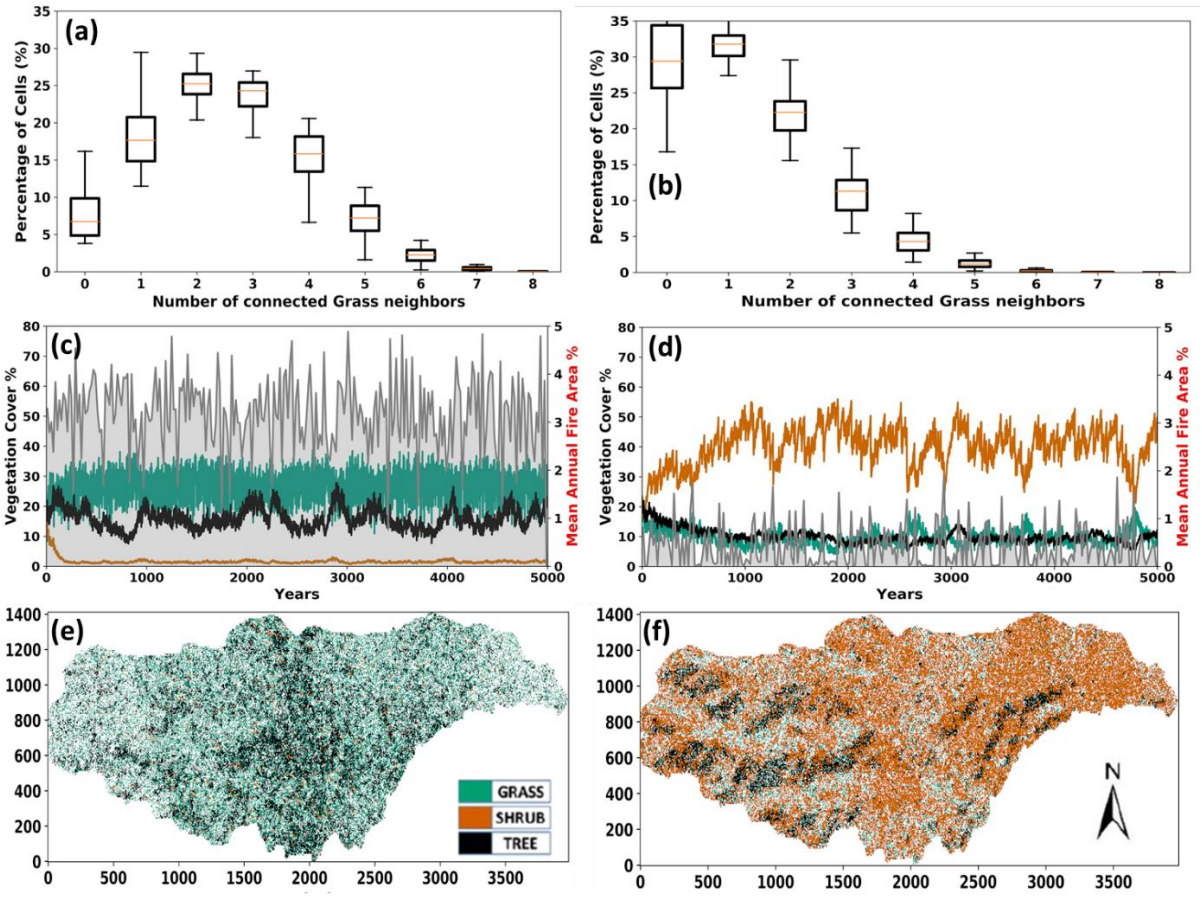


Figure 4-9: Aspect-dependent ecosystem response for cool-wet (MAP=325 mm, Late Pleistocene) and warm-dry (MAP=207 mm, corresponds to a short period of dry spell around ~1800 yr BP) extremes of the reconstructed Paleoclimatic range for a central New Mexico site (Figure 4-2).

Results show two stable ecosystems under a steady-state but stochastic climate (Figure 4-9a, 4-9c, 4-9e are wet climate; 4-9b, 4-9d, 4-9f are dry climate outputs). Shrub is absent in Late Pleistocene as tree-grass coexist with highly variable grass cover, while frequent fires suppress the expansion of trees. Surprisingly, lack of aspect control on tree cover suggests the level of moisture might be sufficient for tree growth across all landforms in Late Pleistocene. A rapid switch to a MWP-like dry and steady climate from wet Late Pleistocene first prompts a transient response that takes approximately 1,000 years during when grass and tree cover gradually give way to shrub expansion. Shrub establishes in much of the landscape except for cooler hillslopes (Figure 4-10). Loss of fires and shifted connectivity distribution to the left indicate reduced connectivity of grass patches. Warm-dry climate causes an aspect-dependent organization of

one-seed Juniper in this watershed, consistent with Lidar-derived estimates of modern cover (MAP=~ 250 mm), within the whisker ranges (Zhou et al., 2013).

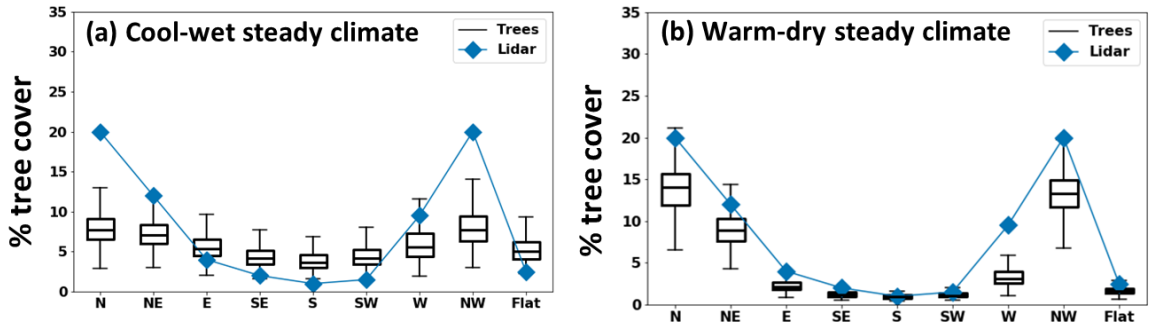


Figure 4-10: Aspect-distribution of one-seed Juniper (J. monosperma): a) Late Pleistocene-like cool-wet and b) MWP-like warm-dry conditions for central New Mexico study watershed. Lidar-derived tree cover represent conditions in 2007 (digitized from Zhou et al., 2013). Box-whisker plots are developed from model output of every 100 years, representing a variability of tree cover over time.

When climate forcing is steady (wet-cool or warm-dry), stable ecoclimatic patterns emerged. *How does ecosystem respond to variable climate forcing with persistent trends?* This question is investigated by running Landlab continuously with reconstructed climate forcing (Figure 4-11). As the climate begins to get warmer and drier in Late Pleistocene tree cover continuously declines until ~9 K yr BP. As warming continues shrub and tree cover both begin to show an advance followed by a setback (9K -7893 yr BP). Ecosystem in this period largely remains as a grassland savanna with aspect-dependent trees while fire sizes get smaller. Persistent warmer and drier climate marks the Mid-Holocene shrubland expansion (~7900 yr BP). Shrub vegetation, initially established in clusters (7493 yr BP), expands into grasslands and fires get smaller in size. Aspect control on tree establishment, and the propagation of shrubs from low elevations towards the headwaters are prominent features of the modeled ecosystem dynamics of Mid-Holocene (7493 – 5493 yr BP, MAP=244 mm-225 mm range). Roughly around 5800 yr BP, peak of the dry period arrives (MAP=225 mm) and the rainfall begins to increase (but still warmer/drier than today), and grasses begin to respond rapidly.

Compared to the tree-shrub seeding simulation on flat domain (Figure 4-7b, 4-8), shrub expansion and the decline of a shrub dominated ecosystem took place earlier on actual topography during the Holocene. This may be due to the influence of aspect-dependent clustering of trees on fire frequency and size. A random lightning that hit a north-facing slope will have a smaller probability to cause a wildfire. Over the long Mid Holocene dry period that favors shrub vegetation because of their greater drought tolerance, loss of fire frequency could have led to a faster shrub expansion but at the same time concentration of more trees on favorable north aspects. Towards the end of the Holocene, as climate gets wetter, shrubs are replaced by grass, but aspect-pattern of trees remains. During the MWP trees buffer the landscape from shrub expansion and the ecosystem remains dominated throughout the simulation until modern climate is reached. Compared to the flat simulation with same conditions, fast encroachment of shrubs in the final ~150 years is not observed which supports this hypothesis.

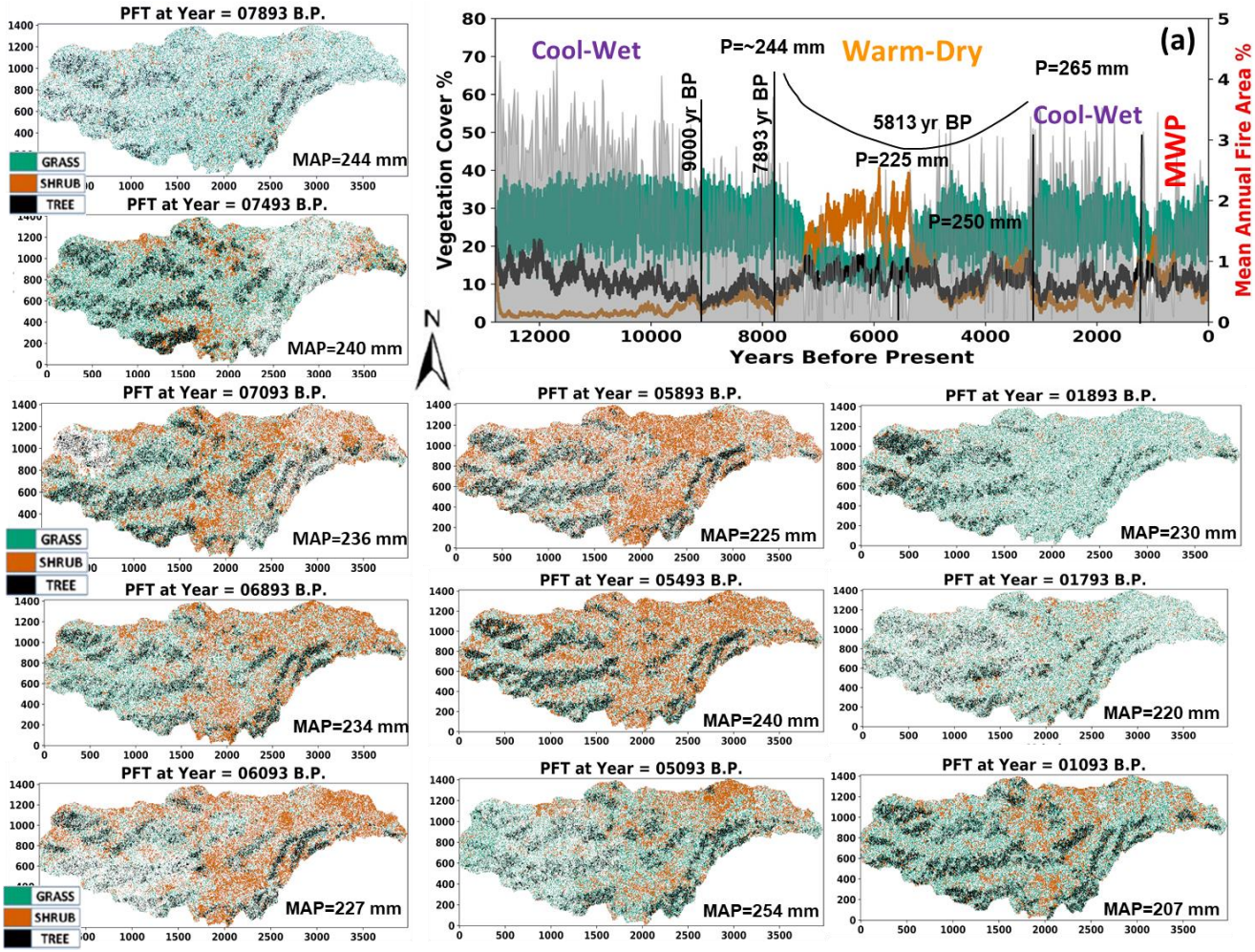


Figure 4-11: Aspect-dependent ecosystem response to continuous simulation of reconstructed Paleoclimatic data. (a) Time series of vegetation cover change. Maps of PFTs

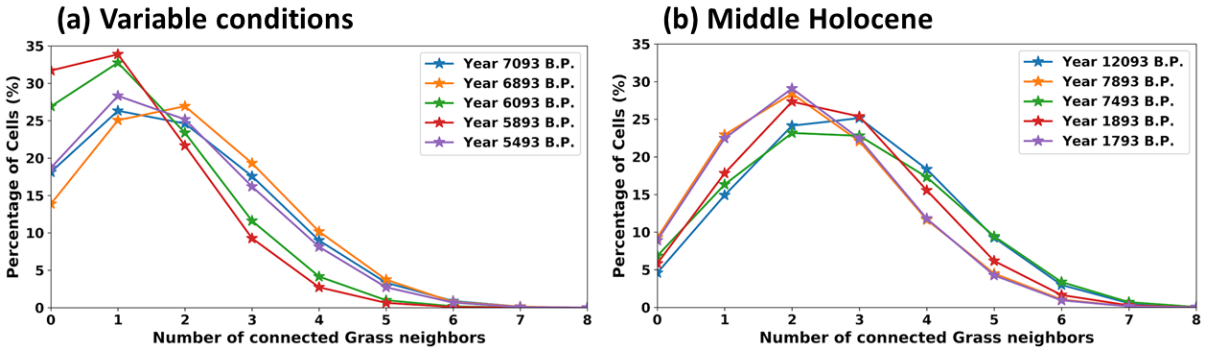


Figure 4-12: Grass connectivity distributions for PFT maps in select years that represent: (a) More variable conditions of the Late Pleistocene and Late Holocene; (b) Persistent Mid-Holocene dry climate.

Model results underscore the importance of the length of dry spells on ecosystem structure. The PFT maps plotted in Figure 4-11 have relatively small differences of MAP among them. The sustained warmer and drier than average periods in the Middle of Holocene lead to PFT maps that more closely resemble to the dry steady-state end-member aspect simulation (Figure 4-9f). When Landlab is driven by a more variable climate that includes drier and wetter than average spells rather than longer periods, the ecosystem diversity is better preserved and shrub invasion is avoided. The key contribution of climate variability is that during wet spells grasslands expand into bare soil patches. This expansion increases the fire frequency and size in the region which begin to impact shrubs as they also burn like grasses but with a lower probability.

## 4.6 Discussion and Conclusion

Conceptual models developed to explain the woody plant encroachment (WPE) in the Western USA offer several phases (Miller et al., 2000; Miller et al., 2005; Archer et al., 2017; D'Odorico et al., 2012). The first phase involves slow establishment of pioneering new plants, largely attributed to grazing, drought conditions, or grassland fire reduction programs. The second phase is rapid expansion of woody plants, often associated with multiple endogenous feedback mechanisms that require vegetation cover interacting with another variable such as fire frequency and size, water and wind erosion, soil moisture and surface energy balance (see reviews by Bond, 2008; D'Odorico et al., 2012; Grimm et al., 2013; Archer et al., 2017). The final phase is canopy closure and change in the fire regime. A limited number of models have tested and numerically confirmed this hypothesis largely within the context of woody plant encroachment since the mid 1800s (Caracciollo et al., 2016; 2017).

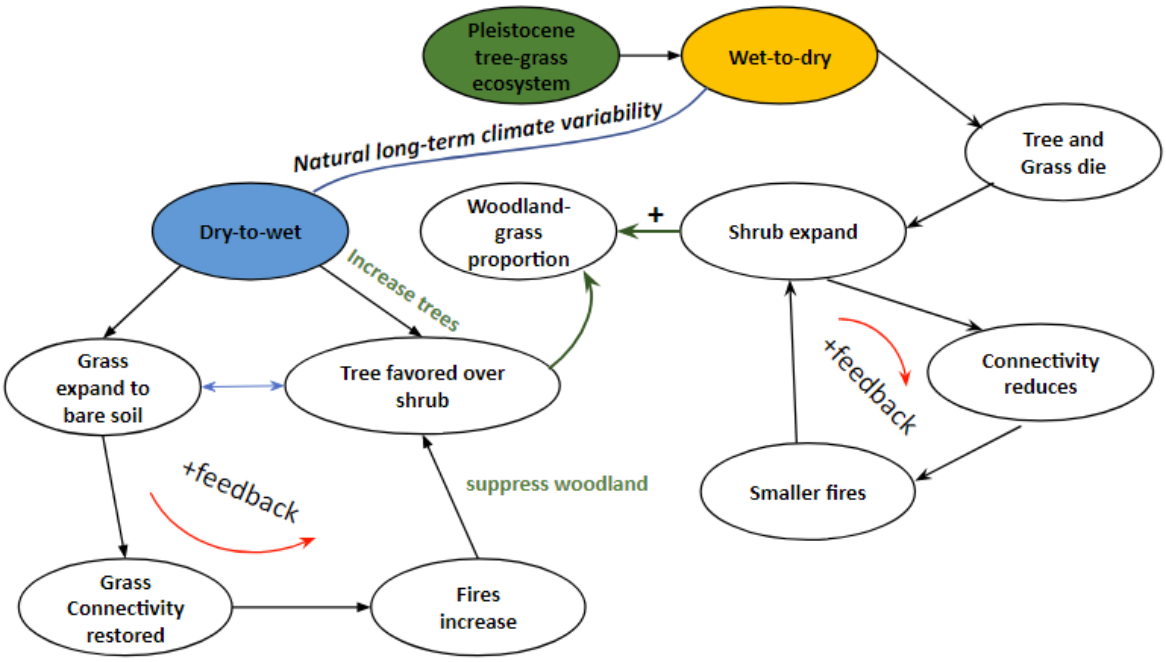


Figure 4-13: Conceptual model of eco-climatic change for a woodland-grassland desert ecosystem similar to Southwestern USA conditions.

Inspired with these earlier studies, in this paper we took a long-term approach and examined the role that climate and fire-grass interactions plays in forming desert ecosystem communities since the Late Pleistocene in the Southwest USA. Our modeling approach leads to the following conceptual model of eco-climatic change since the Late Pleistocene for a woodland-grassland desert ecosystem similar to Southwestern USA conditions (Figure 4-13). A transition from cool-wet climate to a warm-dry climate is responsible for drought-driven tree and grass mortality and their gradual replacement by shrubs. Shrub seeds could have propagated northward during this time or could be available but limited locally. Shrubs are fire tolerant, and with loss of grass fuel they gradually diminish the landscape connectivity for wildfires to spread. A critical loss of connectivity impairs the fire-grass feedback and fires become less frequent and smaller. This acts as a positive feedback to enhance shrub expansion as long as the climate remains ecohydrologically supportive of shrubs over other PFTs that are less tolerant to drought. If there are pockets of trees on cooler aspects, they act to reduce the strength of this feedback.

Our model shows that switch to a tree or grass dominated ecosystem from shrub dominated ecosystem can only happen with a dry-to-wet climate transition. Grass expansion into bare soil patches, and some potential increase in trees that have higher susceptibility to fires than shrubs. Restoring a grassland fire regime as grass connectivity increases in a relatively wetter climate would promote the stabilization of trees rather than shrubs as trees have a competitive advantage over shrubs because of their longer seedling dispersal range.

The modeling framework we proposed in Landlab can be used to identify conditions in terms of connectivity and climatic envelopes that may lead to vegetation change. We show through numerical model simulations that shrubs in the Southwestern USA establish in response to shifts to a warmer and drier climate in the Holocene. Similar mechanisms could be responsible for woody plant encroachment, model runs suggest that even though ecosystems could have seen grass domination in certain parts of the Southwest USA where tree seedlings are available during the LIA and the time of Euro-American settlement, shrubs could rebound in response to climate without the need for extensive grazing and fire suppression. Within the desert elevations, having topographical refugia for trees controlled by aspect modulates the landscape scale ecosystem response to climate change. Aspect control on tree establishment, and the propagation of shrubs from low elevations towards the headwaters are prominent features of the modeled ecosystem change dynamics. This finding is consistent with extensive field observations on ecosystem change in the desert elevations of the Southwest USA (Bond. 2008; Archer et al., 2017).

Sensitivity of our model to the parameter uncertainty of soils and plants is a critical issue that need to be addressed in the future. The key difference of our model compared to other distribution ecohydrology models is the cellular automaton based algorithms for space competition. Ecosystem studies that track the location of individual plants in the field or from Lidar and satellite derived maps would be necessary to advance spatial modeling for resource management of desert ecosystems.

# REFERENCES


Archer, S. R., Andersen, E. M., Predick, K. I., Schwinning, S., Steidl, R. J., & Woods, S. R. (2017). Woody plant encroachment: causes and consequences. In Rangeland systems (pp. 25-84). Springer, Cham.

Alley, R. B. (2000). The Two-Mile Time Machine: Ice Cores. Abrupt Climate Change, and Our Future, Princeton University Printer.

Betancourt, J. L., Van Devender, T. R., & Martin, P. S. (Eds.). (1990). Packrat middens: the last 40,000 years of biotic change. University of Arizona Press.

Caracciolo, D., Istanbulluoglu, E., Noto, L. V., & Collins, S. L. (2016). Mechanisms of shrub encroachment into Northern Chihuahuan Desert grasslands and impacts of climate change investigated using a cellular automata model. Advances in water resources, 91, 46-62.

Caracciolo, D., Istanbulluoglu, E., & Noto, L. V. (2017). An ecohydrological cellular automata model investigation of juniper tree encroachment in a western North American landscape. Ecosystems, 20(6), 1104-1123.

Fritz, S. C., Juggins, S., Battarbee, R. W., & Engstrom, D. R. (1991). Reconstruction of past changes in salinity and climate using a diatom-based transfer function. Nature, 352(6337), 706-708.

Gutiérrez-Jurado, H. A., Vivoni, E. R., Istanbulluoglu, E., & Bras, R. L. (2007). Ecohydrological response to a geomorphically significant flood event in a semiarid catchment with contrasting ecosystems. Geophysical Research Letters, 34(24).

Hall, S. A., Penner, W. L., Palacios-Fest, M. R., Metcalf, A. L., & Smith, S. J. (2012). Cool, wet conditions late in the Younger Dryas in semi-arid New Mexico. Quaternary research, 77(1), 87-95.

Holmgren, C. A., Norris, J., & Betancourt, J. L. (2007). Inferences about winter temperatures and summer rains from the late Quaternary record of C4 perennial grasses and C3 desert shrubs in the northern Chihuahuan Desert. Journal of Quaternary Science: Published for the Quaternary Research Association, 22(2), 141-161.

Kurc, S. A., & Small, E. E. (2004). Dynamics of evapotranspiration in semiarid grassland and shrubland ecosystems during the summer monsoon season, central New Mexico. Water Resources Research, 40(9).

Moreno-de las Heras, M., Díaz-Sierra, R., Turnbull, L., & Wainwright, J. (2015). Assessing vegetation structure and ANPP dynamics in a grassland-shrubland Chihuahuan ecotone using NDVI-rainfall relationships. Biogeosciences discussions., 12(1), 51-92.

Ravi, S., & D'Odorico, P. (2009). Post-fire resource redistribution and fertility island dynamics in shrub encroached desert grasslands: a modeling approach. Landscape Ecology, 24(3), 325-335.

Waller, S. S., & Lewis, J. K. (1979). Occurrence of C3 and C4 photosynthetic pathways in North American grasses. Rangeland Ecology & Management/Journal of Range Management Archives, 32(1), 12-28.

Waters, M. R., & Haynes, C. V. (2001). Late Quaternary arroyo formation and climate change in the American Southwest. Geology, 29(5), 399-402.

Van Auken, O. W. (2009). Causes and consequences of woody plant encroachment into western North American grasslands. Journal of environmental management, 90(10), 2931-2942.

Van Devender, T. R. (1995). Desert grassland history: changing climates, evolution, biogeography, and community dynamics In: JA McClaran and TR Van Devender, eds. The Desert Grassland.

McClaran, M. P., & Van Devender, T. R. (Eds.). (1997). The desert grassland. University of Arizona Press.

Yang, Y., Roderick, M. L., Zhang, S., McVicar, T. R., & Donohue, R. J. (2019). Hydrologic implications of vegetation response to elevated CO 2 in climate projections. Nature Climate Change, 9(1), 44-48.

Yetemen, O., Istanbulluoglu, E., Flores-Cervantes, J. H., Vivoni, E. R., & Bras, R. L. (2015). Ecohydrologic role of solar radiation on landscape evolution. Water Resources Research, 51(2), 1127-1157.

Zhou, X., Istanbulluoglu, E., & Vivoni, E. R. (2013). Modeling the ecohydrological role of aspect-controlled radiation on tree-grass-shrub coexistence in a semiarid climate. Water Resources Research, 49(5), 2872-2895.